University of Southampton

Faculty of Engineering, Science and Mathematics

Institute of Sound and Vibration Research

THE EFFECT OF SUSPENSION DAMPING ON VEHICLE RESPONSE TO TRANSIENT ROAD INPUTS

by

Youngjin Hyun

A thesis submitted for the degree of

Master of Philosophy

August 2005

ABSTRACT

This thesis considers the transient response of suspension models of a vehicle traversing a versed-sine shaped bump. In the first instance, the damper is assumed to be linear which enables analytical solutions to be obtained for the displacement and acceleration shock spectra. Numerical solutions are also obtained using the Runge-Kutta method. The analysis differs from much of the general shock and transient vibration literature in that the acceleration response is considered for a displacement input. By considering bump traversal time of short and long durations relative to the natural period of the system, a simple expression has been determined for the peak acceleration in terms of the system's parameters, bump length and vehicle speed.

Using a two degree-of freedom (DOF) quarter car model, the effect of the unsprung mass on the peak acceleration is investigated by numerical simulations. The acceleration shock response spectrum of the two DOF system is compared with that of the SDOF system. Experimental work involving the measurement of accelerations of the sprung mass and unsprung mass of a passenger car has also been carried out to test the validity and limitations of the approximate relationship derived for the single degree-of-freedom (SDOF) system.

A practical hydraulic automotive damper is considered and the principle of operation is discussed. Using experimental data from an automotive non-linear damper, a piece-wise linear damping model is established.

Two types of bi-state damping are introduced to model a non-linear automotive damper in terms of shock isolation. One is piece-wise linear to represent different damping coefficients in the jounce and rebound directions. Another is switching damping coefficients so that the damper is switched off whilst the vehicle is traversing the bump and on again once the vehicle has traversed the bump. Numerical simulations are presented for the transient response of a SDOF model with a versed-sine base displacement input. The results of the piece-wise linear damper are compared with that of the switchable damper. The maximum benefit of the switchable damper in reducing the peak acceleration is investigated analytically using the approximate equations. A significant reduction in acceleration is observed when the switchable damper is considered in the SDOF model. This study of non-linear passive damping models in transient shock vibration may be used in a new strategy for semi-active damping control.

Contents

LIST OF NOTATION

c, c_s	:	damping coefficient of damper in SDOF system,
		damping coefficient of damper in two DOF system.
c_a, c_d, c_j, c_r	:	damping coefficient after bump is being traversed,
		damping coefficient during bump,
		damping coefficient in jounce direction,
		damping coefficient in rebound direction
f_d	:	damping force
h_b	:	height of bump
k, k_s, k_u	:	stiffness of spring in SDOF system, stiffness of spring on sprung
		mass in two DOF system, stiffness of spring on unsprung mass
		in two DOF system
l_b	:	length of bump
m, m_s, m_u	:	mass in SDOF system, sprung mass, unsprung mass in two DOF system
r	:	frequency ratio (ω/ω_n)
t_n, t_p	:	undamped natural period, duration of bump (pulse)
v	:	longitudinal velocity of vehicle or its models
x, $\dot{x}$, $\ddot{x}$	:	absolute vertical displacement, velocity and acceleration of sprung mass
y, $\dot{y}$, $\ddot{y}$	:	absolute vertical displacement, velocity and acceleration of base
z, $\dot{z}$, $\ddot{z}$	:	relative vertical displacement, velocity and acceleration

α_p, α_s	:	ratio of damping coefficients of piece-wise linear damper,
		ratio of damping coefficients of alternative bi-state damper
ζ, ζ_s, ζ_w	:	damping ratio of SDOF system,
		damping ratio of bounce mode of two DOF system,
		damping ratio of wheel hop mode of two DOF system,
ζ_a, ζ_d, ζ_j, ζ_r	:	damping ratio after bump is being traversed,
		damping ratio during bump,
		damping ratio in jounce direction,
		damping ratio in rebound direction
ω, ω_n	:	forcing frequency from base motion,
		undamped natural frequency of SDOF system
ω_{n1}, ω_{n2}	:	undamped bounce natural frequency of sprung mass,
		undamped wheel-hop natural frequency of unsprung mass
$(\omega_{n1})_f$, $(\omega_{n2})_r$	:	front pitch natural frequency of vehicle,
		rear pitch natural frequency of vehicle

ACKNOWLEDGEMENTS

I would like to thank my supervisors, Professor Mike Brennan and Dr Tim Waters for the continuous encouragement and guidance for my research. I would also like to thank Professor Brian Mace and Dr Neil Ferguson for their valuable advice at the first review of my project. I am grateful to Dave Rhodes and Gihwan Kim for their helps in conducting the experiment in my thesis. The financial support for my study by Hyundai Motor Company is greatly appreciated.

I would like to express the deepest gratitude to my parents and parents-in-law and friends for their understanding and support of my study. Finally, I would especially like to thank my wife, Yunjung Cho and my daughter, Alim Hyun for their patience and love.

CHAPTER 1

INTRODUCTION

1.1 BACKGROUND

Vehicle ride is important for reasons of safety and human comfort. When a vehicle is driven over rough terrain, vibration is transmitted from the road, via the vehicle suspension system, to the vehicle body and occupants. The vibration transmitted through the vehicle suspension system is a major contributor to vibration levels in vehicles. Changes to this transmission path may play an important part in reducing vibration due to road inputs. The study of vibration transmission is reported extensively in the literature, see for example [1] and [2].

Vibration transmission is dependent on system properties such as natural frequencies and damping. For example, in a dynamic system at steady state that is excited with harmonic input, even a relatively small excitation can cause an undesirably large response near resonance. In this case, vibration isolation measures can be focussed on reducing the amplitude at the resonance frequency. However, for transient vibration like shock, it is more important to limit the peak force transmitted to the surroundings of the equipment in which shock originates. Shock is transferred to a system in a short period of time and with large acceleration. Therefore, the role and effect of system properties such as stiffness and damping in isolating shock may be different to that of isolating steady-state vibration.

Simple models such as a single-degree-of-freedom (SDOF) system are frequently investigated to study the effect of system parameters on vehicle ride. Various models for vehicle suspension, both linear and non-linear, have been proposed. In many instances a linear model

is insufficient to describe the behaviour of the physical system adequately. However, non-linear models cannot often be treated analytically. A convenient compromise is sometimes to characterise non-linear relations by piece-wise linear behaviour.

The most common cause of non-linearity in vehicle suspensions is the damper, which is non-linear in two respects. Firstly, the magnitude of the damping force increases disproportionately with relative velocity due to the orifice damping mechanism and flow control valves in the damper. Secondly, the damper is designed to have more damping in rebound than compression (jounce).

In this thesis, a suspension system is first modelled as a SDOF system with a mass, linear spring and linear damper, in order to investigate the influence of damping and vehicle speed on the displacement and acceleration of a vehicle traversing a bump. This study differs from most of the literature on shock isolation which is concerned with input and output displacement or input and output acceleration. Numerical and analytical solutions for a displacement input are obtained using the Runge-Kutta method and Laplace Transforms respectively. From analytical solutions, physical insight and the simple relationships between system parameters and response can be found using the shock response spectrum and simplified expressions derived by making some approximations.

Under this transient vibration, the role of the damper in the response of a SDOF system may be different to that of a damper in a directly forced SDOF system. Generally, the role of a damper in forced response of a SDOF system is in dissipating energy and reducing the vibration. However, in a SDOF system with base excitation, the damper transmits force to the vehicle (mass) as well as dissipating energy.

The relationship between the system parameters and responses of a SDOF system may or

may not be different to that of a two DOF system. A typical two DOF system for a quarter car model additionally has a mass and a spring on the base which is directly excited by the road input. Therefore, the system responses are also influenced by a base mass which is usually called an unsprung mass. For practical passenger cars, it is not always justifiable to neglect the effect of unsprung mass (wheel, tyre and axle etc.). The weight of the unsprung mass is generally about ten percent that of the vehicle body [3].

Having examined a linear system, non-linear damping is introduced in the SDOF system and this is discussed in Chapter 4. One convenient approach is to model a damper in a piece-wise linear fashion in which the damping coefficient is different in the jounce and rebound directions. The system responses are found numerically using the Runge-kutta method. The results are compared with a newly proposed switchable damper where the damping coefficient is switched on at the end of the bump. Finally, the piece-wise linear damping is compared to the switchable damper in terms of shock isolation.

1.2 LITERATURE REVIEW

1.2.1 Shock isolation

The response of a SDOF system to transient base motion has been widely researched and is presented in many standard texts including Harris [1] and Rao [2]. Often, transient base motion may be dealt with using classical shock and vibration theory in which the duration of the excitation pulse is short compared to the natural period of the spring-mass oscillator [4]. In shock induced vibration, it is the maximum peak response that is of interest for structural design. For a lightly damped SDOF system, the transient vibration due to the shock input

can be determined analytically using the impulse response function and convolution integral [2]. However, for a heavily damped system, it is more complicated to solve directly. The analysis is further complicated when, as in the case of a vehicle traversing a bump, the input disturbance and system response are different dynamic quantities. For example, the input may be of a displacement type whereas the acceleration response is of interest. This situation is rarely encountered in the literature.

Mindlin [5] considered the relation between damping and maximum acceleration in a drop test of a package cushion. When the system is excited by a half-sine acceleration pulse, the acceleration response is a damped sinusoid with an initial value whose magnitude depends on the duration of pulse and the amount of damping. For small damping (damping ratio, $\zeta < 0.5$), the maximum acceleration response reduces as $e^{-\zeta t_m}$ where t_m is the time at which the maximum response occurs [5]. For high damping ($\zeta > 0.5$), the maximum acceleration response increases in direct proportion to 2ζ [5]. Harris [4] showed that the maximum acceleration response can be solved in the case of a series of acceleration pulse inputs. However, in references [4, 5] the relationship between acceleration and damping is not explained when the system is excited by a displacement pulse.

Snowdon [6] studied the response of one-dimensional damped mechanical systems to input transients. In his work, the input disturbances are physically realistic and their first and second derivatives are continuous. Therefore, two transient displacement input functions are proposed, a so-called rounded displacement step and a unidirectional rounded displacement

pulse. These transient inputs are defined as

$$x(t) = X_{\max}[1 - e^{-\gamma\omega_n t}(1 + \gamma\omega_n t)] \qquad \text{(rounded step displacement)} \quad (1.1a)$$

$$x(t) = X_{\max}(e^2/4)(\gamma\omega_n t)^2 e^{-\gamma\omega_n t} \qquad \text{(rounded pulse displacement)} \quad (1.1b)$$

where $X_{\max}$ is maximum amplitude of these functions and ω_n is a natural frequency and γ is defined as a shock severity factor given by the duration of the pulse, t_p in terms of the half natural period t_n ($\gamma = t_n/2t_p$). For the two transient inputs, the relationship between the system parameters and maximum response is found using Laplace transforms. Snowdon determined that for the rounded pulse displacement, the magnitude of the initial acceleration spike, which occurs for relatively large value of γ and the damping ratio ζ, is approximately proportional to the damping ratio, the natural frequency and the severity factor.

Hundal [7] investigated the response of shock isolators with linear and quadratic damping. He considered a SDOF system where the input was a base acceleration pulse of rectangular shape. It was found in this paper that with quadratic damping the optimum damping ratio in reducing the maximum acceleration varies for different durations of the pulse.

In this thesis, the exact solution of the system responses for a versed-sine displacement input in a SDOF system are found analytically by using Laplace transforms and numerically using the Runge-Kutta method. The physical relations between the peak acceleration and system parameters are investigated for short and long durations of the displacement input.

1.2.2 Semi-active damping controls

In passive vibration isolation systems, the stiffness and damping properties are fixed at the design stage to achieve an acceptable compromise in performance over various operating conditions. Semi-active isolation, however, allows the stiffness or damping of the system to adapt to current conditions.

Semi-active damping control systems were proposed in the 1970s when patents were issued for automotive shock absorbers using a hydraulic valve or a solenoid valve to achieve good ride quality [8]. Semi-active damping control can be used in isolation systems for harmonic, transient shock and random inputs, although most literature focuses on harmonic and random vibration. One of the semi-active damping control strategies is the semi-active sky hook damping where the damper is switched on and off in order to emulate a damper attached between the mass and a fixed reference [8-11]. This concept can improve an inherent compromise between high frequency isolation and resonance amplification in a passive system [9]. One limitation is that a sky hook damper cannot be replicated throughout a vibration cycle. Ahmadian et al. [10] studied the trade-off between control of resonant response and isolation at higher frequencies, using a SDOF model of a vehicle suspension with a harmonic input at the base. According to this paper, a semi-active damper which has either on-off or continuously-variable characteristics exhibits the ability to reduce the amplitude of the resonance peak without worsening isolation at higher frequencies under harmonic vibration. Jalili [11] reviewed the fundamental principles of the sky hook control strategies in semi-active control systems and surveyed recent developments and control techniques for these systems related practical applications in vehicle suspensions.

The role and effect of damping in isolating shock input may be different to harmonic and

random excitation. Alanoly and Sankar [12] presented the advantages of using a semi-active strategy in systems subject to transient shock displacement inputs using numerical simulations. According to this paper, when a SDOF isolator is subject to a rounded pulse or step input as defined in equations (1.1a) and (1.1b), the performance of a semi active isolator is better than that of the passive isolator in reducing the peak acceleration. Another paper by Ahmadian [13] investigated the performance of semi-active damping control strategies when a two DOF system is subjected to a transient vibration such as a step input. In this paper, sky hook control was used on the sprung mass and groundhook control was used on unsprung mass. The ground hook control that is used for the unsprung mass is a similar method to sky hook control. The results were evaluated by peak to peak displacement and acceleration responses of a two DOF system. Yang et al. [14] compared the performance of passive, active and semi-active isolators for shock isolation. They investigated optimal damping control laws for compromised performance between peak displacement and acceleration.

1.2.3 Human response to shock

Generally, human response to shock can be considered as the perception of transient disturbances in a time much shorter than the natural response period of the body [15]. The literature seeks to classify the tolerance limits of injury and the ride discomfort in whole body response of shock. The tolerance limits of injury relate to health and safety of exposed persons, and ride discomfort assesses feelings about vibration and shock subjectively, such as displeasure and dissatisfaction.

British Standard 6841 [16] suggests that for assessment of subjective response to transient, shock and non-stationary motions, the *vibration dose value* (VDV) is more appropriate

than either the root mean square (RMS) or peak values. The VDV is given by the fourth root of the integral of the fourth power of the acceleration after it has been frequency-weighted, and is defined as

$$VDV = \left[\int_{t=0}^{t=t_n} a^4(t)dt \right]^{1/4} \tag{1.2}$$

where, $a(t)$ is the frequency-weighted acceleration and t_n is the total period during which vibration may occur. The VDV uses a fourth power time dependency to accumulate vibration severity over the exposure period from the shortest possible shock to a full day of vibration [17].

Howarth and Griffin [18] studied experimentally the human response to a single and repeated vertical shock. According to this paper, for a single shock, the growth of discomfort with increasing shock magnitude is independent of frequency, duration and direction of motion. This means that the VDV may underestimate the evaluation for the duration of low-frequency shocks. However, for repeated shock, the VDV provides a more accurate method of evaluating the discomfort of shocks.

Zong and Lam [19] studied the human body subject to shock motion using simulation of a lumped parameter model of the body. The numerical simulations are compared with experiment results for a drop test of a human on a chair in order to assess the injury level. In the study, the influence of the structure stiffness and damping for the injury level of the human was determined by measuring the peak acceleration.

The subjective ride discomfort and tolerance limit of injury can be evaluated by several methods such as the VDV and frequency weightings. However, the peak displacement and acceleration are used as objective measurements of ride discomfort [15]. In this thesis,

ride comfort is considered objectively using peak values of the response of the system. The consideration of subjective ride discomfort is beyond the scope of this thesis.

1.2.4 Non-linear models of automotive hydraulic damper

The hydraulic damper (shock absorber) is a crucial component in the automotive suspension to enhance the ride comfort and handling performance [20]. It dissipates vibrational kinetic energy due to the wheel and body motion into heat.

As the automotive hydraulic damper is typically nonlinear, a suitable dynamic model is often required for analysis of nonlinear vibration characteristics. Duym [21] studied a model of a spring disc type valve with fluid dynamics to express a non-linear relationship between the damping force and operating velocity. Mollica and Youcef-Toumi [22] suggested a non-linear model for a high pressure monotube shock absorber for analysing dynamic behaviour. The model assumed a relationship between fluid flow and damping force, and included various phenomena such as fluid inertia effects, laminar orifice flow, air entrained in the hydraulic fluid, and cavitation.

Weigel et al. [23] proposed a non-parametric model of a hydraulic damper which can establish a relationship between measured quantities, such as damping force, displacement or velocity. Oyadiji and Sarafianos [24] studied the damping forces in the jounce and rebound directions for a conventional hydraulic damper and an electro-rheological fluid-filled shock absorber. More recently, the study of a stroke dependent damper for a vehicle subject to different load conditions has been developed in order to reach a better compromise between ride comfort and handling performance [25], [26].

1.3 OBJECTIVE AND SCOPE

This thesis aims to investigate the role and effect of linear and non-linear damping in transient vibration of a vehicle traversing a bump using a SDOF and two DOF model. The primary objectives of the thesis are to:

(1) present numerical and analytical solutions for the response of a SDOF system with a versed-sine base displacement input;

(2) provide physical interpretation of the relationship between the peak response and certain vehicle parameters;

(3) discuss the damping mechanisms in a non-linear automotive damper, and the validity of linear and piece-wise linear damping models to represent an automotive damper;

(4) propose a switchable damper that gives better shock isolation than a conventional automotive damper.

This thesis is concerned with a SDOF and two DOF quarter car suspension model excited by a versed-sine shaped bump, comprising a linear or non-linear damper with a linear spring in parallel for shock isolation.

Chapter 2 presents the SDOF model, the governing equation and its solutions using numerical and analytical methods. The system responses are given by a non-dimensional form and linear damping is assumed.

In Chapter 3, the physical relationship between system responses and parameters is investigated by simplifying the analytical solutions. A two DOF quarter car model is also studied

to assess unsprung mass and tyre stiffness effects. The validity and limitation of simplified relationships derived in the SDOF system are discussed. Experimental work is carried out to find the practical relationship between the peak acceleration and suspension parameters. The theoretical relationship between the peak acceleration and the system parameters in the SDOF and two DOF systems is also validated for a bump of short duration.

In Chapter 4, a practical automotive damper is discussed in terms of its non-linear characteristics and the way in which a damping force generated is explained in relation to the structure and the fluid flow of hydraulic damper. A non-linear relationship between damping force and velocity is formulated by fitting a piece-wise linear damping model to experimental data.

Chapter 5 investigates the response of a system where the damping values are switched between two states: a piece-wise linear damper in the jounce and rebound direction and a switching damper where the damping coefficients are switched at the end of the bump. The two types of automotive damper are compared directly by numerical simulations of a SDOF system for shock isolation.

Finally, Chapter 6 summarises the main conclusions from this thesis and makes suggestions for future work.

1.4 CONTRIBUTIONS OF THESIS

The contributions of this thesis are as follows:

(1) An analytical solution for the response of a SDOF system with versed-sine base excited displacement input is derived;

(2) A physical interpretation of the relationship between the peak response of vertical acceleration and system parameters is provided when a vehicle is traversing a bump;

(3) The theoretical relationship between the peak acceleration and system parameters is validated by the numerical simulation of a two DOF quarter car model and an experimental measurement of vertical acceleration in a passenger car;

(4) One of the reasons for an asymmetric characteristic of an automotive damper in jounce and rebound directions is proposed in terms of shock isolation;

(5) A strategy of switching damping coefficients for reducing the shock response is proposed.

CHAPTER 2

SDOF SYSTEM WITH VERSED SINE BASE MOTION

2.1 INTRODUCTION

In order to analyse the ride comfort of a vehicle, the dynamic behaviour of the suspension system of a vehicle should be investigated. Real suspension systems are difficult to model and analyse in a simple manner due to non-linear components and irregular road conditions. However, a simplified and linearised suspension model such as a SDOF system with lumped mass, a linear spring, and a linear viscous damper, is able to offer physical insight and approximate relationships between physical quantities of interest. Therefore, in this chapter, a vehicle going over a single bump is analysed by using a SDOF system subject to a transient base input. In analysis involving transient vibration, it is more appropriate to study the response in the time domain than in the frequency domain. The peak response can then be determined from time histories of the responses.

In Section 2.2, a SDOF suspension model is reviewed, and base excitation is considered as a displacement input with a versed-sine shape. In order to solve the equation of motion, a numerical solution is presented in Section 2.3 using the Runge-Kutta method. In Section 2.4, an analytical solution for the response during and after the bump is presented using the Laplace transforms. In Section 2.5, the analytical solutions are normalised with respect to bump height and natural period. This paves the way for approximate analytical solutions to be derived in Chapter 3, from which greater physical insight can be gained.

2.2 EQUATION OF MOTION

A schematic of a base excited SDOF system is shown in Figure 2.1, where m, c, and k are the mass, linear viscous damping coefficient, and spring constant. The sprung mass is considered as a lumped mass and the spring and damper are assumed to be of negligible mass. The system is also assumed to move only in the vertical direction. The input displacement is denoted by $y(t)$ and the displacement response is denoted by $x(t)$. The equation of motion is given by

$$m\ddot{x} = c(\dot{y} - \dot{x}) + k(y - x) \tag{2.1}$$

where the time dependence of x and y is omitted for clarity. Substituting for $z = x - y$ where z is the relative displacement, equation (2.1) can be written as

$$m\ddot{z} + c\dot{z} + k\,z = -m\ddot{y} \tag{2.2}$$

Equation (2.2) can be expressed more conveniently in terms of modal parameters. Recalling that the damping ratio is given by $\zeta = c/c_c$, where $c_c = 2m\omega_n$ is the critical damping coefficient and ω_n is natural frequency of system, then equation (2.2) can be rewritten as

$$\ddot{z} + 2\zeta\omega_n\dot{z} + \omega_n^2 z = -\ddot{y} \tag{2.3}$$

Suppose the base input $y(t)$ is considered to be a versed-sine displacement, as shown in Figure 2.2, which is widely used as an input for transient vibration analysis [1]. The displacement,

velocity and acceleration input to the SDOF system traversing the bump are then given by

$$y = \frac{h_b}{2}\left[1 - \cos(\frac{2\pi}{t_p}t)\right] , \qquad 0 < t < t_p \qquad (2.4a)$$

$$\dot{y} = \frac{\pi h_b}{t_p}\sin(\frac{2\pi}{t_p}t) , \qquad 0 < t < t_p \qquad (2.4b)$$

$$\ddot{y} = \frac{h_b}{2}\left(\frac{2\pi}{t_p}\right)^2 \cos(\frac{2\pi}{t_p}t) , \qquad 0 < t < t_p \qquad (2.4c)$$

where h_b is the height of the bump and t_p is the period of time that the SDOF system takes to travel the length of the bump. The period of time t_p can be expressed as

$$t_p = \frac{l_b}{v} \qquad (2.5)$$

where, v is the longitudinal velocity of the SDOF system and l_b is the length of the bump. A unit height of bump is used in this dissertation for convenience of calculations. Setting $h_b = 1$ and the forcing frequency $\omega = 2\pi/t_p$, equation (2.3) and (2.4c) can be combined to give

$$\ddot{z} + 2\zeta\omega_n\dot{z} + \omega_n^2 z = -\frac{1}{2}\omega^2\cos(\omega t) , \qquad 0 < t < t_p \qquad (2.6)$$

$$\ddot{z} + 2\zeta\omega_n\dot{z} + \omega_n^2 z = 0 , \qquad t \geq t_p \qquad (2.7)$$

Second order ordinary differential equations such as equation (2.6) and (2.7) can be solved by numerical methods or analytical methods given initial conditions. In Section 2.3, a time domain solution is obtained using the fourth order Runge-Kutta method. In Section 2.4, the exact solution is presented using Laplace transforms with partial fractions.

2.3 NUMERICAL SOLUTION

The numerical solution of ordinary differential equations is an important technique in dynamics. Since many ordinary differential equations are not soluble analytically, numerical integration is often the only way to obtain a solution. Many different methods have been proposed and used to solve accurately various types of ordinary differential equations. However, there are a handful of methods known and used universally, for example Runge–Kutta, Adams–Bashforth–Moulton and Backward Differentiation Formulae methods [29]. All these methods discretise the differential equation to produce a difference equation. Differential equations contain information about the rate of change of a dependent variable with respect to some independent variable [29]. To solve the equation, these changes are integrated to obtain a final solution.

The classical 4^{th} order Runge-Kutta method is a good choice for a numerical method of solution because it is both fast and accurate. In this section, the fourth order Runge-kutta method is used to solve the equation of motion in the time domain. In the Runge-Kutta method, the second-order differential equation is first reduced to two first-order equations. Equation (2.6) can be written as

$$\ddot{z} = f(t) - 2\zeta\omega_n\dot{z} - \omega_n^2 z = F(z, \dot{z}, t) \tag{2.8}$$

where,

$$f(t) = -\frac{1}{2}\omega^2 \cos(\omega t) \tag{2.9}$$

By letting $\dot{z} = w$, this equation is reduced to the following two first-order equations

$$\begin{aligned} \dot{z} &= w \\ \dot{w} &= F(z, w, t) \end{aligned} \tag{2.10}$$

where $F(z, w, t)$ is a function of z, w, and t. The differential equation given in equation (2.6) is defined in MATLAB [27] by a function file which has, as an input, the time and variable parameters. The detailed algorithm is presented in Appendix A.

Figure 2.3 shows an example of the numerical solutions for the time response of the SDOF system excited at the base by a versed-sine bump of short and long durations (t_p) compared to natural period (t_n) of the system. The responses shown are the normalised displacement, velocity and acceleration of the system. Time t is also normalised by the time taken to traverse the bump t_p. When the duration of the bump excitation is short as shown in Figure 2.3 (a), the acceleration response of the system is very sudden and occurs whilst the vehicle is traversing the bump and the peak displacement occurs after the vehicle has traversed the bump. Even if the fourth order Runge-Kutta method can solve stiff differential equations [29], care should be taken in choosing the step size. As a general rule, the step size should be much smaller than t_p (bump duration). In this thesis, simulations were conducted using a time step of one tenth of the bump duration. From Figure 2.3 (b), for a long duration of bump, it can be seen that the displacement of the sprung mass is similar to the shape of the base input. The peak acceleration is much smaller than for a bump of short duration.

2.4 ANALYTICAL SOLUTION

The vibration of a viscously damped SDOF with versed-sine base motion can be considered as a transient vibration problem. Generally, the transient response of a system can be found using various methods such as the Fourier integral, convolution integral, impulse response method and Laplace transform [31]. The impulse response method is most commonly used whereby the momentum is assumed to be imparted to the mass instantaneously resulting in an infinite acceleration during the shock. However, since in this thesis it is the acceleration

response due to a transient displacement input that is of interest, the method is not applicable here.

The Laplace transform is a powerful tool to formulate exact solutions of some amenable ordinary differential equation and is the method chosen here. The Laplace transformation of equation (2.6) governing motion during the bump can be written as

$$\mathcal{L}\left[\ddot{z} + 2\zeta\omega_n\dot{z} + \omega_n^2 z\right] = \mathcal{L}\left[-\frac{1}{2}\omega^2\cos(\omega t)\right] \quad , \qquad 0 < t < t_p \tag{2.11}$$

where $\mathcal{L}$ denotes the Laplace transform. The transformed equation is given by

$$s^2 Z(s) - sz(0) - \dot{z}(0) + 2\zeta\omega_n s Z(s) - 2\zeta\omega_n z(0) + \omega_n^2 Z(s) = \frac{-\frac{1}{2}\omega^2 s}{s^2 + \omega^2} \tag{2.12}$$

where $Z(s)$ denotes the Laplace transform of the relative displacement, $z(t)$.

Rearranging equation (2.12) gives

$$Z(s) = \left(\frac{\dot{z}(0) + (s + 2\zeta\omega_n)z(0)}{s^2 + 2\zeta\omega_n s + \omega_n^2}\right) + \left(\frac{-\frac{1}{2}\omega^2 s}{s^2 + \omega^2}\right)\left(\frac{1}{s^2 + 2\zeta\omega_n s + \omega_n^2}\right) \tag{2.13}$$

The Laplace transform of the relative displacement, $Z(s)$ in equation (2.13) consists of two terms which have distinct physical meanings. The first term involves the initial conditions of the system, and the second term involves the input acceleration of the base during the period when the system is traversing the bump. Therefore, equation (2.13) can be written in the form

$$Z(s) = Z_1(s) + Z_2(s) \tag{2.14}$$

where,

$$Z_1(s) = \frac{\dot{z}(0) + (s + 2\zeta\omega_n)z(0)}{s^2 + 2\zeta\omega_n s + \omega_n^2} \tag{2.15}$$

represents the free vibration during the bump due to the initial conditions at the start of the bump and

$$Z_2(s) = \left(\frac{-\frac{1}{2}\omega^2 s}{s^2+\omega^2}\right)\left(\frac{1}{s^2+2\zeta\omega_n s+\omega_n^2}\right) \tag{2.16}$$

represents both free and forced vibration during the bump.

The force is removed at the end of the bump and the response is then described by equation (2.7). In this case, the Laplace transform of equation (2.7) gives the relative displacement $Z(s)$ which is

$$Z(s) = \frac{\dot{z}(t_p) + (s+2\zeta\omega_n)z(t_p)}{s^2+2\zeta\omega_n s+\omega_n^2} \tag{2.17}$$

where, $z(t_p)$ and $\dot{z}(t_p)$ are the relative displacement and velocity at the end of the bump.

The exact solution for the response of a SDOF system both during and after a versed-sine base motion can be found by the inverse Laplace transformation of $Z(s)$ using the table of Laplace transforms listed in Appendix B. Because the governing equations in the time periods $0 \leq t \leq t_p$ and $t > t_p$ are different, the solutions for the time periods should be considered separately.

2.4.1 During the bump ($0 \leq t \leq t_p$)

Assuming initial conditions of zero displacement and velocity at time $t = 0$, it follows that $Z_1(s) = 0$ in equation (2.15). Consequently, the relative displacement is simply the inverse Laplace transform of $Z_2(s)$ which is derived in Appendix B. Adding the base input to

the solution gives the following expression for the absolute displacement of the mass:

$$\begin{aligned} x(t) &= \left(\frac{-0.5\omega^2(\omega_n^2-\omega^2)}{(2\zeta\omega\omega_n)^2+(\omega_n^2-\omega^2)^2}\right) \\ &\left((\cos\omega t+\frac{2\zeta\omega\omega_n}{\omega_n^2-\omega^2}\sin\omega t)-e^{-\zeta\omega_n t}(\cos\omega_d t+\frac{\zeta\omega_n(\omega_n^2+\omega^2)}{(\omega_n^2-\omega^2)\omega_d}\sin\omega_d t)\right) \\ &+0.5(1-\cos\omega t) \end{aligned} \tag{2.18}$$

The velocity and acceleration of the mass are given by differentiating $x(t)$ to give respectively

$$\begin{aligned} \dot{x}(t) = &\left(\frac{0.5\omega^2(\omega_n^2-\omega^2)}{(2\zeta\omega\omega_n)^2+(\omega_n^2-\omega^2)^2}\right)\left(\omega(\sin\omega t-\frac{2\zeta\omega\omega_n}{\omega_n^2-\omega^2}\cos\omega t)\right. \\ &\left.-\left(1-\frac{(\omega_n^2+\omega^2)}{(\omega_n^2-\omega^2)}\zeta\omega_n\right)e^{-\zeta\omega_n t}\cos\omega_d t-\left(1+\frac{\zeta^2\omega_n^2(\omega_n^2+\omega^2)}{(\omega_n^2-\omega^2)\omega_d^2}\omega_d\right)e^{-\zeta\omega_n t}\sin\omega_d t\right) \\ &+0.5\omega\sin\omega t \end{aligned} \tag{2.19}$$

$$\begin{aligned} \ddot{x}(t) &= \left(\frac{0.5\omega^2(\omega_n^2-\omega^2)}{(2\zeta\omega\omega_n)^2+(\omega_n^2-\omega^2)^2}\right) \\ &\left(\omega^2(\cos\omega t+\frac{2\zeta\omega\omega_n}{\omega_n^2-\omega^2}\sin\omega t)+\left((\zeta\omega_n)^2-\frac{2\zeta^2\omega_n^2(\omega_n^2+\omega^2)}{(\omega_n^2-\omega^2)}-\omega_d^2\right)e^{-\zeta\omega_n t}\cos\omega_d t\right. \\ &\left.+\left(\frac{(\zeta\omega_n)^3(\omega_n^2+\omega^2)}{(\omega_n^2-\omega^2)\omega_d}+2\zeta\omega_n\omega_d-\frac{\zeta\omega_n^2\omega_d(\omega_n^2+\omega^2)}{(\omega_n^2-\omega^2)}\right)e^{-\zeta\omega_n t}\sin\omega_d t\right) \\ &+0.5\omega^2\cos\omega t \end{aligned} \tag{2.20}$$

2.4.2 After the bump ($t > t_p$)

After the bump the displacement $x(t)$ can be determined by solving equation (2.17) with known conditions at time t_p. The inverse Laplace transform of $Z(s)$ for $t > t_p$ in equation

(2.17) can be obtained using the table of Laplace transforms in Appendix B to give

$$x(t) = \left(z(t_p) \cos \omega_d (t - t_p) + \frac{\dot{z}(t_p) + \zeta \omega_n z(t_p)}{\omega_d} \sin \omega_d (t - t_p) \right) \tag{2.21}$$

where in general the initial conditions at $t = t_p$, $z(t_p)$ and $\dot{z}(t_p)$, are non zero. The absolute velocity $\dot{x}(t)$ and acceleration $\ddot{x}(t)$ can be obtained by differentiating equation (2.21).

Figure 2.4 shows the responses of the system excited by base motion of a bump of short and long duration compared to natural period (t_n). This exact solution is consistent with the numerical solution calculated using the Runge-Kutta method shown previously in Figure 2.3. Further comparisons are shown and discussed in Chapter 3.

The analytical solution, whilst cumbersome to obtain, can be exploited to gain insight into the effect of the damper on the peak acceleration response. In particular, approximate relations can be sought for the peak acceleration for bumps of short and long duration by the application of Taylor-series expansions. This is the subject of Chapter 3. Further non-dimensionalisation of the solution is first required.

2.5 NON-DIMENSIONALISATION

The analytical solutions presented in the previous section are too complicated to infer the effect of parameters on the peak response. Instead, it is desirable to establish approximate relationships. Normalising the fundamental variables with respect to typical values and constructing dimensionless parameters provides a measure of the relative importance of the various terms in the equations and highlights the dominant physical behaviour. It also facilitates parametric studies through the variation of fewer parameters in simulations.

The displacement, $x(t)$ can be normalised by h_b, the maximum height of the versed-sine

bump to give $x(t)/h_b$. The velocity and acceleration, $\dot{x}(t)$ and $\ddot{x}(t)$ can also be normalised to give $\dot{x}(t)/\omega_n h_b$ and $\ddot{x}(t)/\omega_n^2 h_b$. Using these dimensionless forms of the parameters, equations (2.18), (2.19), and (2.20) can be rewritten as

$$\begin{aligned}
\frac{x(t)}{h_b} &= \left(\frac{-\frac{1}{2}(\frac{\omega}{\omega_n})^2(1-(\frac{\omega}{\omega_n})^2)}{(2\zeta\frac{\omega}{\omega_n})^2+(1-(\frac{\omega}{\omega_n})^2)^2}\right) \\
&\quad \left(\left(\cos 2\pi\frac{t}{t_p}+\frac{2\zeta\frac{\omega}{\omega_n}}{1-(\frac{\omega}{\omega_n})^2}\sin 2\pi\frac{t}{t_p}\right)\right. \\
&\quad \left.-e^{-2\pi\zeta\frac{\omega_n}{\omega}\frac{t}{t_p}}\left(\cos 2\pi\sqrt{1-\zeta^2}\frac{\omega_n}{\omega}\frac{t}{t_p}+\frac{\zeta}{\sqrt{1-\zeta^2}}\frac{1+(\frac{\omega}{\omega_n})^2}{1-(\frac{\omega}{\omega_n})^2}\sin 2\pi\sqrt{1-\zeta^2}\frac{\omega_n}{\omega}\frac{t}{t_p}\right)\right) \\
&\quad +\frac{1}{2}\left(1-\cos 2\pi\frac{t}{t_p}\right), \qquad 0\le\frac{t}{t_p}\le 1
\end{aligned} \tag{2.22}$$

$$\begin{aligned}
\frac{\dot{x}(t)}{\omega_n h_b} &= \left(\frac{\frac{1}{2}(\frac{\omega}{\omega_n})^2(1-(\frac{\omega}{\omega_n})^2)}{(2\zeta\frac{\omega}{\omega_n})^2+(1-(\frac{\omega}{\omega_n})^2)^2}\right) \\
&\quad \left(\frac{\omega}{\omega_n}\left(\sin 2\pi\frac{t}{t_p}-\frac{2\zeta\frac{\omega}{\omega_n}}{1-(\frac{\omega}{\omega_n})^2}\cos 2\pi\frac{t}{t_p}\right)\right. \\
&\quad -\left(1-\frac{(1+(\frac{\omega}{\omega_n})^2)}{(1-(\frac{\omega}{\omega_n})^2)}\right)\zeta e^{-2\pi\zeta\frac{\omega_n}{\omega}\frac{t}{t_p}}\cos 2\pi\sqrt{1-\zeta^2}\frac{\omega_n}{\omega}\frac{t}{t_p} \\
&\quad \left.-\left(1+\frac{\zeta^2(1+(\frac{\omega}{\omega_n})^2)}{(1-\zeta^2)(1-(\frac{\omega}{\omega_n})^2)}\right)\sqrt{1-\zeta^2}e^{-2\pi\zeta\frac{\omega_n}{\omega}\frac{t}{t_p}}\sin 2\pi\sqrt{1-\zeta^2}\frac{\omega_n}{\omega}\frac{t}{t_p}\right) \\
&\quad +\frac{1}{2}\frac{\omega}{\omega_n}\sin 2\pi\frac{t}{t_p}, \qquad 0\le\frac{t}{t_p}\le 1
\end{aligned} \tag{2.23}$$

$$
\begin{aligned}
\frac{\ddot{x}(t)}{\omega_n^2 h_b} = & \left(\frac{\frac{1}{2}(\frac{\omega}{\omega_n})^2(1-(\frac{\omega}{\omega_n})^2)}{(2\zeta\frac{\omega}{\omega_n})^2+(1-(\frac{\omega}{\omega_n})^2)^2} \right) \\
& \left((\frac{\omega}{\omega_n})^2 \Big(\cos 2\pi\frac{t}{t_p} + \frac{2\zeta\frac{\omega}{\omega_n}}{1-(\frac{\omega}{\omega_n})^2} \sin 2\pi\frac{t}{t_p} \Big) \right. \\
& + \Big(2\zeta^2 - \frac{2\zeta^2(1+(\frac{\omega}{\omega_n})^2)}{(1-(\frac{\omega}{\omega_n})^2)} - 1 \Big) e^{-2\pi\zeta\frac{\omega_n}{\omega}\frac{t}{t_p}} \cos 2\pi\sqrt{1-\zeta^2}\frac{\omega_n}{\omega}\frac{t}{t_p} \\
& + \Big(\frac{\zeta^3}{\sqrt{1-\zeta^2}} \frac{(1+(\frac{\omega}{\omega_n})^2)}{(1-(\frac{\omega}{\omega_n})^2)} + 2\zeta(1-\zeta^2)^2 - \zeta(\sqrt{1-\zeta^2}) \frac{(1+(\frac{\omega}{\omega_n})^2)}{(1-(\frac{\omega}{\omega_n})^2)} \Big) \\
& \left. e^{-2\pi\zeta\frac{\omega_n}{\omega}\frac{t}{t_p}} \sin 2\pi\sqrt{1-\zeta^2}(\frac{\omega_n}{\omega}\frac{t}{t_p}) \right) \\
& + \frac{1}{2}(\frac{\omega}{\omega_n})^2 \cos 2\pi\frac{t}{t_p}, \qquad 0 \le \frac{t}{t_p} \le 1
\end{aligned} \tag{2.24}
$$

Equations (2.22), (2.23) and (2.24) are valid during the bump ($0 \le t/t_p \le 1$). The expressions for the responses for $t/t_p > 1$ can be normalised in a similar fashion.

However, equations (2.22), (2.23) and (2.24) are still too complicated to exhibit any simple relationships between the system parameters and responses. These equations may be simplified for the cases when $\omega/\omega_n \gg 1$ or $\omega/\omega_n \ll 1$ to provide physical insight into the system for "*short*" or "*long*" bump inputs. Therefore, each term of these equations can be expressed as a function of frequency ratio, $r = \omega/\omega_n$.

The closed form solutions can be rewritten for short and long bumps in terms of the frequency ratio. The acceleration response given by equation (2.24) can be rewritten simply as

$$
\frac{\ddot{x}(\tilde{t})}{\omega_n^2 h_b} = a(r)\left\{b(r)+c(r)+d(r)\right\}+e(r)\,, \quad 0 \le \tilde{t} \le 1 \tag{2.25}
$$

where, $\tilde{t}$ is a dimensionless form of time t/t_p,

$$a(r) = \frac{\frac{1}{2}r^2(1-r^2)}{(2\zeta r)^2+(1-r^2)^2} \tag{2.26}$$

$$b(r) = r^2\left(\cos 2\pi\tilde{t} + \frac{2\zeta r}{1-r^2}\sin 2\pi\tilde{t}\right) \tag{2.27}$$

$$c(r) = \left(2\zeta^2 - \frac{2\zeta^2(1+r^2)}{(1-r^2)} - 1\right)e^{-2\pi\zeta\frac{1}{r}\tilde{t}}\cos 2\pi\sqrt{1-\zeta^2}\frac{1}{r}\tilde{t} \tag{2.28}$$

$$d(r) = \left(\frac{\zeta^3}{\sqrt{1-\zeta^2}}\frac{(1+r^2)}{(1-r^2)} + 2\zeta(1-\zeta^2)^2 - \zeta(\sqrt{1-\zeta^2})\frac{(1+r^2)}{(1-r^2)}\right) e^{-2\pi\zeta\frac{1}{r}\tilde{t}}\sin 2\pi\sqrt{1-\zeta^2}\frac{1}{r}\tilde{t} \tag{2.29}$$

$$e(r) = \frac{1}{2}r^2\cos 2\pi\tilde{t} \tag{2.30}$$

In Chapter 3, a first order approximation will be sought for equation (2.25) to obtain the time response and hence the peak response when the bump can be considered to be of "short" ($r \gg 1$) or "long" ($r \ll 1$) duration.

2.6 CONCLUSION

A SDOF model subject to versed-sine base motion has been presented as a representative model for a vehicle traversing a bump. Numerical and analytical solutions have been obtained by the Runge-Kutta method and the Laplace transform respectively. It has been shown that the analytical and numerical solutions give the almost identical results.

Non-dimensional parameters were introduced to make more apparent the importance of individual terms and the physical attributes. In the next chapter, the relative importance of these terms is considered for short and long bumps.

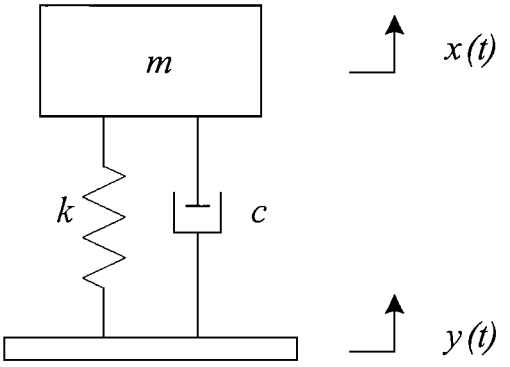

Figure 2.1: Schematic of a SDOF model with base motion

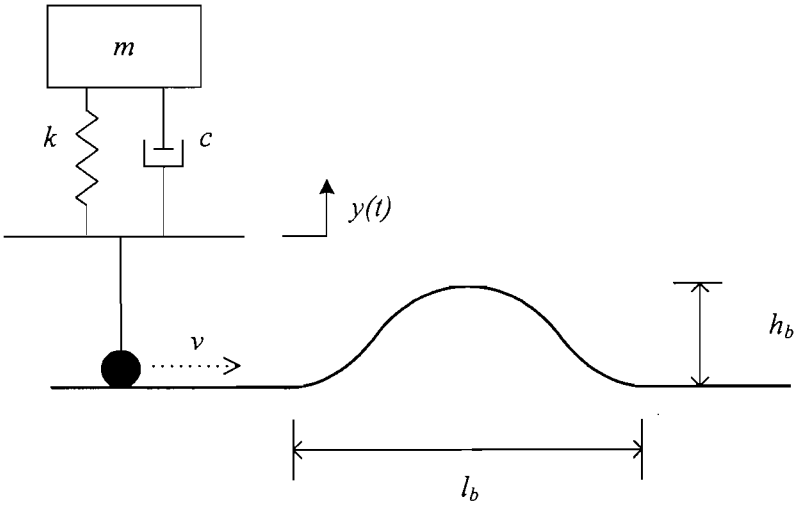

Figure 2.2: Versed-sine base motion for a SDOF system. v is the vehicle speed, h_b is the maximum height of the bump, and l_b is the length of the bump.

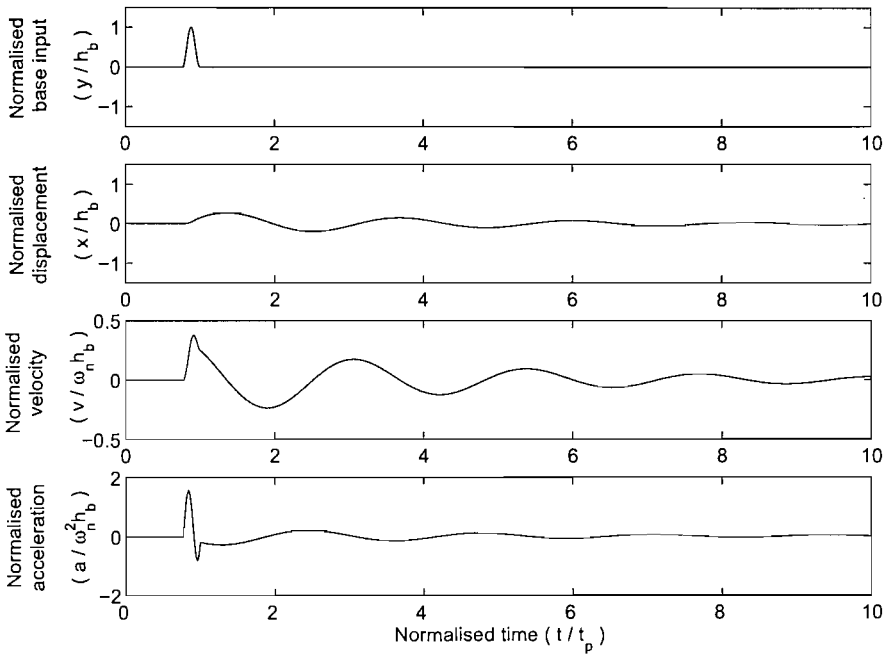

(a)

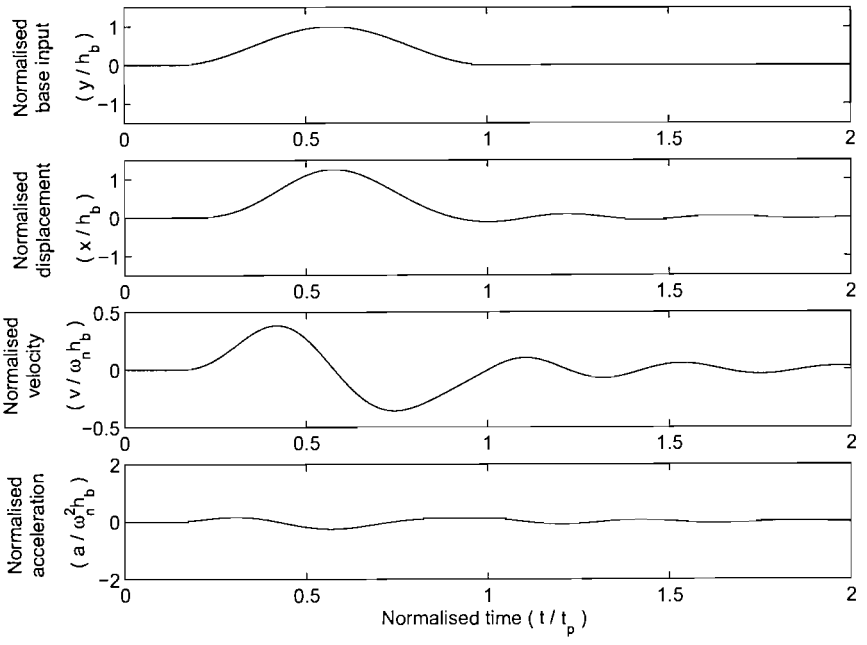

(b)

Figure 2.3: Numerical solutions for the responses of a SDOF vehicle model with damping ratio $\zeta = 0.3$ to a versed-sine displacement base input, where, x is displacement, v is velocity, a is acceleration, ω_n is natural frequency and h_b is the bump height. (a) short duration of bump ($t_n/t_p = 10$), (b) long duration of bump ($t_n/t_p = 0.5$).

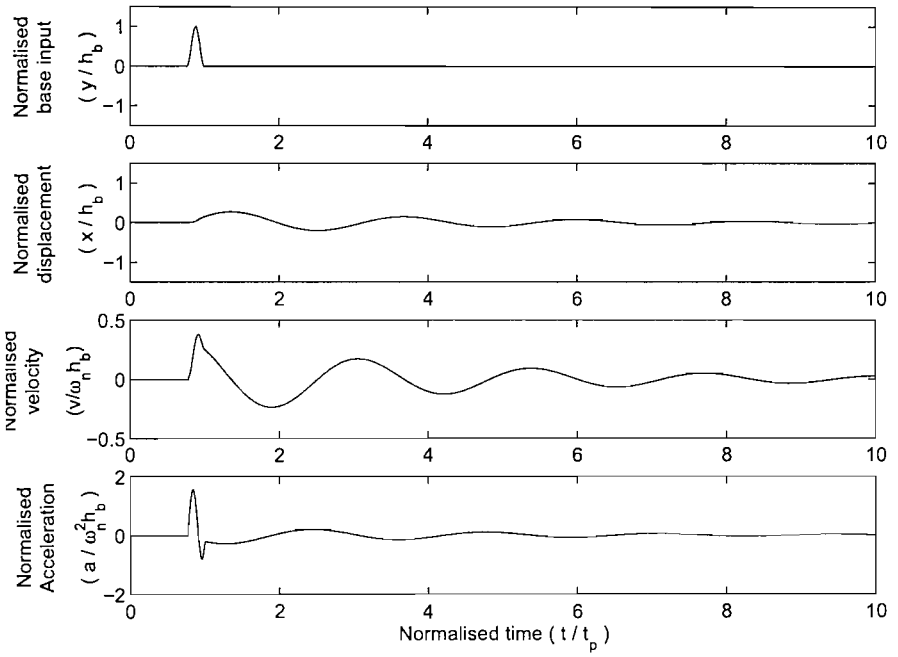

(a)

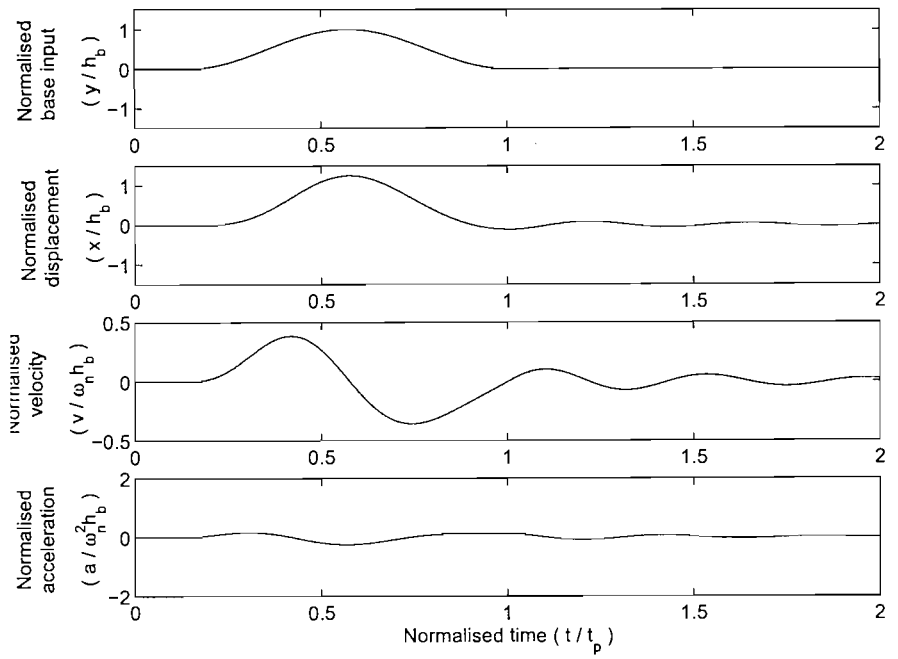

(b)

Figure 2.4: Exact solutions for the responses of a SDOF vehicle model with damping ratio $\zeta = 0.3$ to a versed-sine displacement base input, where, x is displacement, v is velocity, a is acceleration, ω_n is natural frequency and h_b is the bump height. (a) short duration of bump ($t_n/t_p = 10$), (b) long duration of bump ($t_n/t_p = 0.5$).

CHAPTER 3

DYNAMICS OF A VEHICLE TRAVERSING A BUMP

3.1 INTRODUCTION

In the previous chapter, a SDOF system excited at the base with a versed-sine displacement input was considered as a simple model of a vehicle traversing a bump. A closed form solution for the response was obtained using the Laplace transform. The main purpose of this chapter is to exploit this closed form solution to gain understanding of the role of the damper and the spring in governing the shock response of the vehicle and to determine the relationship between the peak acceleration and system parameters in a SDOF system. The validation and limitation of this relationship are also discussed in relation to a two DOF model and experimental results of a passenger car.

In the response of a system to transient excitation such as step or pulse, the maximum value of the response is often of considerable physical significance [1]. In practice, a mechanical system may be most affected by the maximum response due to a shock input rather than the mean square response of steady state vibration. Therefore, in this chapter, the peak values of displacement and acceleration responses are found using numerical and exact solutions.

The peak acceleration response can be approximated by using a Taylor series expansion of the exact solutions. Eliminating small terms for the case of short and long bumps yields simple approximate relationships for the response from which simple physical descriptions of the system can be justified.

To investigate the effect of the unsprung mass on the peak response, the response of

a two DOF quarter car model is calculated numerically. Approximate relationships between the peak acceleration and system parameters of a SDOF system are compared with a two DOF system. The peak acceleration response of the two DOF quarter car model is found using Matlab/Simulink for short and long bumps. Finally, experimental work carried out on a passenger car traversing a bump to evaluate the validity and limitations of the single and two DOF models is described.

3.2 SINGLE DEGREE OF FREEDOM MODEL

3.2.1 Maximum displacement

The maximum value of displacement, velocity and acceleration are widely used to express the shock response spectrum in many text books [1], [4], and [5]. This concept is useful in mechanical design in estimating the potential damage to a mechanical component due to shock. The shock response spectrum is a plot of the maximum peak response of a SDOF system as a function of the natural period of the system [4]. The shock response spectrum is a convenient method to determine the peak response for purposes such as assessing the rattle space or stress failure.

Figure 3.1 shows two different forms of shock response spectrum for a versed-sine input. Figure 3.1 (a) is a typical form of shock response spectrum for a versed-sine pulse plotted as a function of a pulse duration divided by a natural period (t_p/t_n) and Figure 3.1 (b) is a plot of the shock response as a function of excitation frequency divided by a natural frequency (ω/ω_n), which is the reciprocal of t_p/t_n. In both plots, the maximum displacement is plotted for various values of damping ratio, ζ. In the general case of steady-state forced harmonic vibration, even very small values of the damping have a great effect in limiting the displacement response at or near resonance. However, Figure 3.1 illustrates that if the excitation is a single pulse such as

a vehicle going over a bump, the effect of damping on the maximum response is modest. For a bump of long duration ($t_p/t_n \gg 1$ or $\omega/\omega_n \ll 1$), the curves approach a limiting value of $x(t)/h_b = 1$. Physically, this simply corresponds to a vehicle going over a bump very slowly, which results in a maximum displacement that is the same as the bump height.

Figure 3.2 (a) shows the maximum displacement $x(t)$ normalised by the bump height h_b as a function of ω/ω_n using the numerical and analytical methods outlined in Chapter 2. The curves of the numerical solution are well matched with those of the analytical solution. The curves are plotted for three damping ratios $\zeta = 0$, 0.3 and 0.9. The effect of damping on the peak displacement is small to modest depending on the duration of the bump. This is shown more clearly in Figure 3.2 (b) where, for a number of fixed bump durations, the peak displacement is plotted as a function of damping ratio. In each case, the peak displacement is normalised by the peak displacement when the damping ratio of the SDOF system ζ is *zero*.

For a short duration bump there is an optimal level of damping that minimises the peak displacement. For a very short bump, for example, $\omega/\omega_n = 10$, then $\zeta \simeq 0.25$ is optimal. For a long bump, the effect of damping is always beneficial but small.

3.2.2 Maximum acceleration

Most analyses of shock response to displacement disturbances consider displacement as the response quantity of interest. However, in this thesis, the analysis differs from much of the general shock and transient vibration literature in that the acceleration response is considered for a displacement input. It is useful to investigate the effects of system parameters on displacement and acceleration responses which can impact on ride discomfort. Therefore, both the displacement and acceleration response are considered in this analysis.

Figure 3.3 (a) shows the peak acceleration normalised by $\omega_n^2 h_b$ plotted as a function of

ω/ω_n using the numerical and analytical methods outlined in Chapter 2. The curves from the numerical solutions closely match those of the analytical solutions. The curves are plotted for three damping ratios $\zeta = 0, 0.3$ and 0.9. The characteristics of the curves may be explained by considering three regions, a lower, middle, and higher region of frequency ratio, ω/ω_n. Firstly, in the region of low ω/ω_n (a long bump), even if the damping ratio ζ varies widely from 0 to 0.9, the normalised peak acceleration $\ddot{x}_{peak}/\omega_n^2 h_b$, does not vary much as shown in Figure 3.3 (a). This means that the damping ratio, ζ is not a very important parameter on the peak acceleration. However, the peak acceleration is nearly proportional to the square of frequency which in turn depends on the speed of the vehicle going over the bump. Secondly, in the region of high frequency ratio ω/ω_n, the curves are affected by two parameters, the damping ratio ζ and the frequency ratio ω/ω_n, but increasing the damping ratio ζ consistently results in higher values of peak acceleration. The peak acceleration is also nearly proportional to the frequency ratio ω/ω_n and hence vehicle speed. Finally, the intermediate frequency region shows the peak acceleration to be significantly affected by changing the damping ratio ζ. In this region, the maximum acceleration $\ddot{x}_{peak}/\omega_n^2 h_b$, may occur during or after the period when the system is traversing the bump, depending on the frequency ratio ω/ω_n and the damping ratio ζ.

Figure 3.3 (b) shows the normalised peak acceleration as a function ζ for several bump durations. For $\omega/\omega_n = 10$, the peak acceleration increases in proportion to damping ratio ζ. However, for ω/ω_n less than 3, the peak acceleration is largely unaffected by damping ratio ζ. Therefore, from Figures 3.2 (b) and 3.3 (b), for very large values of ω/ω_n, it can be concluded that both the peak displacement and acceleration are dependent on the damping ratio ζ. However, the peak displacement is less sensitive to the damping ratio ζ than is the peak acceleration.

3.2.3 Role of spring and damper

To understand the function of the spring and damper in a shock isolation system, it is useful to consider individually the spring and damper forces transmitted to the mass. Figure 3.4 shows the force transmitted to the mass in a SDOF system for a short duration bump ($\omega/\omega_n = 10$) and a long bump ($\omega/\omega_n = 0.2$).

As shown in Figure 3.4 (a), when the bump duration, t_p is very small compared to the natural period t_n, the force transmitted to the mass is dominated by the damping force and less affected by the spring force. The time variation and scaling of the damping force is similar to the force transmitted to the mass. Conversely, when the bump duration, t_p is much larger than the natural period t_n, the force transmitted to the mass is dominated by the spring force as shown in Figure 3.4 (b). Therefore, the maximum acceleration of a SDOF system with versed-sine base motion can be expected to be largely independent of the damper for bumps of long duration.

Figure 3.5 shows the maximum forces from the spring and damper separately and the maximum transmitted force (which will in general occur at different instances in time). From Figure 3.5, it can be seen how the force transmitted to the mass is dominated by either the spring or damping force according to the size of the damping ratio. For $\omega/\omega_n = 10$, the maximum force transmitted to the mass is very dependent on the damping force as shown in Figure 3.5 (a); For $\omega/\omega_n = 0.2$, the maximum force transmitted to the mass is largely dependent on the spring force as shown in Figure 3.5 (b).

3.2.4 Approximation for acceleration shock response spectrum

(1) Short bump

The shock response spectrum can be used to estimate the potential damage to mechanical components or discomfort to a human occupant. An approximate shock response spectrum valid over a limited frequency range can be helpful in understanding the physical relationship between the responses and system parameters and to aid the design of mechanical components [6].

In Section 2.4, an analytical solution for the response of a SDOF system to a versed-sine displacement pulse input was found. In this section, the exact acceleration time response given by equation (2.24) is approximated in the case of short bump by eliminating some terms using Taylor series expansions. The result is a simple equation which can be used to explain the role of the spring and damper in shock isolation of road vehicles.

Equation (2.25), the concise form of equation (2.24), is

$$\frac{\ddot{x}(\tilde{t})}{\omega_n^2 h_b} = a(r)\left\{b(r) + c(r) + d(r)\right\} + e(r)\,, \quad 0 \le \tilde{t} \le 1 \tag{3.1}$$

where,

$$a(r) = \frac{\frac{1}{2}r^2(1-r^2)}{(2\zeta r)^2+(1-r^2)^2} \tag{3.2a}$$

$$b(r) = r^2\left(\cos 2\pi\tilde{t} + \frac{2\zeta r}{1-r^2}\sin 2\pi\tilde{t}\right) \tag{3.2b}$$

$$c(r) = \left(2\zeta^2 - \frac{2\zeta^2(1+r^2)}{(1-r^2)} - 1\right)e^{-2\pi\zeta\frac{1}{r}\tilde{t}}\cos 2\pi\sqrt{1-\zeta^2}\frac{1}{r}\tilde{t} \tag{3.2c}$$

$$d(r) = \left(\frac{\zeta^3}{\sqrt{1-\zeta^2}}\frac{(1+r^2)}{(1-r^2)} + 2\zeta(1-\zeta^2)^2 - \zeta(\sqrt{1-\zeta^2})\frac{(1+r^2)}{(1-r^2)}\right) e^{-2\pi\zeta\frac{1}{r}\tilde{t}}\sin 2\pi\sqrt{1-\zeta^2}\frac{1}{r}\tilde{t} \tag{3.2d}$$

$$e(r) = \frac{1}{2}r^2\cos 2\pi\tilde{t} \tag{3.2e}$$

and $\tilde{t}$ is dimensionless form of time t/t_p.

terms in equation (3.1)	$a(r)$	$b(r)$	$c(r)$	$d(r)$	$e(r)$
order of terms	r^0	r^2	r^{-1}	r^{-1}	r^2
smallest terms required	r^{-2}	r^0	r^0	r^0	r^0

Table 3.1: Order of terms $a(r)$ to $e(r)$ in equation (3.1) and terms required in the Taylor series expansion for $r \gg 1$.

Considering a short bump $r \gg 1$, the peak acceleration occurs during the bump regardless of the damping ratio. This can be observed from the simulation. Equation (2.24), the exact solution of acceleration during the bump, should therefore be used in the approximation. The process of approximation is detailed in Appendix C and briefly outlined here. It is assumed that the zeroth order or higher terms are kept and the terms smaller than the zeroth order are

neglected in equation (3.1). By inspection, the order of the terms $a(r)$ to $e(r)$ are as listed in table 3.1. In order to keep the zeroth order or higher terms, then when expanding $a(r)$ to $e(r)$, care should be taken over which terms are kept. Table 3.1 also lists the smallest terms to be retained in the expanded Taylor series. After applying the above to equation (3.1), the approximate expression for the normalised acceleration is given by

$$\frac{\ddot{x}(\tilde{t})}{\omega_n^2 h_b} = \zeta r \sin 2\pi\tilde{t} - \frac{1}{2}(1-4\zeta^2)(\cos 2\pi\tilde{t} - 1) + O(r^{-1}), \qquad 0 \leq \tilde{t} \leq 1 \tag{3.3}$$

where, $O(r^{-1})$ is all terms of order r^{-1} which can be neglected for $r \gg 1$. Therefore, equation (3.3) can be rewritten as

$$\frac{\ddot{x}(\tilde{t})}{\omega_n^2 h_b} = \frac{1}{2}\sqrt{4\zeta^2 r^2 + (1-4\zeta^2)^2}\sin(2\pi\tilde{t} + \alpha) + \frac{1}{2}(1-4\zeta^2) \tag{3.4}$$

where,

$$\tan\alpha = \frac{1-4\zeta^2}{2\zeta r} \tag{3.5}$$

Equation (3.4) consists simply of one time-dependent term and a constant term. In the special case when the damping ratio ζ is $\frac{1}{2}$, only the first term in equation (3.3) is non-zero, and the peak normalised acceleration during the bump is simply $\frac{1}{2}r$. In general, when $\zeta \neq \frac{1}{2}$, the peak acceleration depends on whether the maximum or minimum acceleration has the largest amplitude. If ζ is larger than $\frac{1}{2}$, the maximum acceleration has the largest amplitude, which is given by

$$\frac{\ddot{x}_{\max}}{\omega_n^2 h_b} = \frac{1}{2}\sqrt{4\zeta^2 r^2 + (1-4\zeta^2)^2} + \frac{1}{2}(1-4\zeta^2) \tag{3.6}$$

If ζ is smaller than $\frac{1}{2}$, then the minimum acceleration has the largest amplitude as

$$\frac{\ddot{x}_{\min}}{\omega_n^2 h_b} = -\frac{1}{2}\sqrt{4\zeta^2 r^2 + (1-4\zeta^2)^2} + \frac{1}{2}(1-4\zeta^2) \tag{3.7}$$

Figure 3.6 shows the exact solution from equation (2.24) and the approximation from equation (3.4) as a function of time for $r = 10$ and 2. Figure 3.6 (a) shows that the approximated curves are well matched to the exact solution for a large frequency ratio ($r = 10$), regardless of the damping ratio. In Figure 3.6 (b), the approximated curves are only a close match with the exact solution for high damping ratio.

If ζr is much larger than $\frac{1}{2}(1 - 4\zeta^2)$, then the peak acceleration reduces to

$$\left(\frac{\ddot{x}}{\omega_n^2 h_b}\right)_{\text{max / min}} \approx \zeta r \tag{3.8}$$

Figure 3.7 shows a comparison of the peak acceleration from the exact solution and the two approximations given by equation (3.3) and (3.8) as a function of ω/ω_n for four different damping ratios ζ. As can be seen in the figure, the approximate equations are in close agreement with the exact solution in the relatively short duration impulse. In particular, the two curves of approximate equations are well matched with that of the exact solution for a damping ratio $\zeta = 0.6$ since the peak acceleration is dominated by the first term of equation (3.3) when the damping ratio $\zeta \approx 0.5$, as shown in Figure 3.7 (c).

Considering the errors in the peak acceleration of the two approximate equations using Figure 3.7, the curve of the peak acceleration from equation (3.3) is valid over a much wider frequency range than that of equation (3.8) which assumes that ζr is much larger than $\frac{1}{2}(1 - 4\zeta^2)$.

(2) Long bump

Considering when the duration of the bump is long compared to the natural time period, it is possible to explain the relation between system properties and the peak acceleration by physical argument. Suppose the duration of the bump is very long (eg. because the speed of vehicle is very low), then the relative velocity between the base and mass on the SDOF system is low. It means that the effect of damping in the system cannot dominate due to very low velocity. Furthermore, in section 3.4, it was shown that the force transmitted to mass is mainly dominated by the spring force when the time to traverse the bump t_p, is much smaller than the natural period t_n. This also means that the damping has little effect on the vertical acceleration of vehicle when it is traversing the bump.

To find the relationship between the frequency ratio r and the peak acceleration response, the influence of damping on the system for a long bump can be considered to be negligible. Thus, using the frequency ratio r, equation (2.24) can be simplified by setting the damping ratio $\zeta = 0$.

$$\frac{\ddot{x}(\tilde{t})}{\omega_n^2 h_b} = \frac{1/2r^2}{1-r^2}\left(\cos 2\pi\tilde{t} - \cos 2\pi\frac{1}{r}\tilde{t}\right) \tag{3.9}$$

Equation (3.9) can be rewritten as

$$\frac{\ddot{x}(\tilde{t})}{\omega_n^2 h_b} \simeq \frac{-r^2}{1-r^2}\sin((1+\frac{1}{r})\pi\tilde{t})\sin((1-\frac{1}{r})\pi\tilde{t}) \tag{3.10}$$

For a frequency ratio r much smaller than 1, equation (3.10) can be simplified to

$$\frac{\ddot{x}(t)}{\omega_n^2 h_b} \simeq r^2 \sin^2(\pi\frac{t}{t_n}) \tag{3.11}$$

since the frequency ratio r can be expressed as t_n/t_p. The maximum of equation (3.11) occurs when $\sin(\pi t/t_n) = \pm 1$, thus, the peak acceleration for a long duration bump can be

approximated as

$$\left(\frac{\ddot{x}(t)}{\omega_n^2 h_b}\right)_{peak} \approx r^2 \tag{3.12}$$

From equation (3.12), it is clear that the peak acceleration is nearly proportional to the square of input frequency ω, which in turn is proportional to the vehicle speed. This asymptotic behaviour is plotted as a function of frequency ratio r in Figure 3.8. Also plotted is the peak acceleration from the exact solution. For frequency ratio r, much lower than 1, the asymptote line from equation (3.12), is fairly consistent with the line of the exact solution. For frequency ratio r, much higher than 1, the asymptote line from equation (3.8) is also consistent with the peak acceleration from the exact solution in high frequency region.

3.2.5 Effect of natural frequency on peak acceleration

An approximate acceleration response spectrum has been found for bumps of short and long durations. Expressions for the peak acceleration are normalised by $\omega_n^2 h_b$ where ω_n is the natural frequency of the system. This is a convenient choice when fixing the system and considering the effects of bump duration due to speed variation, for example. However, when considering the effect of changes to the natural frequency of the system, then the peak acceleration can be normalised by $\omega^2 h_b$ where ω is the input frequency related with the vehicle speed v as

$$\omega = \frac{2\pi v}{l_b} \tag{3.13}$$

where l_b is the length of the bump.

For a short duration bump, equation (3.8) can be rewritten as

$$\ddot{x}_{\text{max / min}} \approx \zeta\omega\omega_n h_b \tag{3.14}$$

Equation (3.14) can be normalised as dividing by $\omega^2 h_b$:

$$\left(\frac{\ddot{x}}{h_b\omega^2}\right)_{\text{max / min}} \approx \frac{\zeta}{r} \tag{3.15}$$

From equation (3.15), it can be seen that for a short duration bump, the peak acceleration is proportional to the natural frequency ω_n. Figure (3.9) shows the normalised peak accelerations plotted as a function of the frequency ratio r using the exact solution from equation (2.24). The natural frequency is varied whilst the input frequency ω and damping ratio ζ are kept constant. For example, in a practical vehicle, this would represent increasing the stiffness and at the same time increasing the damping coefficient c in proportional to $\sqrt{k}$. The peak normalised acceleration is plotted as the three different damping ratios. It can be seen that the normalised peak accelerations decrease in proportional to $1/r$ for short bumps.

3.3 DISCUSSION

In the previous sections, a SDOF system model of a vehicle traversing a bump has been analysed. Approximations to the response spectra have been derived from which the physical relations between the parameters and responses have been inferred. The general relationships between parameters and responses for a short duration bump ($r \gg 1$) can be listed as follows:

(1) The peak displacement is largely unaffected by damping;

(2) The peak acceleration is approximately proportional to the damping ratio and vehicle speed for the frequency ratio, $r \gg |1/2\zeta - 2\zeta|$;

(3) The peak acceleration is independent of the spring stiffness but is inversely proportional to the mass.

For a long bump ($r \ll 1$), the general relationships between parameters and responses are as follows:

(1) The displacement traces the shape of the bump and the peak is the same as the height of bump;

(2) Neither the peak displacement nor the peak acceleration are affected much by damping;

(3) The peak acceleration is approximately proportional to the square of frequency ratio r;

(4) The peak acceleration is independent of the spring stiffness.

3.4 TWO DEGREE OF FREEDOM QUARTER-CAR MODEL

3.4.1 Introduction

In the previous sections, the relationship between the peak acceleration and system parameters has been found using approximate shock spectra for short and long bumps in a SDOF system. However, a SDOF system may or may not express the behaviour of a vehicle suspension sufficiently. In particular, it may be difficult to neglect the effect of the unsprung mass (wheel, tyre and axle) in a vehicle suspension. The unsprung mass is generally about ten percent of the body mass for passenger cars. In certain frequency ranges, the effect of the unsprung mass has to be considered in the peak response. Therefore, the relationship between the peak acceleration and system parameters is investigated numerically in this section using a two DOF quarter car model.

The peak acceleration of a two DOF system is found for a bump of short duration using simulations from Matlab/Simulink. This enables the validity of a SDOF model to be assessed.

3.4.2 Free vibration of the two DOF model

Figure (3.10) shows the general configuration of a quarter car modelled as a two DOF system. This consists of a sprung mass supported on a suspension system which has stiffness and damping characteristics. The suspension system is connected to the unsprung mass of the tyre and axle. The tyre stiffness can be expressed as an undamped linear spring.

The free vibration of a two DOF model can be analysed by applying Newton's second law of motion to each mass in turn [3]. The displacement response of the sprung mass and unsprung masses are denoted by x_s and x_u respectively. Therefore, the equation of motion for

the sprung mass m_s can be expressed as

$$m_s\ddot{x}_s + c_s(\dot{x}_s - \dot{x}_u) + k_s(x_s - x_u) = 0 \tag{3.16}$$

and the equation of motion for the unsprung mass m_u is

$$m_u\ddot{x}_u + c_s(\dot{x}_u - \dot{x}_s) + (k_s + k_u)x_u - k_s x_s = 0 \tag{3.17}$$

These equations can be rewritten in matrix form as

$$\begin{bmatrix} m_s & 0 \\ 0 & m_u \end{bmatrix} \begin{Bmatrix} \ddot{x}_s \\ \ddot{x}_u \end{Bmatrix} + \begin{bmatrix} c_s & -c_s \\ -c_s & c_s \end{bmatrix} \begin{Bmatrix} \dot{x}_s \\ \dot{x}_u \end{Bmatrix} + \begin{bmatrix} k_s & -k_s \\ -k_s & k_s + k_u \end{bmatrix} \begin{Bmatrix} x_s \\ x_u \end{Bmatrix} = \begin{bmatrix} 0 \\ 0 \end{bmatrix} \tag{3.18}$$

It can be seen from equation (3.18) that the responses of the sprung mass and unsprung mass are coupled via the spring and damper.

Modal parameters of the two DOF model can be used to normalise the peak acceleration and compare to that of the SDOF model. Such a two DOF system has two resonance frequencies which for the quarter car model are usually termed the bounce mode and the wheel hop mode. To determine an approximate expression for the undamped natural frequency of the bounce mode, it is convenient to use the effective stiffness of the suspension and tyre springs in series as shown in Figure 3.12 (a). Therefore, the undamped resonance frequency of the bounce mode, ω_{n1} and its damping ratio ζ_s can be approximated as [3]

$$\omega_{n1} \simeq \sqrt{\frac{k_s k_u}{(k_s + k_u)m_s}} \tag{3.19}$$

$$\zeta_s \simeq \frac{c_s}{2\sqrt{m_s k_s}} \tag{3.20}$$

The unsprung mass is generally substantially less than that of the vehicle body, so an approximate wheel hop mode may be performed by considering the body to fixed as shown in Figure 3.12 (b) [34]. Hence, the undamped natural frequency of the wheel hop mode, ω_{n2} and its damping ratio ζ_w can be expressed as

$$\omega_{n2} \simeq \sqrt{\frac{k_s + k_u}{m_u}} \tag{3.21}$$

$$\zeta_w \simeq \frac{c_s}{2\sqrt{(k_s + k_u)m_u}} \tag{3.22}$$

Using these modal parameters of the two DOF system, the peak acceleration can be normalised and compared with that of the SDOF system in next section.

3.4.3 Two DOF model with a displacement input

When the two DOF model is excited by a displacement input, the equation of motion can be expressed as

$$\begin{bmatrix} m_s & 0 \\ 0 & m_u \end{bmatrix} \begin{Bmatrix} \ddot{x}_s \\ \ddot{x}_u \end{Bmatrix} + \begin{bmatrix} c_s & -c_s \\ -c_s & c_s \end{bmatrix} \begin{Bmatrix} \dot{x}_s \\ \dot{x}_u \end{Bmatrix} + \begin{bmatrix} k_s & -k_s \\ -k_s & k_s + k_u \end{bmatrix} \begin{Bmatrix} x_s \\ x_u \end{Bmatrix} = \begin{bmatrix} 0 \\ k_u \end{bmatrix} y \tag{3.23}$$

To solve equation (3.23) numerically, this two DOF system can be modelled and simulated using the Matlab/Simulink. Figure 3.13 shows the Simulink block diagram model of the two DOF system. The sprung mass in Figure 3.13 is subject to the spring and damping forces, which can be used to determine the acceleration of the sprung mass. This acceleration is then integrated once to find the velocity and again to find the displacement. For the unsprung mass, the input force arises from displacement input multiplied by tyre stiffness. The coupled spring

and damping force are transmitted to the unsprung mass. The responses of the unsprung mass can be found by the same procedure as for the sprung mass.

3.4.4 Acceleration shock response spectrum for two DOF model

In this section, the peak acceleration response of a two DOF quarter car system subject to a versed-sine base input is found using the Runge-Kutta method in Matlab/Simulink. The acceleration shock response spectrum of the two DOF model is compared with that of the SDOF system as shown in Figures 3.14 (a) and (b). The damping ratio of the bounce mode of the two DOF system is set to be equal to the mode of the SDOF system. Two values of ζ_s are 0.2 and 0.4. The peak acceleration of the SDOF model is normalised by the bump height and the square of the natural frequency whilst the peak acceleration of the two DOF model is normalised by the bump height and the square of the natural frequency of the bounce mode. It can be seen in Figure 3.14 that the peak acceleration of the two DOF model reaches a maximum at a frequency ratio of about 12. This maximum is caused by the wheel hop mode which occurs at a frequency ratio of about 12.

For a frequency ratio $r < 3$, the peak acceleration of the two DOF model is in good agreement with the SDOF model as shown in Figures 3.14 (a) and (b). This means that the peak acceleration is proportional to the square of the frequency ratio r for long bumps, the same relationship as for the SDOF model as discussed in the previous section. However, for $r > 3$, the amplitude of the peak acceleration of the two DOF model is different from that of the SDOF model as shown in Figure 3.14 (a). In particular, for $r > 10$, the peak acceleration of the two DOF system decreases as the frequency ratio r increases whilst that of the SDOF increases steadily. This means that the relationship between the peak acceleration

and the frequency ratio in the SDOF system cannot be extended to the two DOF system. For $3 < r < 10$ and $\zeta_s = 0.2$ even though the amplitude of the peak acceleration of the SDOF system is different to that of the two DOF system, the peak acceleration of the two DOF system is still approximately proportional to the frequency ratio r. For $\zeta_s = 0.4$, the amplitude of the peak acceleration of the two DOF model is the same as that of the SDOF model. However, the frequency range where there is a proportional relationship between the peak acceleration and the frequency ratio is more narrow as shown in Figure 3.14 (b).

For short and long duration bumps, the approximate relationship between the peak acceleration and system parameters in a SDOF system as discussed in previous section can be adopted in the lower frequency range of a two DOF quarter car system. In particular, for a short duration bump such that the frequency ratio is in the range $3 < r < 10$, the peak acceleration is approximately proportional to the frequency ratio and the damping ratio. However, for a very short bump, the peak acceleration of the two DOF system is reduced unlike that of the SDOF model. This is due to the two-stage isolation affected by the unsprung mass. For the two-stage isolation, the force transmitted to the base of the suspension spring and damper combination is less because some force is taken up in accelerating the unsprung mass as shown in Figure 3.11.

3.5 EXPERIMENTAL WORK

3.5.1 Aim of experiment

This section presents experimental work to investigate the practical relationship between the vehicle speed and the peak acceleration of a passenger car for short duration bumps and

to validate qualitatively the relationship between the peak acceleration and the frequency ratio derived from the SDOF and two DOF models. The limitations of these models is also discussed for short duration bumps.

3.5.2 Procedure

An experiment was conducted that involved the measurement of the acceleration of a vehicle body and suspension at various vehicle speeds. Figure 3.15 (a) shows the experimental set up for a passenger car traversing a bump. In this experiment, the vehicle speed was chosen to be large enough such that the duration of the bump was short compared with the natural period of the vehicle body, so that the effect of the bump shape could be neglected. To eliminate the effect of the vehicle roll motion, two speed bumps were so that the nearside and offside tyres traversed the bumps simultaneously.

Figure 3.16 shows typical front and rear pitch modes of a passenger car. If the length of a bump is much shorter than the wheel base of a vehicle, then the transient vibration after each wheel has traversed the bump may resemble that of a SDOF system. For example, when the front tyres traverse the bump, the pitching mode about the rear axle is not excited significantly. In the same way, when the rear tyres traverse bumps, the excitation is near nodal point of the other mode. Using this physical phenomenon, the vertical acceleration should be measured on the vehicle body and axle near the wheel centre. The accelerometers were attached near the upper body mounts of the nearside front and rear shock absorber and axle in the vehicle as shown in Figure 3.17.

The vertical acceleration was measured using Bruel & Kjaer Piezoelectric accelerometers (type 4384) and charge amplifiers as shown in Figure 3.18 (a). Five channels of data were

captured simultaneously. Two of those channels were from the front upper body mount of the shock absorber and the front axle. Another two channels were from the rear upper body mount of the shock absorber and the rear axle. Finally, the fifth channel was used for the speedometer. The data acquisition system was designed by the Vehicle Noise and Vibration Group of ISVR Consulting in the University of Southampton using commercial data acquisition cards. The data was captured using a 1 KHz the sampling frequency and was filtered by a low pass filter with a corner frequency of 50 Hz to observe the frequencies for rigid body motion. The time histories of measured data were captured for various vehicle speeds.

The vehicle speed was measured by a pulse type speedometer as shown in Figure 3.18 (b) which can be calibrated by the number of pulses per one meter and data recording time in data acquisition software. For example, if 55 pulses occur in one meter, the distance of one pulse is 1/55 (0.0182) meter. Therefore, the velocity of the vehicle can be calculated using the number of pulses and the time taken to traverse the bump. A complete list of the experiment used can be found in Appendix D.

Commercially available speed bumps were used in this experiment. The bump profile is a trapezoidal shape with a length of 0.45m and height of 0.06m as shown in Figure 3.15 (b). The vehicle was carefully driven in the 2^{nd} gear (automatic transmission) in order to maintain constant speed. The speed range used was from 4 km/hr to 30 km/hr with an increment of about 2-3 km/hr.

3.5.3 Time response of vehicle

Typical time history data for the measured acceleration of the practical vehicle body and suspension are presented in figure 3.19. The duration of the travel over the bumps was 0.19

seconds and the instant at which each wheel encounters the bump is denoted by X and Y. After each wheel goes over the bump, the body responds primarily at a low frequency corresponding to each of the pitch modes, but also at a higher frequency corresponding to the wheel hop mode. This is more apparent at the front of the vehicle than the rear which is indicative of more significant coupling between the wheel and body. This is confirmed by the fact that the wheel hop mode of the front suspension occurs at a lower frequency than that of the rear suspension. The wheel hop frequencies of the front and rear suspensions were found to be approximately 11Hz (front) and 15 Hz (rear) from the Fourier transform of the data and also counting the periods in the time history.

It is difficult to measure the pitch natural frequency accurately by Fourier transform due to frequency resolution. However, it can be deduced approximately from the time separation of the first two positive maximum peaks of low frequency in the time history after the bumps have been traversed. Therefore, using the first two positive peaks in acceleration after the bump has been traversed in Figure 3.19 (a) and (b), the front and rear pitch natural frequencies were found to be approximately

$$(\omega_{n1})_f = 2\pi\,(1.4) \text{ rad/sec} \tag{3.24a}$$

$$(\omega_{n1})_r = 2\pi\,(1.7) \text{ rad/sec} \tag{3.24b}$$

where, $(\omega_{n1})_f$ is the front pitch natural frequency and $(\omega_{n1})_r$ is the rear pitch natural frequency. Generally, the pitch natural frequency is from about 1 Hz up to 3 Hz and the wheel hop natural frequency is in the range of 8 to 15 Hz for most passenger cars [42].

3.5.4 Acceleration shock Response Spectra

In this section, the peak acceleration response can be found from the measurement of acceleration responses of the practical vehicle body and suspension and qualitatively compared with the numerical results from the two DOF quarter car model.

Figures 3.20 (a) and (b) show the normalised peak acceleration responses plotted as a function of $(\omega/\omega_{n1})_f$ and $(\omega/\omega_{n1})_r$ from the experimental results and numerical simulation. The peak acceleration of the numerical model is normalised by the bump height and the square of the pitch mode natural frequency ($h_b\omega_{n1}^2$), using equation (3.19). Similarly, the front and rear body of the peak acceleration in experimental results can be normalised by $h_b\,(\omega_{n1})_f$ and $h_b\,(\omega_{n1})_r$ using equations (3.24a) and (3.24b).

To compare qualitatively the peak acceleration between the experiment and the two DOF system, the damping ratio of the pitch modes has been estimated as an damping ratio of the bounce mode of the two DOF system in order to achieve a good fit. For the front suspension, when the damping ratio of the two DOF system is approximately 0.33, the peak acceleration from the experimental results compare well to that of the two DOF system. For rear suspension, the damping ratio is approximately 0.3.

The peak acceleration response of the quarter car model is consistent with the experimental results in limited frequency ranges (front: $4 < r < 6$, rear: $4 < r < 9$) as shown in Figures 3.20 (a) and (b). This means that the proportional relationship between the peak acceleration and the frequency ratio in SDOF and two DOF systems appears to hold in practice. Beyond these frequency regions, this proportional relationship may not be valid due to the effects of other structural modes of vibration.

3.6 CONCLUSION

This chapter has investigated the physical parameters which affect the vibration responses of a vehicle traversing a bump. It has been modelled as a SDOF system and a two DOF system and some experimental work has also been conducted on a vehicle.

An approximation for the transient peak acceleration response in a SDOF system has been found in a simple form using the closed form solution to the equation of motion. The influence of physical parameters such as the damping ratio ζ and the frequency ratio r to the system were analysed. These approximate equations can be used to explain the role of the damper and the physical relationship between the system parameters and peak acceleration response. For a short duration bump, the peak acceleration occurs whilst the bump is being traversed and is influenced by damping and the duration of bump. The approximate acceleration shock spectrum shows that the peak acceleration is proportional to the frequency ratio r and damping ratio ζ. For a long duration bump, the peak acceleration is proportional to the square of the frequency ratio r, but it is not influenced greatly by the damping.

The two DOF quarter car model has been numerically simulated in Matlab/Simulink and compared with the SDOF system to investigate the effect of the unsprung mass on the peak acceleration. The approximate relationship between the peak acceleration and system parameters in the SDOF system also holds for the two DOF system for long bumps. However, for a short duration bump, the approximate relationship determined for the SDOF system is valid in a relatively narrow frequency region ($3 < r < 10$). When the frequency ratio is much higher than 10, the peak acceleration response of the two DOF system is very different to that of the SDOF system due to the effect of the unsprung mass.

Some experimental work has been carried out for a short duration bump to investigate

the practical relationship between the peak acceleration and system parameters in a passenger car and to validate the approximate equations from the SDOF and two DOF systems. From the measurement results, a damping ratio of the bounce mode of the two DOF system has been proposed as an estimate of the practical damping ratio of the pitch mode of a passenger car. Using the damping ratio of the bounce mode of the two DOF system, the peak accelerations of the two DOF system and practical measured data have been compared for the validation and assessment of the limitation of the models. The peak acceleration from the measurement of the sprung mass is proportional to the frequency ratio and the damping ratio. This means that the approximate relationship between the peak acceleration and the system parameters derived from a SDOF system is valid only in a limited speed of a practical vehicle.

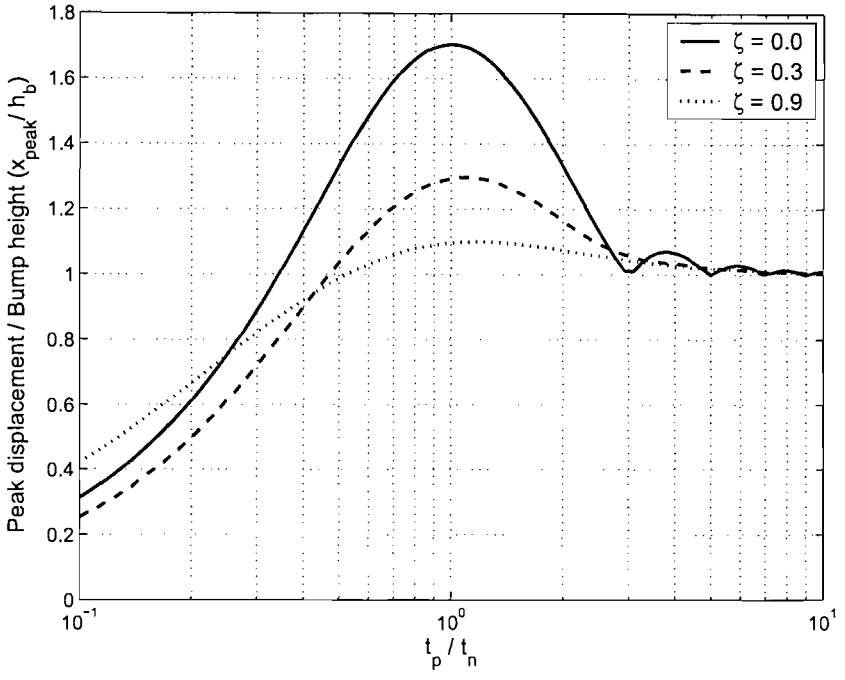

(a)

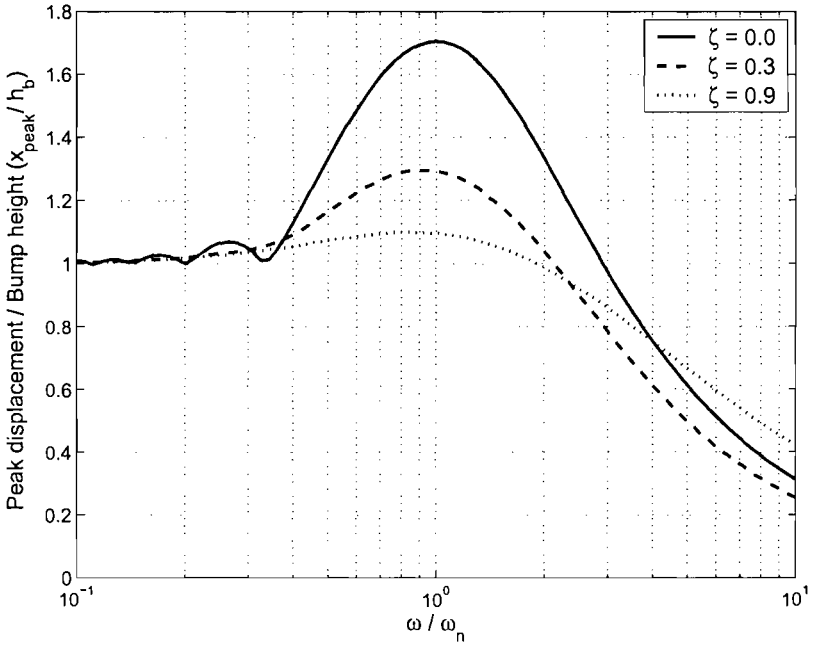

(b)

Figure 3.1: Dimensionless representation of maximum displacement for viscously damped SDOF system with versed-sine input. (a) shock response spectra for versed-sine input as a function of t_p/t_n, (b) shock response spectra for versed-sine input as a function of ω/ω_n .

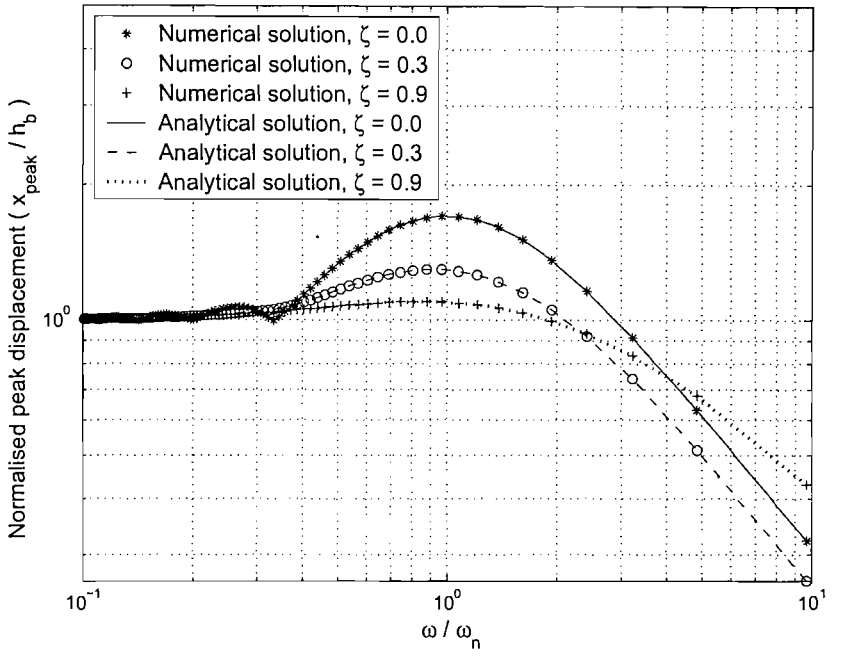

(a)

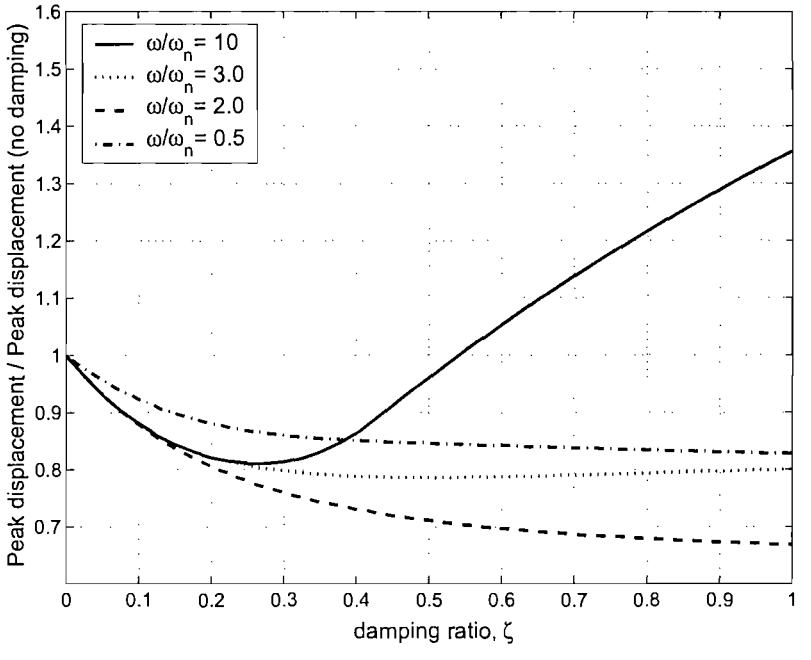

(b)

Figure 3.2: Normalised peak displacement response as a function of frequency ratio ω/ω_n and damping ratio ζ. (a) comparison of numerical and analytical solutions for the peak displacement spectra, (b) the peak displacement response as a function of damping ratio ζ for various bump durations.

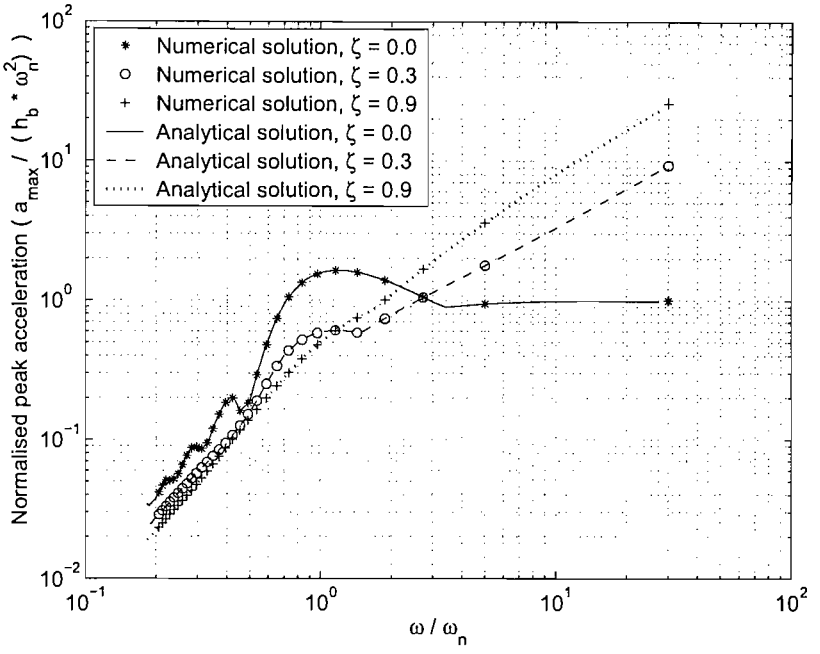

(a)

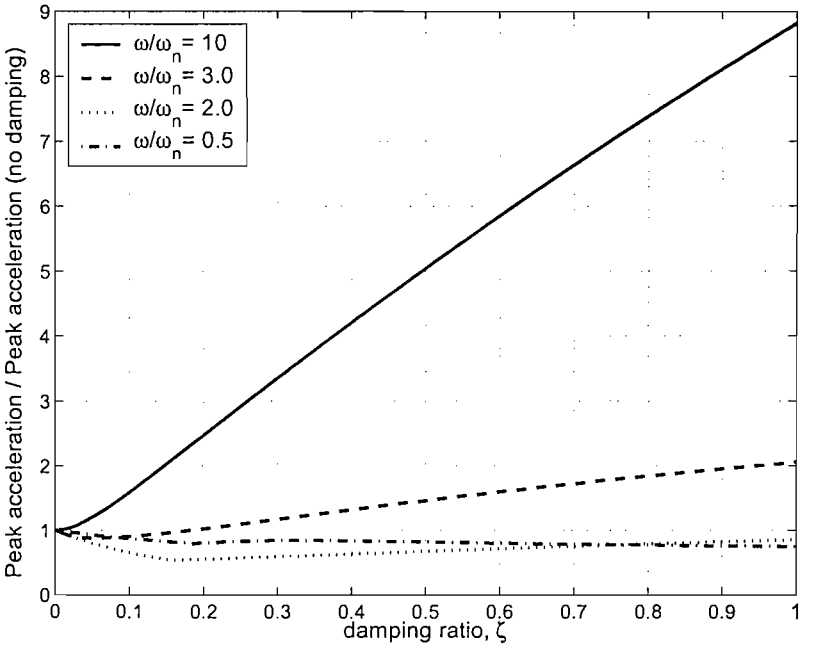

(b)

Figure 3.3: Normalised peak acceleration response as a function of frequency ratio ω/ω_n and damping ratio ζ. (a) comparison of numerical and analytical solutions for the peak acceleration spectra, (b) the peak acceleration response as a function of damping ratio ζ for various bump durations.

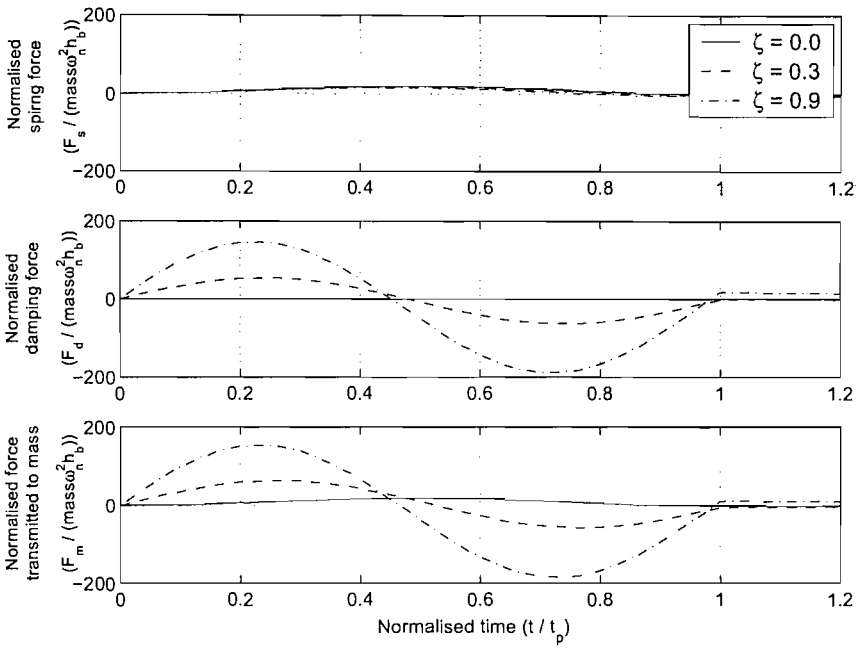

(a)

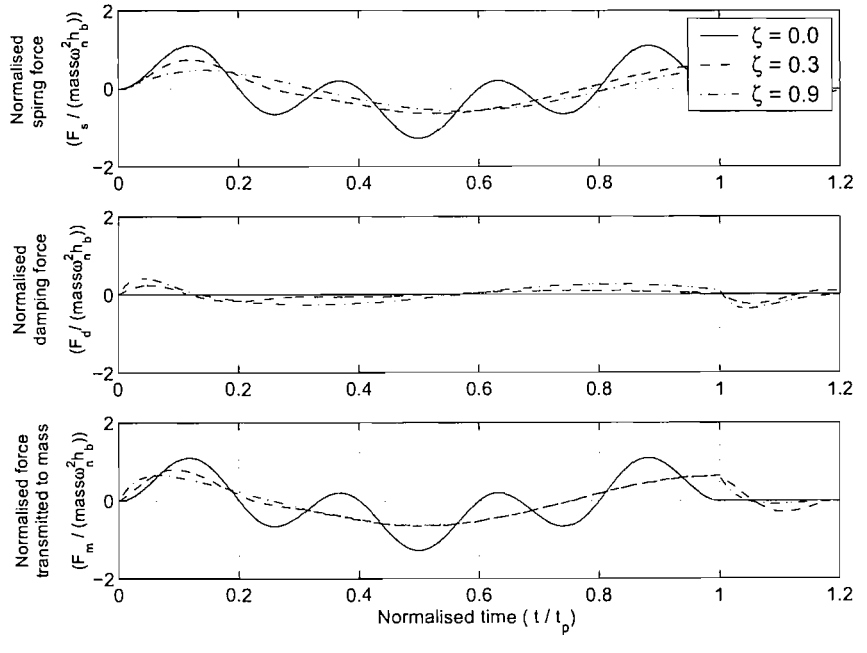

(b)

Figure 3.4: Comparison of spring force, damping force and force transmitted to the mass for a SDOF system with versed-sine base motion, corresponding to damping ratio 0.0, 0.3, and 0.9 (a) time responses for $\omega/\omega_n = 10$, (b) time responses for $\omega/\omega_n = 0.2$.

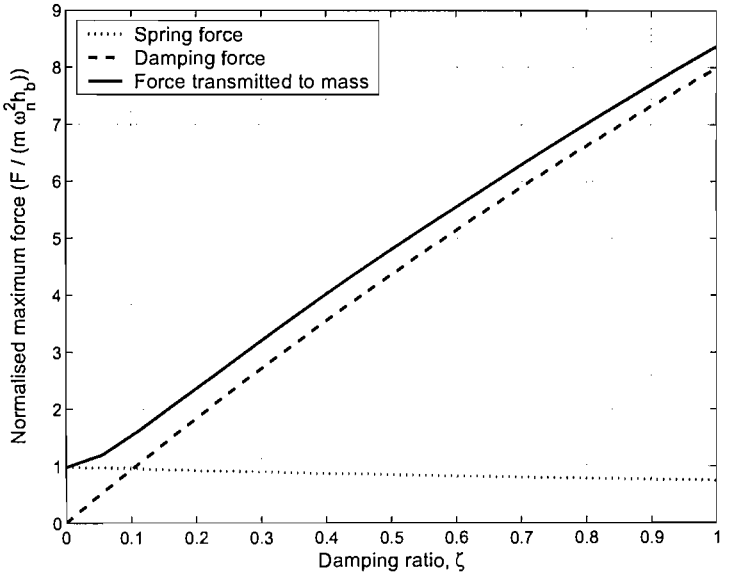

(a)

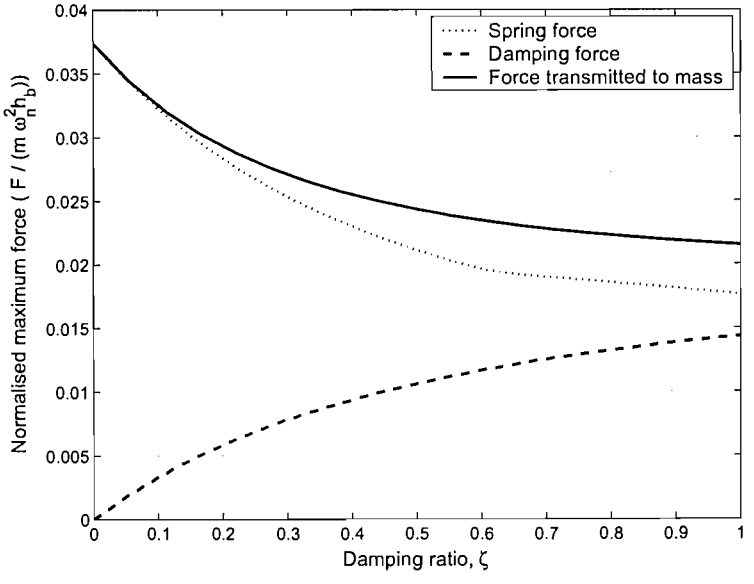

(b)

Figure 3.5: Maximum spring or damping force and the force transmitted to the mass for a SDOF system with versed sine base motion (a) $\omega/\omega_n = 10$, (b) $\omega/\omega_n = 0.2$.

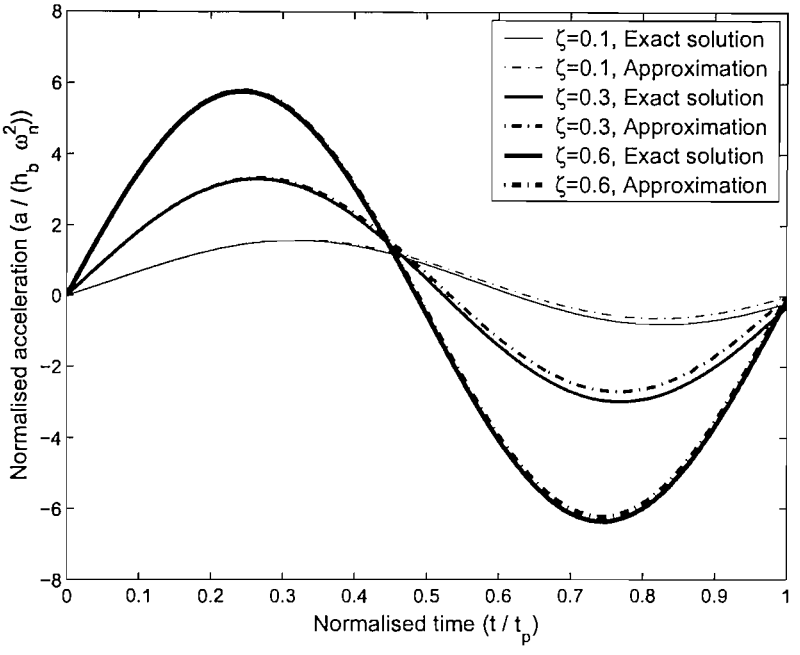

(a)

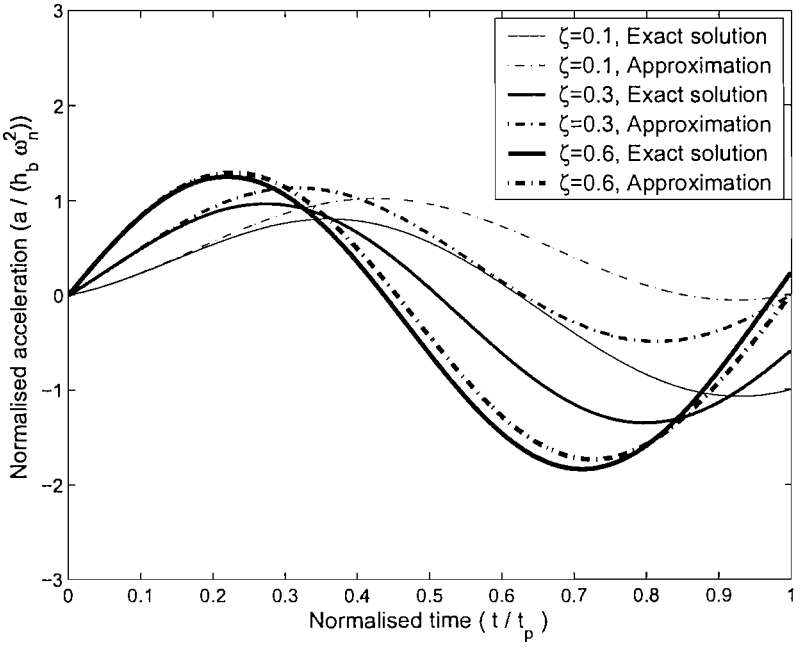

(b)

Figure 3.6: The comparison of exact solved equation (2.24) and approximated equation (3.4) as a function of normalised time, corresponding to damping ratio 0.1, 0.3, and 0.6. (a) time response at $\omega/\omega_n = 10$ (b) time response at $\omega/\omega_n = 2$.

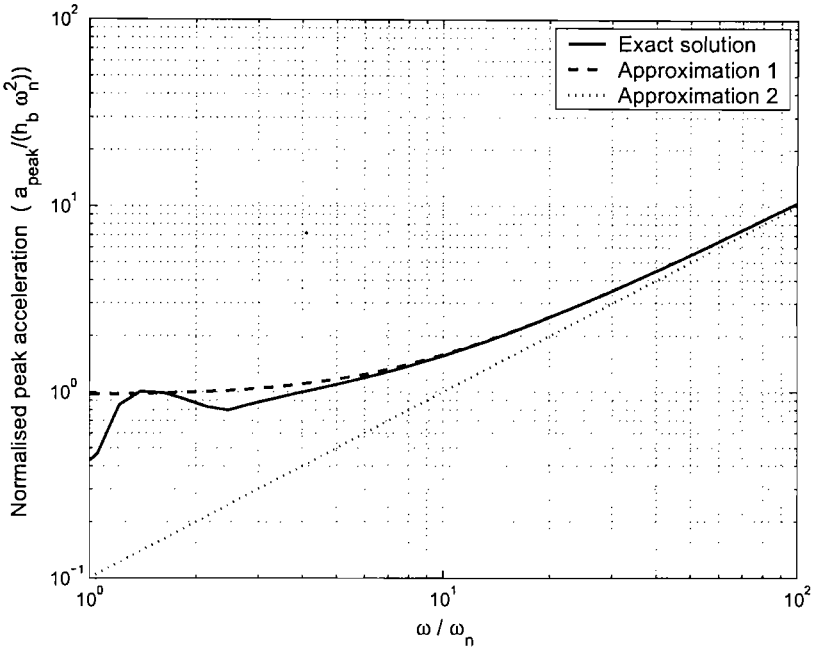

(a)

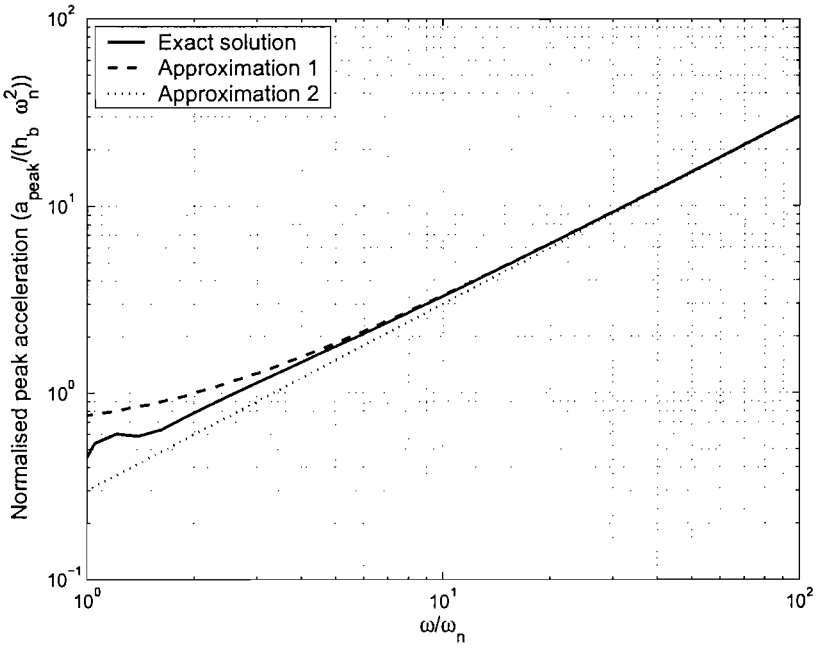

(b)

Figure 3.7: The comparison of the peak acceleration from the exact equation (2.24) and approximate equations as a function of ω/ω_n. Approximation 1- from equation (3.4). Approximation 2 - from equation (3.8). (a) damping ratio $\zeta = 0.1$, (b) damping ratio $\zeta = 0.3$.

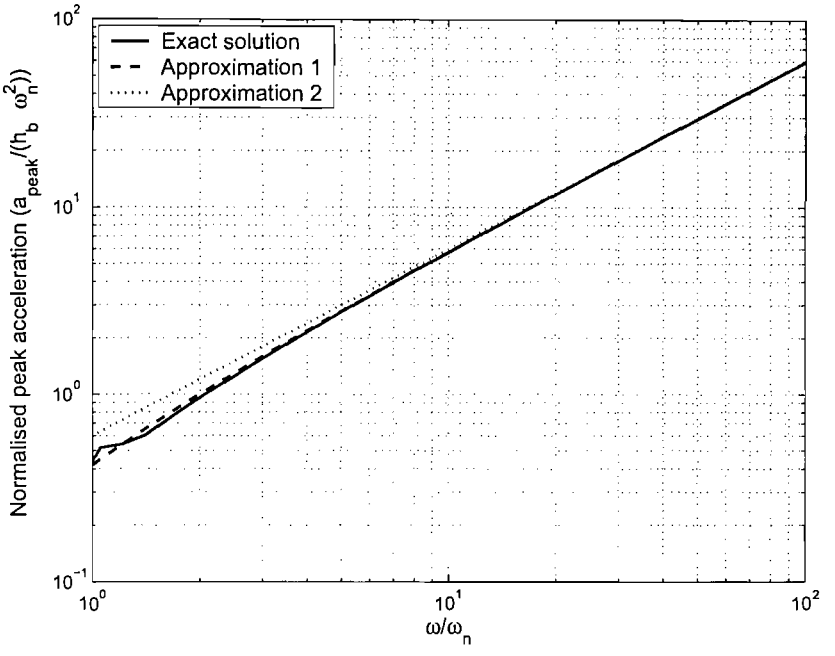

(a) c

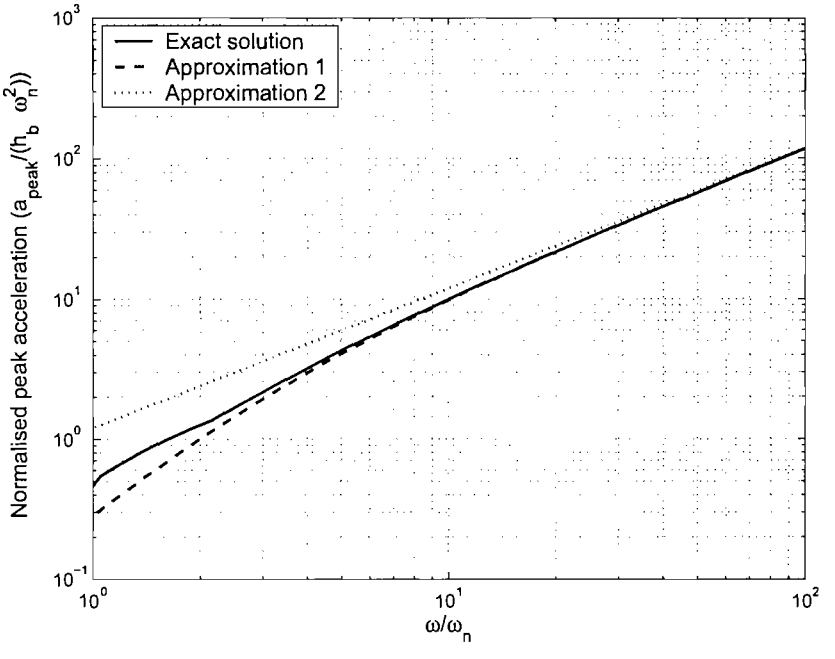

(b) d

Figure 3.7: The comparison of the peak acceleration from the exact equation (2.24) and approximate equations as a function of ω/ω_n. Approximation 1- from equation (3.4). Approximation 2 - from equation (3.8). (c) damping ratio $\zeta = 0.6$, (d) damping ratio $\zeta = 1.2$.

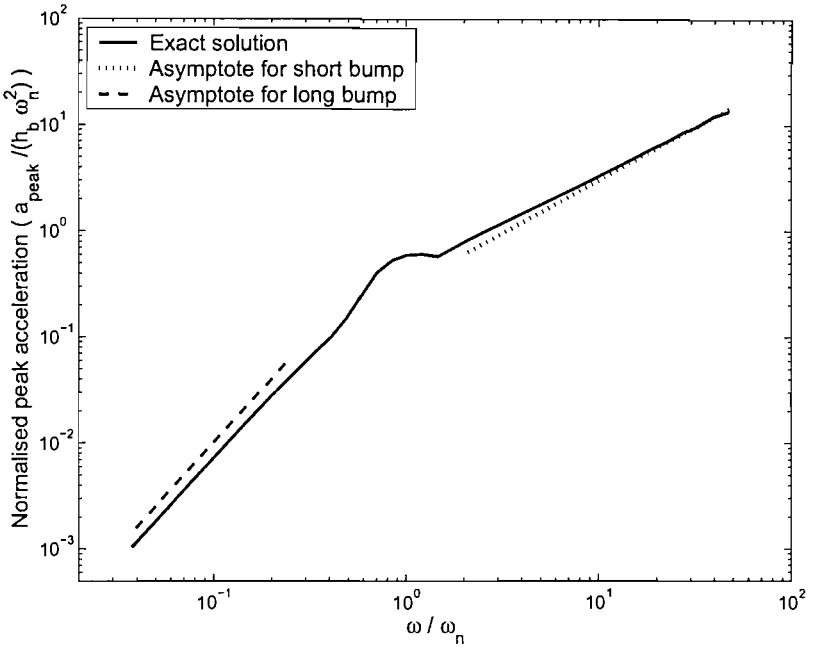

Figure 3.8: The asymptotes of acceleration shock response spectrum for $\zeta = 0.3$ for short and long durations of bump. The asymptote for a short duration bump is $a_{peak}/(h_b\omega_n^2) = \zeta r$ and asymptote for a long bump is $a_{peak}/(h_b\omega_n^2) = r^2$.

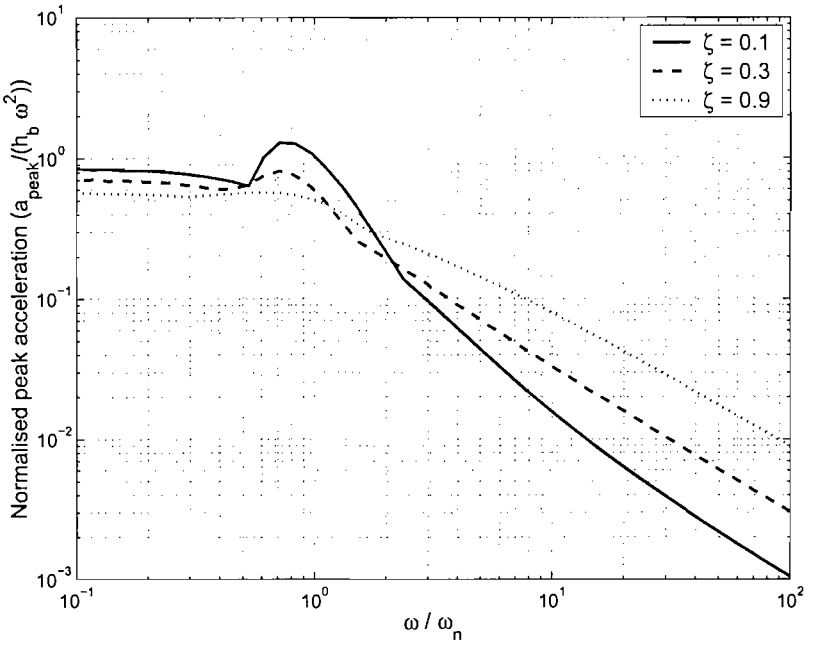

Figure 3.9: The effect of natural frequency on the peak acceleration responses.

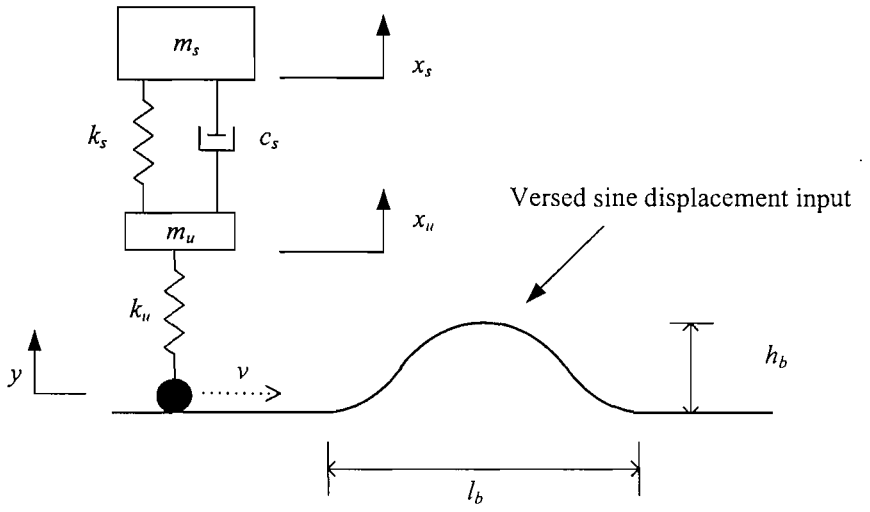

Figure 3.10: Schematic of versed-sine base motion for a 2DOF quarter car model. v is the vehicle speed, h_b is the maximum height of the bump, and l_b is the length of the bump.

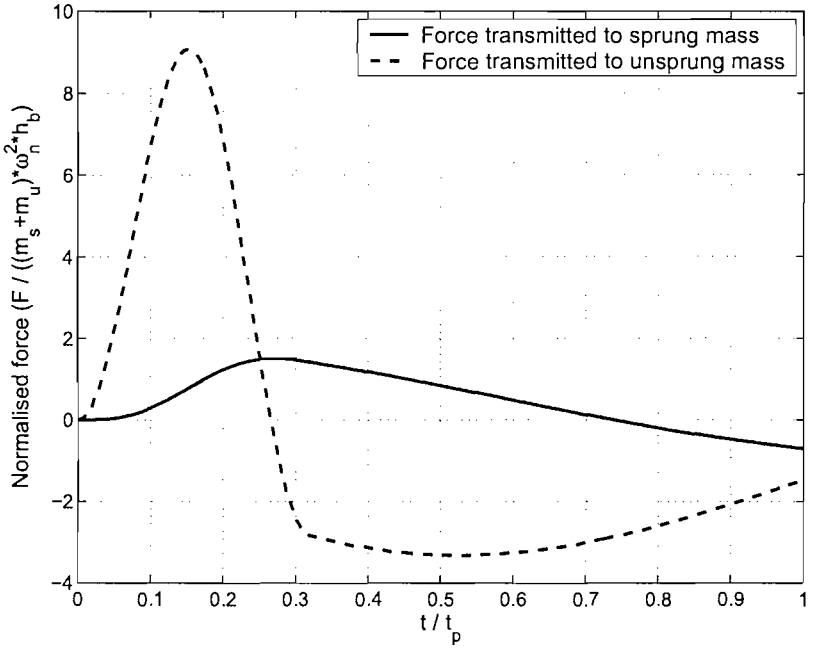

Figure 3.11: Comparison between the forces transmitted to the unsprung mass and sprung mass at $\zeta_s = 0.3$ and $r = 10$.

(a) (b)

Figure 3.12: Approximation of bounce and wheel hop modes. (a) Bounce mode (b) Wheel hop mode.

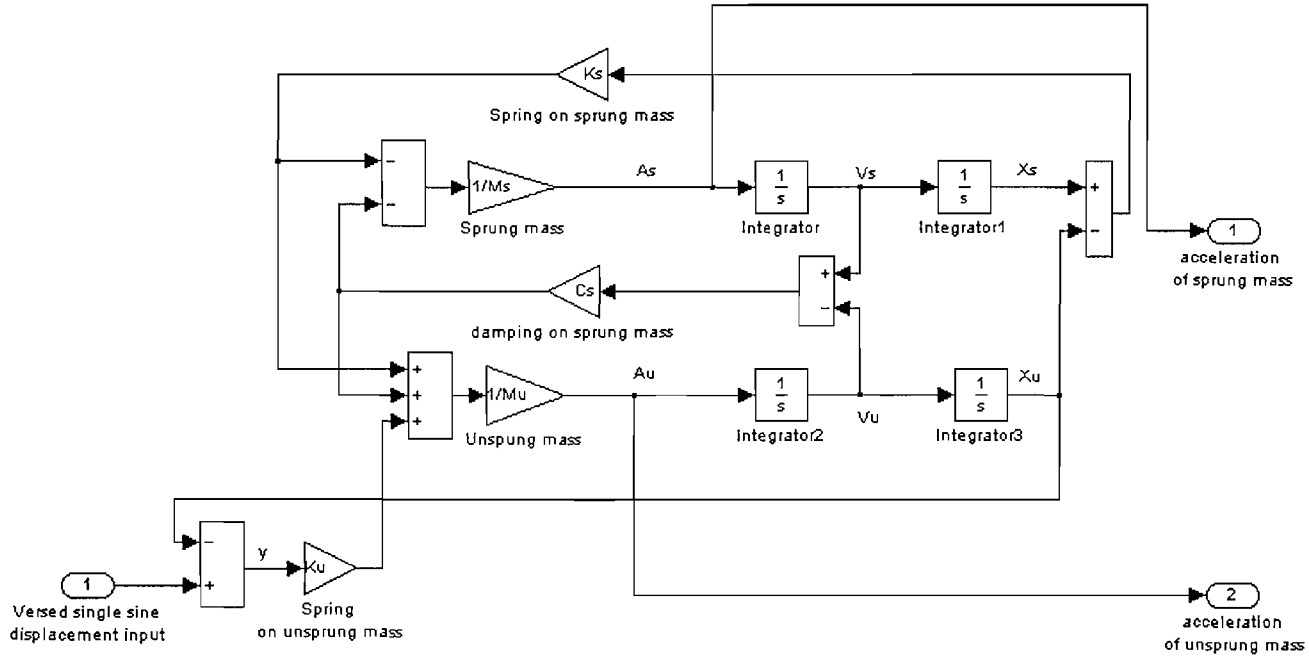

Figure 3.13: Block diagram for a two DOF quarter car model in Matlab/Simulink.

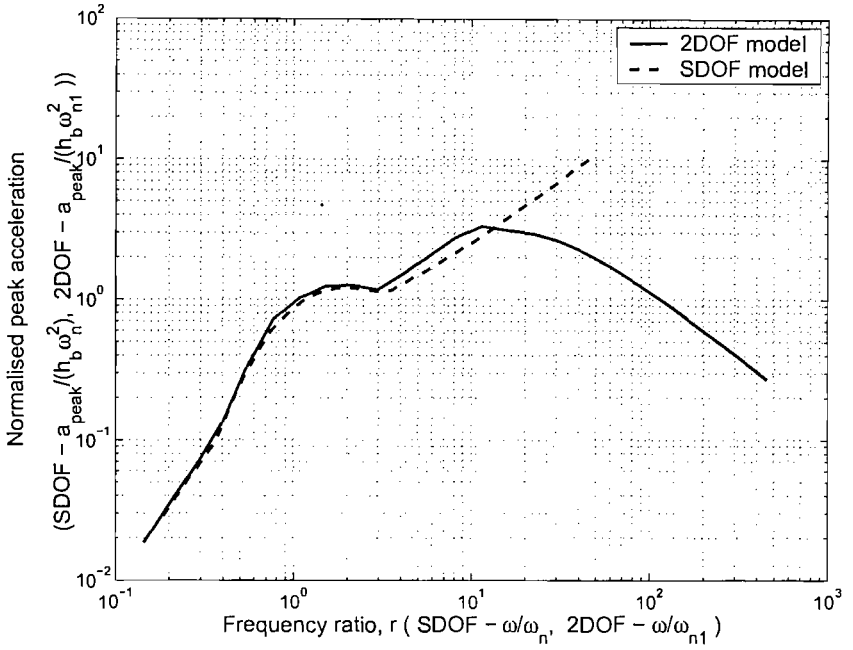

(a)

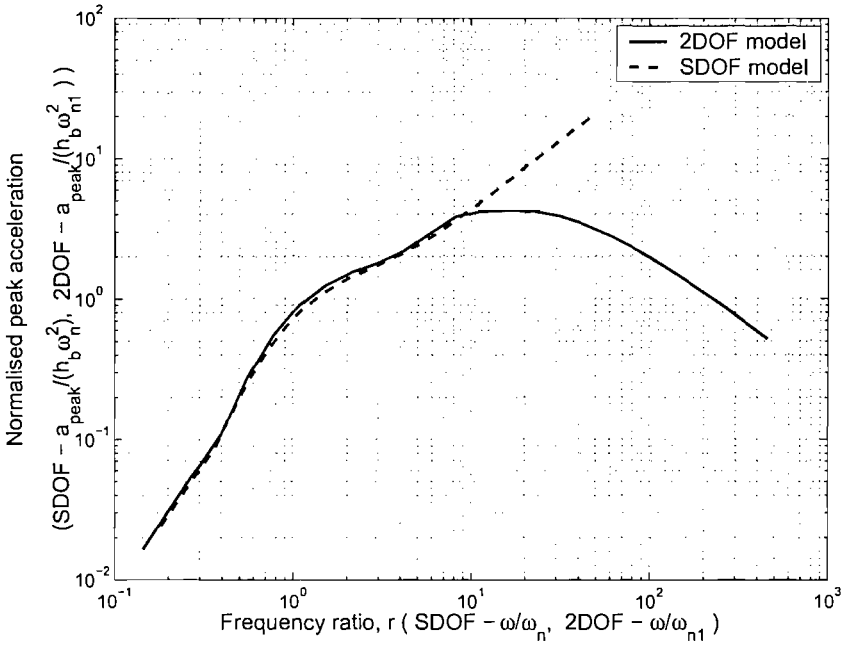

(b)

Figure 3.14: Comparison of the acceleration shock response spectra for the SDOF and two DOF systems. (a) ζ and $\zeta_s = 0.2$ (b) ζ and $\zeta_s = 0.4$

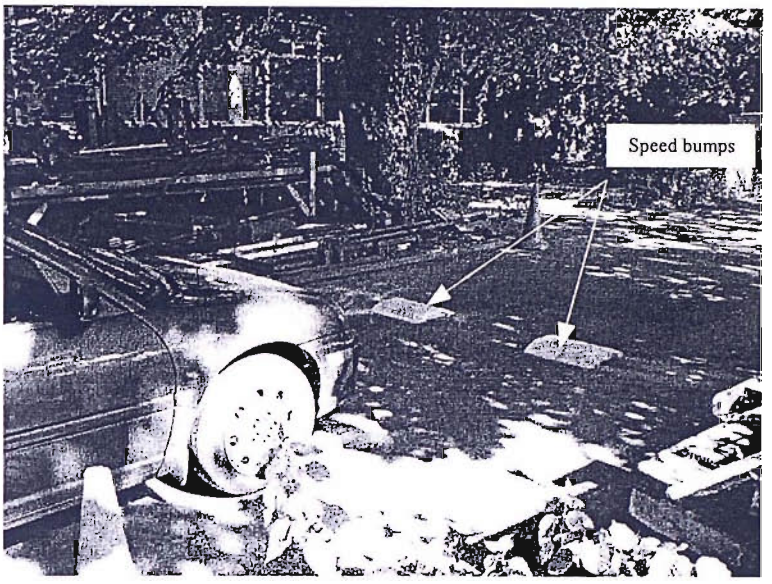

(a)

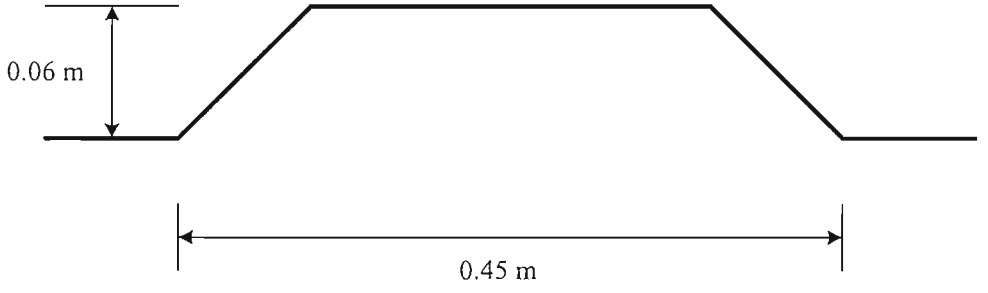

(b)

Figure 3.15: Experimental set up. (a) a vehicle traversing a bump (b) schematic of a bump

(a) (b)

Figure 3.16: Pitch mode shapes. (a) front pitch mode (b) rear pitch mode

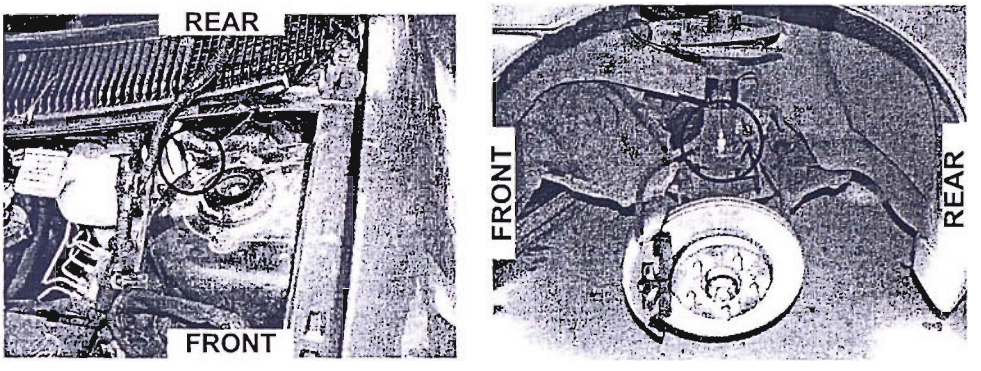

(a) (b)

(c) (d)

Figure 3.17: Attached position of accelerometers on the passenger car. (a) front body (b) front suspension (c) rear body (d) rear suspension. The circles show the accelerometer positions.

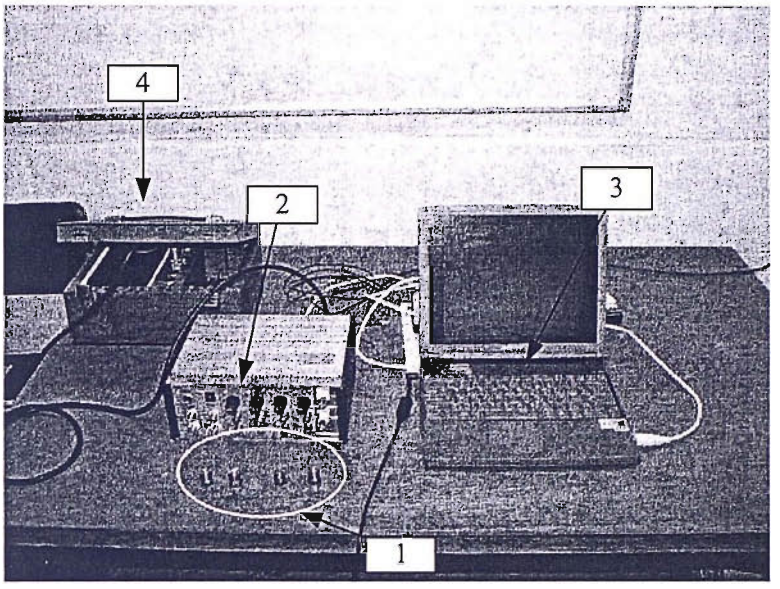

(a)

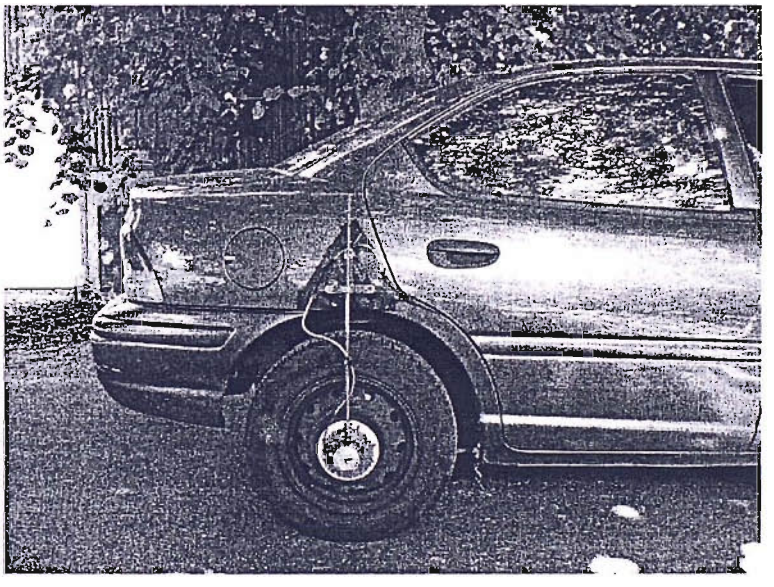

(b)

Figure 3.18: Equipments used. (a) 1. Bruel and Kjaer accelerometers, 2. Charger amplifier, 3. laptop for data acquisition, 4. Battery box. (b) Peiseler pulse type speedometer.

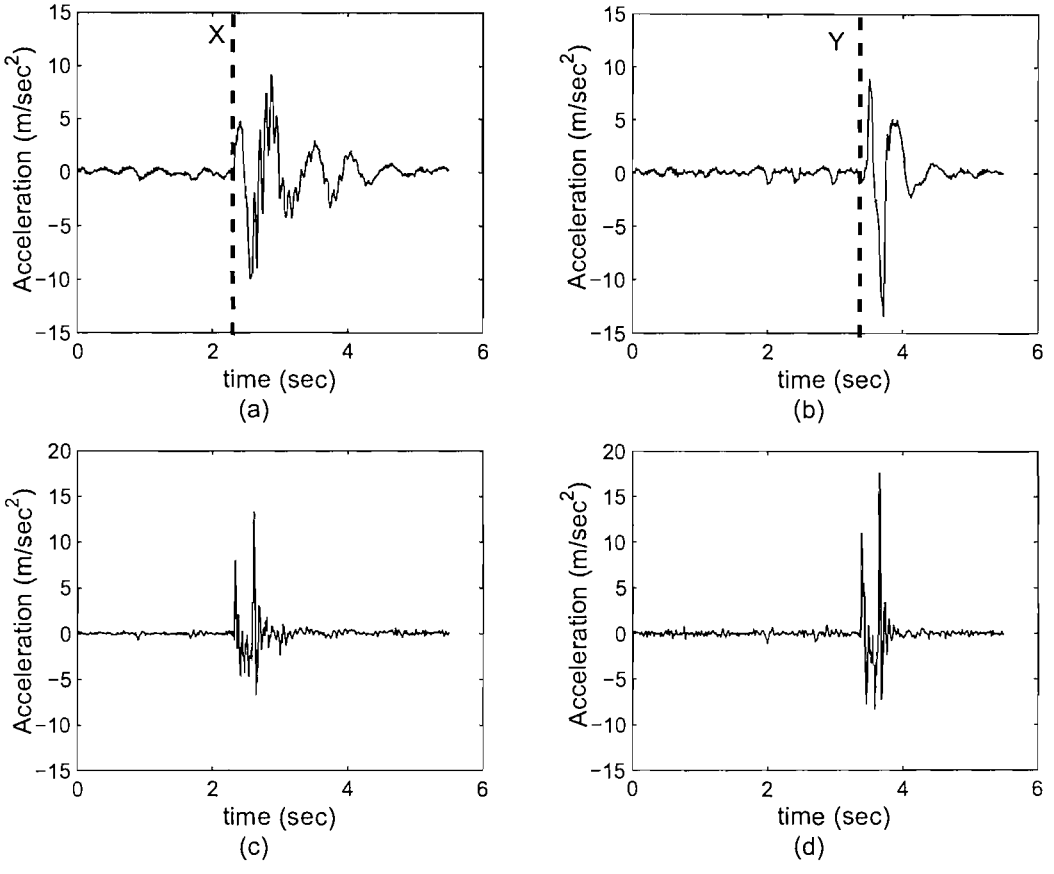

Figure 3.19: Time history data of measured acceleration at $t_p = 0.19$. (a) front body (b) rear body (c) front wheel (d) rear wheel. X : front wheel at start of bump, Y : rear wheel at start of bump.

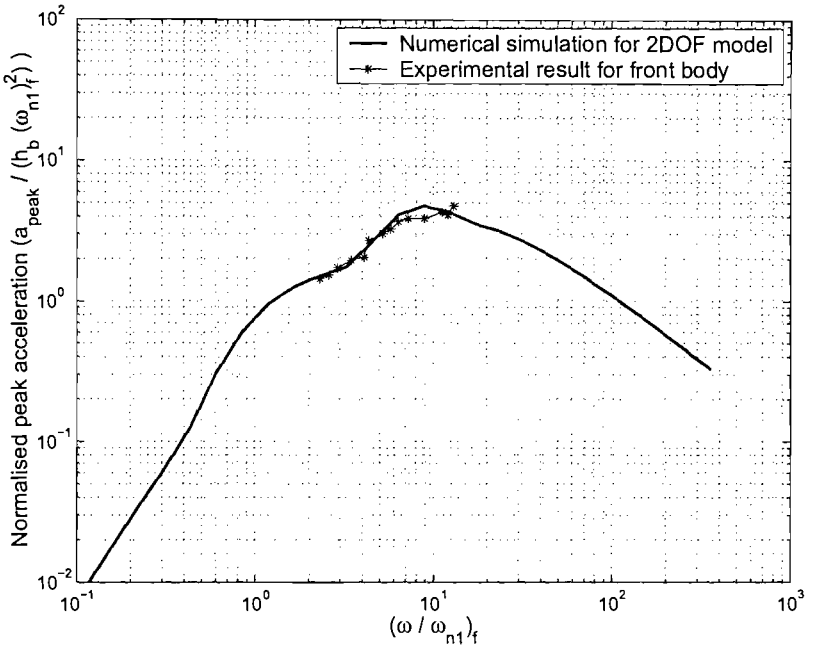

(a)

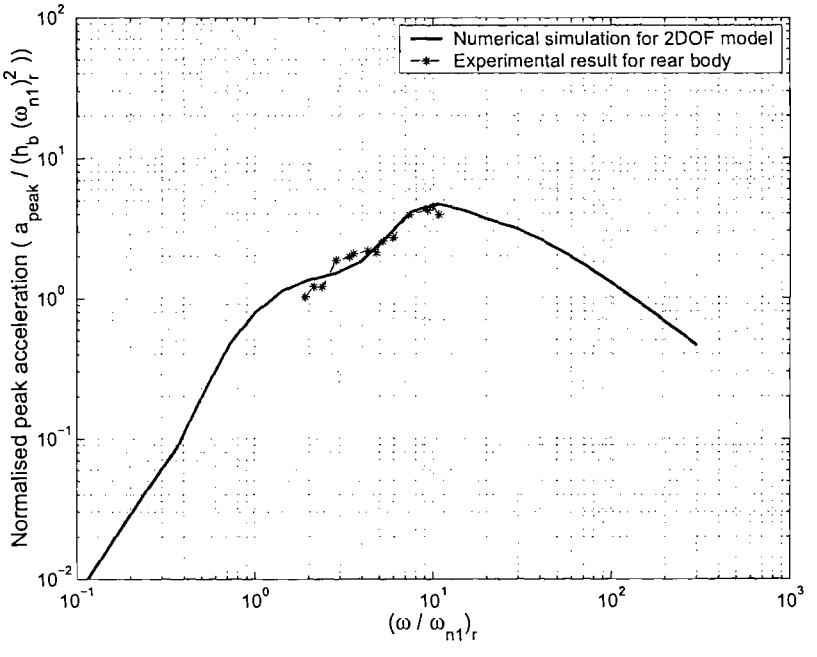

(b)

Figure 3.20: Comparison of acceleration shock response spectra between the 2DOF simulation and experimental results of the peak acceleration from the front and rear body. (a) For front body, $\zeta_{eq} = 0.33$, (b) For the rear body, $\zeta_{eq} = 0.3$.

CHAPTER 4

NON-LINEAR CHARACTERISTICS OF AN AUTOMOTIVE DAMPER

4.1 INTRODUCTION

The design of an automotive damper has a significant effect on suspension performance. Many automotive dampers have non-linear asymmetric characteristics to accommodate the contradictory requirements of ride comfort and handing stability [40]. For example, high damping can improve the handling performance, but it can deteriorate the ride comfort due to poor isolation. Therefore, the relationship between the damping force and relative velocity is deliberately chosen to be non-linear in order to achieve a better compromise. Most notably, the damping force of automotive dampers differs according to the direction of relative velocity. Damping in rebound (extension) is usually two to three times greater than damping in jounce (compression) in most passenger cars.

In this chapter, the general mechanism for damping and in particular the non-linear characteristics of a conventional automotive damper are discussed. The relationship between damping force and relative velocity of a real damper is modelled in a piece-wise linear fashion. The piece-wise linear damping model is compared with experimental data from a damper test.

4.2 General Design of an Automotive Damper

4.2.1 Damper type

Many variants of damper are used in the automotive industry. Damper types can be initially classified as friction (solid elements) or hydraulic (fluid elements), the latter being used almost exclusively in recent times [34]. Telescopic dampers are the most commonly used hydraulic dampers. Most automotive telescopic dampers are of either a mono or twin tube type as shown in Figure 4.1.

Damper valves feature a series of orifices of differing areas, some of which vary in area during operation. There are innumerable possible designs, but two types, namely disc with coil spring and shim disc, are widely used [34]. Figure 4.2 shows the design of a disc with a coil spring valve. In this type of valve, a coil spring mainly controls the area of the orifice and hence the damping force. However, in a shim disc valve, the orifices are mainly controlled by a pack of discs as shown in Figure 4.3. The detailed mechanism of damping will be dealt with in the following section.

4.2.2 Principle of a hydraulic damper

An automotive conventional hydraulic damper is primarily a fluid-dynamic device. A damping force can be generated by generating a differential pressure across a piston moving in an incompressible fluid. A valve in the piston allows fluid to be forced through a series of orifices which produces a hydraulic resistive force.

Although there are many complicated valve types in telescopic automotive dampers, the principle of damping force generation is essentially the same. In this study, the damping mechanism of a shim type valve in a twin tube telescopic damper (*shock absorber*) is dis-

cussed. Generally, the twin tube type damper consists of two valves; the piston valve and the body valve, as shown in Figure 4.1 (b).

During rebound motion, the fluid flows into the compression chamber in two ways. One flow (flow-A) passes through the piston valve from the rebound chamber as shown in Figure 4.3. Another flow (flow-B) passes through the body valve from the reservoir. The rebound damping force is generated by these two flows which are resisted by the piston and body valves. However, the rebound damping force is mainly controlled by the piston valve using orifice valves. The jounce damping force is mainly controlled by the body valve. The principle of operation is similar in the jounce direction except that the fluid in the compression chamber flows into the rebound chamber and the reservoir. The asymmetric behaviour between the jounce and rebound direction can be achieved by tuning the piston and body valves differently.

The resistive force from the piston valve can be controlled by three orifices; namely, the bleed orifice valve, the blow-off orifice valve and the port hole, as shown in figure 4.3. The bleed orifice valve is a very small orifice which consists of a thin disc with small slits through which fluid leaks. The blow-off valve consists of a number of small thin discs, bent by the flow. The more bent the discs become, the wider is the area of the orifice. Finally, when the blow-off valve is fully opened then flow resistance is determined by the cross section area of the port hole.

4.2.3 Non-linear characteristics of an automotive damper

The non-linear characteristics of an automotive damper can be characterised by the relation between the damping force and relative velocity. As discussed in the previous section, the damping force is typically controlled by three different orifice valves in either the rebound or jounce direction. Generally, this non-linear characteristic is tuned to achieve an appropriate

compromise between ride comfort and handling.

Figure 4.4 illustrates the non-linear relationship between the damping force and relative velocity across a damper for a twin tube type damper. In the low velocity region, stage 1 (under about 0.3m/s), the damping force is determined largely by the bleed orifice valve. As the velocity of piston rod increases, the blow-off valve gradually opens allowing flow to by-pass the bleed valve (stage 2). Finally, at high velocities (stage 3), the port hole controls the damping force.

The automotive damper is designed to generate force differently in jounce and rebound directions. Generally, the force in rebound is about two or three times higher than in jounce in most passenger cars. A large rebound damping coefficient may help to increase the ability of road holding and also a small jounce damping coefficient may reduce the peak acceleration from bumpy roads, based on the subjective ride assessment [33]. However, it is difficult to find analysis in the literature that substantiates this choice of damping behaviour. In the Chapter 5, the effect of asymmetric damping is investigated quantitatively using a piece-wise linear model of damping.

Undesirable non-linearties for the suspension performance can arise such as the effects of hysteresis, unavoidable friction forces and so on [33]. Figure 4.5 shows hysteretic behaviour of the damping force and relative velocity in a damper for three different amplitudes of harmonic displacement input at the same excitation frequency. In this figure, the hysteresis increases as the amplitude increases. It also shows that the damping force can be different for the same velocity, when a different displacement amplitude is imposed. This may be due to the effects of temperature, compression and cavitation of the operation fluid and friction of the sealing material of the damper [21], [36], [37].

4.3 FITTING A PIECE-WISE LINEAR DAMPER MODEL TO EXPERIMENTAL DATA

A linear damper model is convenient for shock and vibration analysis but often not sufficiently representative of the characteristics of a practical automotive damper. However, it is difficult to build a wholly representative model of a damper due to the complicated non-linear characteristics of the orifice valves. A piece-wise linear model is a convenient compromise whereby the damper has different linear regions depending on the velocity across the damper. In this chapter, a piece-wise linear model is presented and the model is fitted to experimental data from a practical damper.

4.3.1 Linear damper

Considering a linear damper model, the relation between the force exerted by a damper f_d and relative velocity v_{rel} can be expressed as

$$f_d = cv_{rel} \tag{4.1}$$

where c is the damping coefficient. Imposing a harmonic displacement across the ends of damper, then the displacement and velocity can be expressed as

$$x_{rel} = a\sin\omega t \tag{4.2a}$$

$$v_{rel} = a\omega\cos\omega t \tag{4.2b}$$

where ω is the excitation frequency and a is the amplitude of displacement input. Using the identity $\sin^2\omega t + \cos^2\omega t \equiv 1$, the damping force and displacement are related as follows:

$$\left(\frac{x_{rel}}{a}\right)^2 + \left(\frac{f_d}{ac\omega}\right)^2 = 1 \tag{4.3}$$

The force can be plotted against the relative displacement x_{rel} using equation (4.3). The above relation can be recognised as the equation for an ellipse and is shown in Figure 4.6. Therefore, the damping force can be considered to be a function of displacement amplitude, frequency and damping coefficient for a harmonic displacement input. However, in a practical damper, the damping coefficient is not a constant but varies continuously with relative velocity. A convenient approximation is to adopt a piece-wise linear model in which the damping constant is fixed within certain velocity ranges.

4.3.2 Piece-wise linear damper

In the automotive engineering field, various experiments are undertaken in order to measure damper characteristics. One such experiment is to subject the damper to a harmonic displacement input. One end of a damper is mounted directly on a hydraulic actuator which can control the exact displacement and velocity. The other end of the damper is grounded via a load cell. The force from the load cell and the displacement and velocity of the hydraulic actuator are measured. The experimental relationship between the damping force and displacement of a practical automotive damper can be seen in Figure 4.7 which was provided by Hyundai Motors [41]. The damper is excited at various frequencies with a fixed harmonic displacement input. Unlike Figure 4.6, these plots do not have the elliptical shape characteristic of a linear relationship. Comparing Figures 4.6 and 4.7, two main differences can be observed. Firstly, the damping force in the rebound direction is two or three times higher than in the jounce direction. Secondly, the damping force changes rapidly at both ends of the stroke ($\pm$35-40mm) but more modestly in the intermediate region of the stroke. This means that the damping coefficient is not a constant but varies continuously depending on the velocity region.

Using the measured data from a harmonic displacement test, the damping force can also

be plotted against the relative velocity across the two ends of the damper as shown in Figure 4.8 (a). This plot is an alternative way to illustrate damper characteristics. It offers the advantage that the association between damping force and velocity in jounce and rebound can be read immediately. It is advisable to view the damping force in both formats to infer the non-linear characteristics of a damper.

To derive a convenient approximate model for a practical damper, the damping force–velocity curve shown in Figure 4.8 (a) can be fitted to a piece-wise linear model. It is apparent from Figure 4.8 (a) that there are approximately four velocity regions where a constant damping coefficient can be used. For example, in the rebound direction (positive velocity), two velocity regions can be delimited at 170 mm/sec. In the piece-wise linear damper model, the rebound and jounce damping coefficients c_r and c_j can be approximated as

$$c_r = \begin{cases} 5.1 \text{ Ns/mm} & [0 \leq v_{rel} \leq 170 \text{ mm/s}] \\ 1.5 \text{ Ns/mm} & [170 \text{ mm/s} \leq v_{rel}] \end{cases} \tag{4.4a}$$

$$c_j = \begin{cases} 1.9 \text{ Ns/mm} & [-120 \leq v_{rel} \leq 0\text{mm/s}] \\ 0.4 \text{ Ns/mm} & [v_{rel} \leq -120 \text{ mm/s}] \end{cases} \tag{4.4b}$$

The piece-wise linear approximations shown in Figure 4.8 are a reasonable match to the experimental data. This model can be used in the numerical simulations in preference to a simple linear damping model. If the relative velocity across the damper can be assumed small (-120 mm/s $< v_{rel} <$ 170 mm/s in this case) then the damping model can be further simplified to that of a bi-state device. In the next chapter, such a piece-wise linear damper model is used to investigate the effects of jounce and rebound damping values on the peak relative displacement and acceleration response of a vehicle traversing a bump.

4.4 CONCLUSION

This chapter has discussed the principles of operation of a practical automotive hydraulic damper, and the design features which control the non-linear characteristics between damping force and velocity. The fundamental operating principle can be explained in terms of a resistance to fluid flow on the orifices which is caused by the difference of pressure acting on both sides of damper valves.

An automotive damper has a non-linear characteristic between the damping force and relative velocity to achieve a satisfactory compromise between the ride comfort and handling performance. The cause of this non-linear relation is that the damping force is controlled by different valves depending on the range of relative velocity.

Using experimental data from a test on a practical damper, the non-linear damping characteristic has been approximated by a piece-wise linear model. The approach gives a convenient model for considering shock isolation problems. In the next chapter, a bi-state piece-wise linear damper model is used to the shock response of a vehicle traversing a bump.

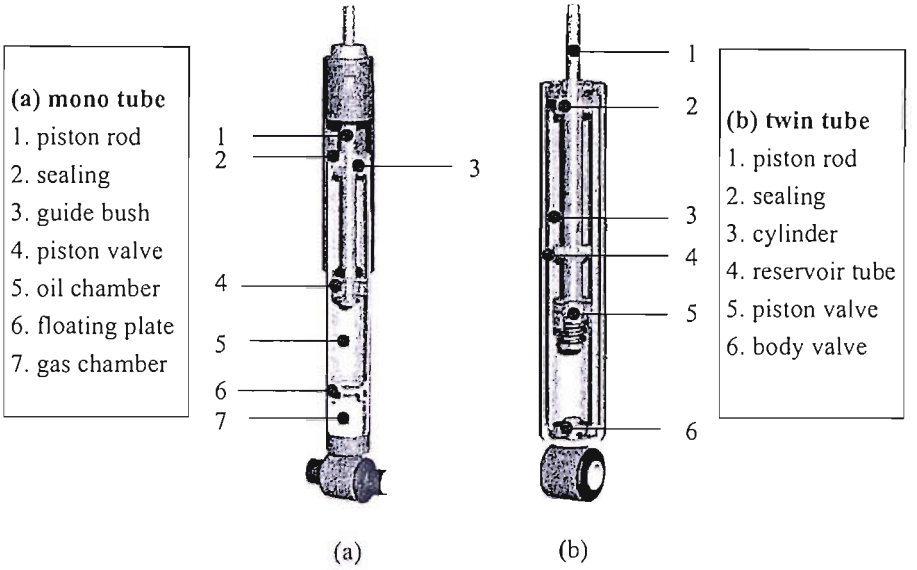

Figure 4.1: Design of a practical automotive damper (a) mono tube type (b) twin tube type [34, 35].

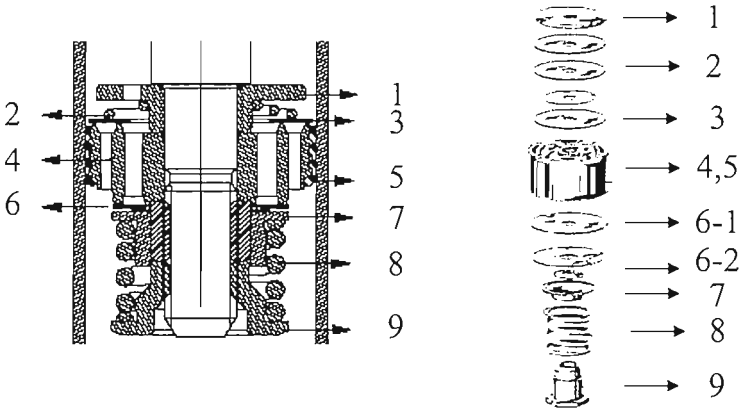

Figure 4.2: Schematic of disc-spring valve and its components. 1. support washer, 2. intake spring, 3. intake valve, 4. piston, 5. piston ring, 6-1. orifice disc, 6-2. orifice valve, 7. spring seat and torque washer, 8. valve spring, 9. rod nut [34].

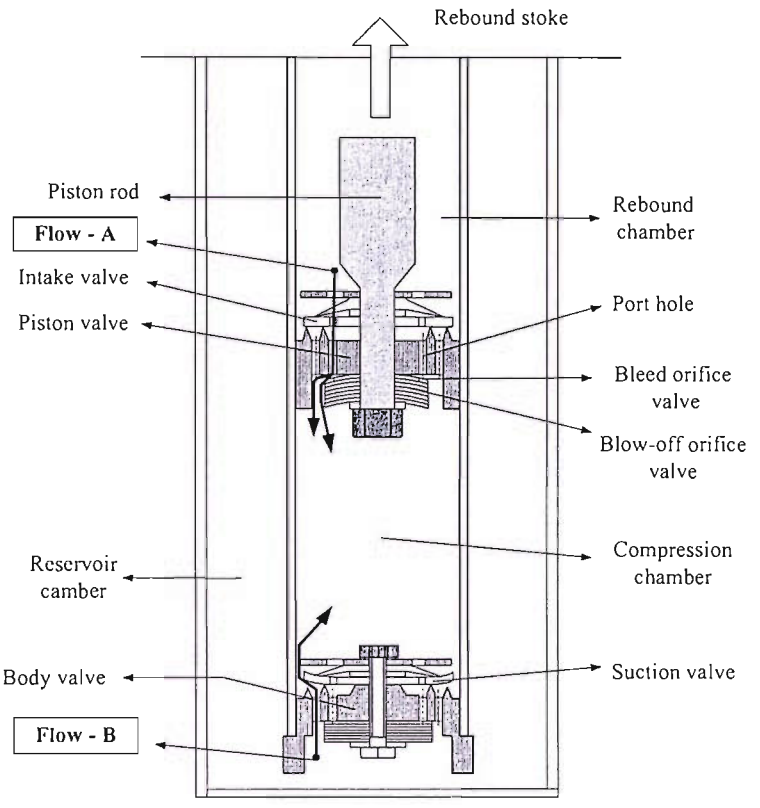

Figure 4.3: Schematic showing the principle of operation of an automotive shock absorber with a shim type valve.

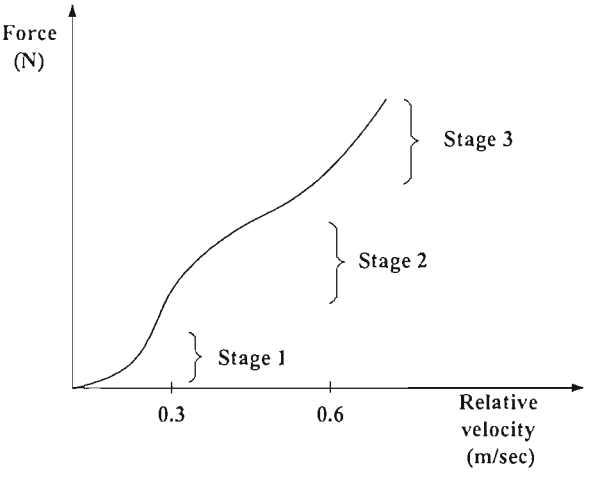

Figure 4.4: Damping force-velocity characteristic of a typical automotive damper in the rebound direction.

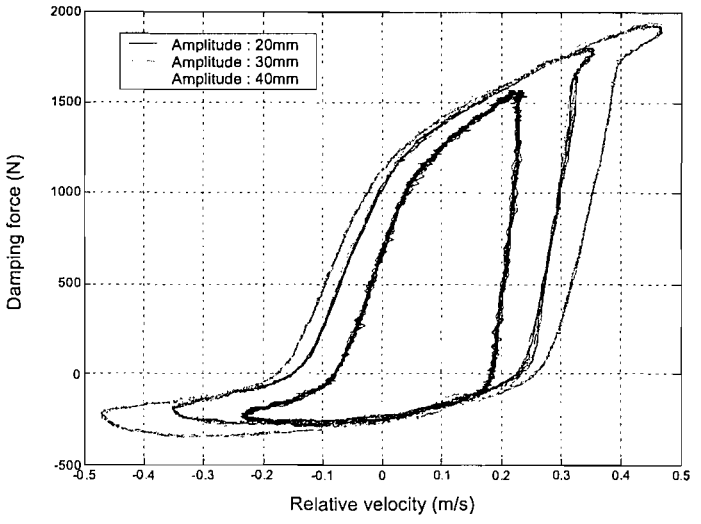

Figure 4.5: Hysteresis behaviour of a practical automotive damper excited by a sinusoidal input [36].

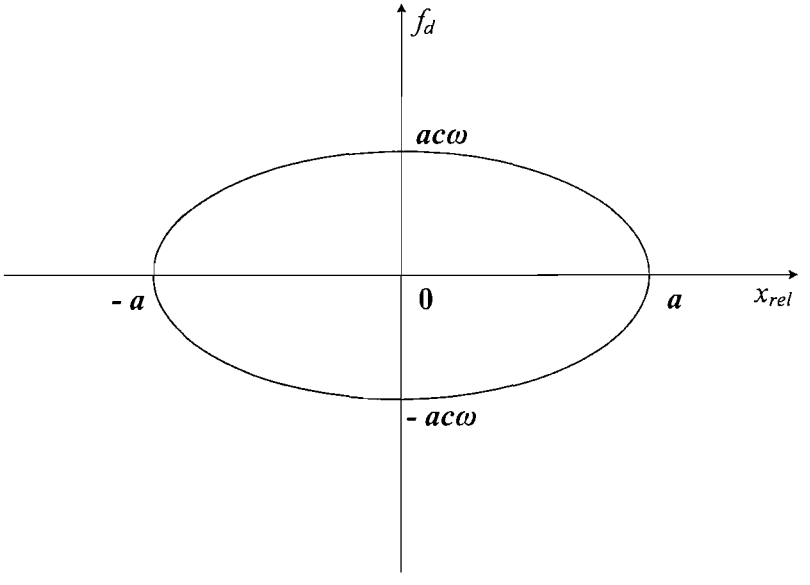

Figure 4.6: The relationship between damping force and displacement for a linear damper subjected to a harmonic input.

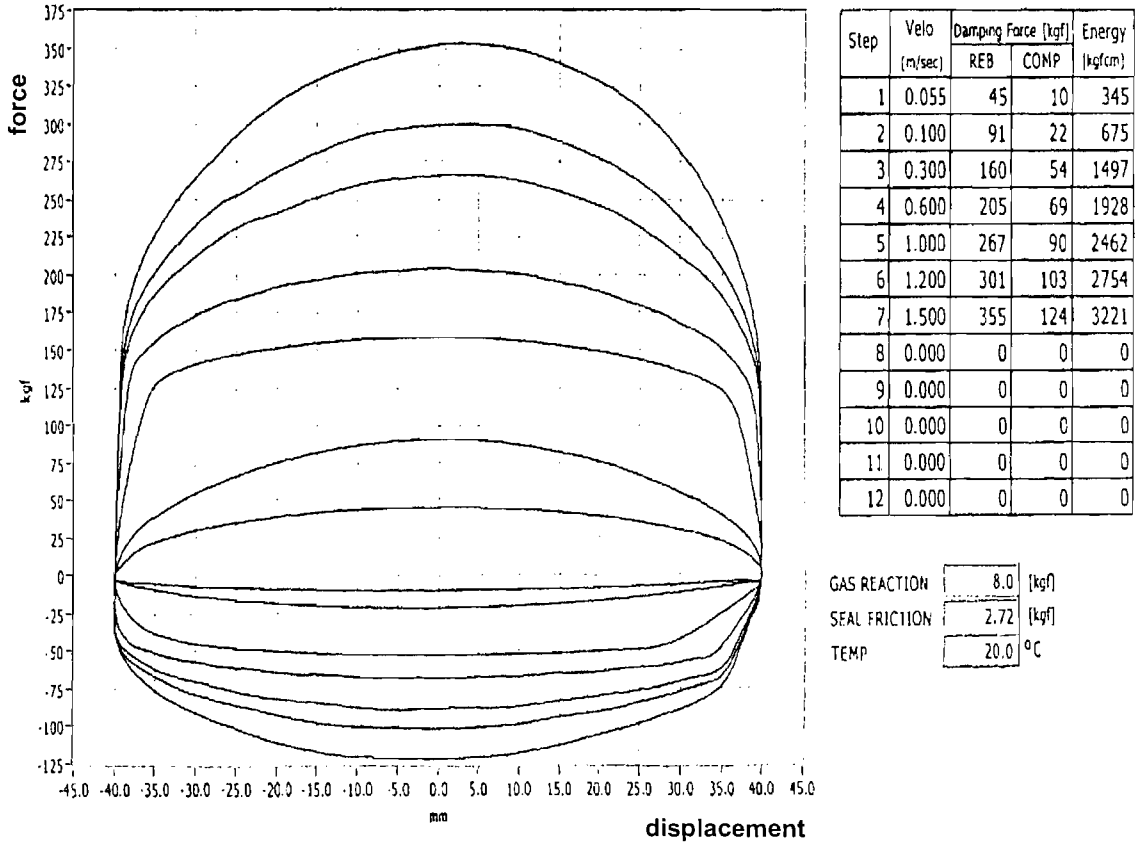

Step	Velo (m/sec)	Damping Force [kgf] REB	COMP	Energy [kgf·cm]
1	0.055	45	10	345
2	0.100	91	22	675
3	0.300	160	54	1497
4	0.600	205	69	1928
5	1.000	267	90	2462
6	1.200	301	103	2754
7	1.500	355	124	3221
8	0.000	0	0	0
9	0.000	0	0	0
10	0.000	0	0	0
11	0.000	0	0	0
12	0.000	0	0	0

GAS REACTION	8.0	[kgf]
SEAL FRICTION	2.72	[kgf]
TEMP	20.0	°C

Figure 4.7: Force versus displacement relation for a practical automotive damper from a harmonic displacement test [41].

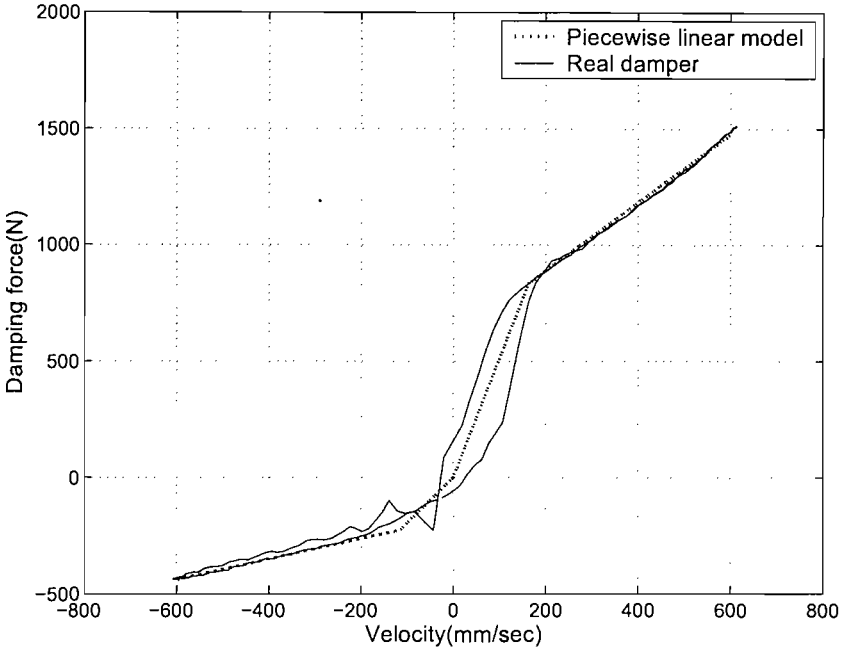

(a)

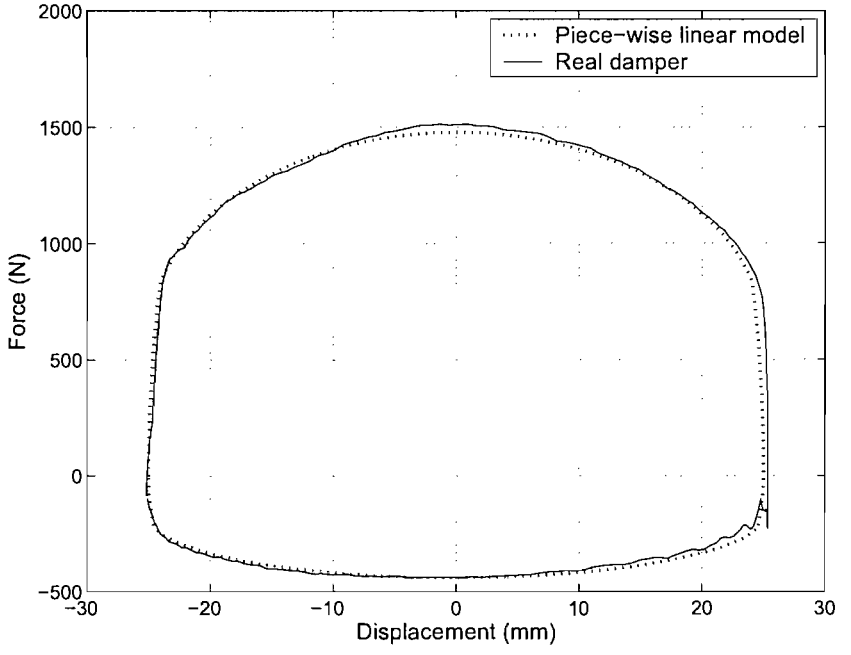

(b)

Figure 4.8: Comparison of real automotive damper and piece-wise linear damping model. (a) damping force-velocity, (b) damping force-displacement.

CHAPTER 5

BI-STATE DAMPING FOR SHOCK ISOLATION

5.1 INTRODUCTION

In the previous chapter, the general non-linear characteristics of an automotive damper have been discussed including the general design features and operating principle. A piece-wise linear damping model has been validated by experimental data from a practical automotive damper.

Most practical dampers of passenger cars are designed to exert lower force in jounce direction than in rebound. In this chapter, using a two-state piece-wise linear damping model, one of the reasons for designing largely different damping coefficients in jounce and rebound direction is investigated and the optimal ratio of damping coefficients for shock isolation is considered. The magnitudes of the peak relative displacement and peak acceleration are presented as a function of damping coefficient in the jounce direction. The maximum achievable benefit from switching the damping coefficient according to relative velocity across the damper is quantified.

The peak acceleration generally occurs during a bump when the bump duration is much shorter than the natural period of the system, as discussed in Chapter 3. Furthermore, the peak acceleration increases with damping coefficients. To reduce the peak acceleration, it follows that the damping should be minimised when the bump is being traversed. However, an adverse consequence of this would be that vehicle body would vibrate freely for longer after the bump.

To solve this conflict, a new strategy is introduced whereby the damper is switched from a low value to a high value at the end of the bump. A significant reduction in acceleration is observed.

5.2 BI-STATE DAMPING MODELS

5.2.1 Piece-wise linear model of a conventional automotive damper

For the piece-wise linear damping model presented in Chapter 4, it is convenient to define the ratio of damping coefficients in the jounce and rebound directions as

$$\alpha_p = \frac{c_j}{c_r} \tag{5.1}$$

where c_j is the damping coefficient when the damper is compressed (negative relative velocity) and c_r is the damping coefficient when the damper is expanded (positive relative velocity). The force-velocity relationship can be seen in Figure 5.1 (a). Using the relationship $\zeta = c/c_c$ where c_c is the critical damping coefficient of the SDOF system, the ratio of damping coefficients α_p can be also expressed as a function of the damping ratios,

$$\alpha_p = \frac{\zeta_j}{\zeta_r} \tag{5.2}$$

For $\alpha_p < 1$, the jounce damping coefficient is smaller than the rebound damping coefficient. For $\alpha_p > 1$, the jounce damping coefficient is bigger than the rebound damping coefficient. For $\alpha_p = 1$, the damper is linear.

Generally, a practical automotive damper has a very different damping coefficient in

jounce and rebound directions as discussed in the previous chapter. Typically, the ratio of damping coefficients α_p is about 0.5 for automotive dampers in most passenger cars.

5.2.2 Alternative bi-state damping model

A new switchable damping model is proposed here. Considering a vehicle traversing a short bump, the peak acceleration occurs during the bump as discussed in Chapter 3. If the vehicle has low suspension damping, the peak acceleration can be reduced but it will oscillate longer after the bump. Therefore, in order to obtain better shock isolation, it may be necessary for the vehicle suspension to have low damping during the bump and high damping after the bump. Hence, an alternative bi-state damping might seem appropriate where the damper is switched off during the bump and on again at the end of the bump.

In this case, it is convenient to define the ratio of damping coefficients α_s as

$$\alpha_s = \frac{c_d}{c_a} = \frac{\zeta_d}{\zeta_a} \tag{5.3}$$

where c_d is the damping coefficient when a vehicle traverses the bump and c_a is the damping coefficient when a vehicle proceeds after the bump. Figure 5.1 (b) shows the force-velocity relation for the alternative bi-state damping model switching at the start and end of the bump. Variations in the ratio of damping coefficients α_s can be interpreted as changes in the damping coefficient during the bump c_d given a fixed damping value c_a after the bump.

For $\alpha_s < 1$, the damping coefficient during the bump is smaller than after the bump. For $\alpha_s > 1$, the damping coefficient during the bump is larger than after the bump. For $\alpha_s = 1$, this model defaults to linear damping.

5.3 ANALYSIS OF RESPONSES FOR BI-STATE DAMPERS

In this section, a SDOF system with a versed-sine base motion is adopted with each of the two types of bi-state damper models defined in Section 5.2. The responses of the SDOF system are found by numerical simulation using the Runge-Kutta method in MATLAB. The effects of the ratios of damping coefficients α_p and α_s and the level of damping are investigated in terms of the peak relative displacement and peak acceleration responses.

Typical time histories for the normalised responses of the SDOF system with the two types of bi-state damper are presented in Figure 5.2. The system has a natural period t_n which is *ten* times longer than the bump duration t_p. For the piece-wise linear damper, the damping ratio in the jounce direction ζ_j is *zero* and in rebound direction, $\zeta_r = 0.3$. For the alternative bi-state model, the damping ratio during the bump, ζ_d is *zero* and the damping ratio after the bump $\zeta_a = 0.3$. The reason for using a *zero* value of ζ_j, and ζ_d is that the effect of bi-state damping can be seen most clearly.

As can be seen in Figure 5.2 (f), the positive peak accelerations of both damping models are the same amplitude but the negative peak of the piece-wise linear model is much larger than the alternative bi-state model. In this example, the largest peak acceleration response of the alternative bi-state damping model can be about 2.5 times smaller than that of the piece-wise linear damping. The largest peak relative displacement of the alternative bi-state damping model, however, is the same as that of the piece-wise linear damping as shown in Figure 5.2 (c).

5.3.1 Effects of the ratio of damping coefficients (α_p, α_s)

Piece-wise linear damper

Figure 5.3 shows the normalised peak responses of the piece-wise linear damping model plotted as a function of the piece-wise linear ratio of damping coefficients α_p. Bump duration ranging from 0.1 to 2 times the natural period are shown. These responses are normalised by those of a linearly damped SDOF system, i.e. where the damping coefficient in the jounce direction c_j, is the same as that of rebound c_r. A fixed rebound damping ratio of $\zeta_r = 0.3$ is used.

From Figure 5.3 (a), it can be seen that the peak relative displacement is not very sensitive to α_p and is similar to that of a linear damper. On the other hand, the peak acceleration can be reduced as α_p becomes less than 1 for $t_p/t_n = 0.1, 0.2$ and 0.5 as shown in Figure 5.3 (b). For $\alpha_p > 1$, the peak acceleration is higher than for a linear damper. These results suggest that the peak acceleration may be reduced for short duration bumps using a piece-wise linear damper with $\alpha_p < 1$ without an appreciable increase in the peak relative displacement.

Most passenger car dampers are designed so that half the damping coefficient of the rebound direction is that of jounce direction [33]. The force depends on the relative velocity which is typically larger in jounce. Therefore, this may be a reason for calling an automotive damper by *Shock absorber.*

Alternative bi-state damper

Figure 5.4 shows the normalised peak responses of the alternative bi-state damper as a function of the ratio of damping coefficients α_s for the same range of bump durations.

When $\alpha_s < 1$, the peak relative displacements are always bigger than those of a linear damper. However, when the duration of the bump becomes shorter, the peak relative displacement becomes less dependent on α_s as shown in Figure 5.4 (a).

Figure 5.4 (b) shows that the peak acceleration decreases as the ratio of damping coefficient α_s becomes smaller for $t_p/t_n = 0.1, 0.2$ and 0.5. This means that the peak acceleration can be reduced by the alternative bi-state damper with $\alpha_s < 1$ for short duration bumps, but the peak acceleration due to long bumps is worse. For $\alpha_s > 1$, the alternative bi-state damper is beneficial for long bumps but detrimental for short duration bumps. Therefore, it can be seen that the alternative bi-state damper has a better shock isolation performance for the ratio of damping coefficients $\alpha_s < 1$ without a large relative displacement for shorter durations of the bump. In particular, for $t_p/t_n = 0.1$, whilst the peak relative displacement is not much smaller than that of a linear damping, the peak acceleration is decreased significantly for $\alpha_s < 1$.

5.3.2 Effects of level of damping for a short duration bump

The preceding section has considered the effect of the ratio between the two damping values for a given damping ratio of 0.3 in rebound (or after the bump). This section investigates the effect of varying the overall level of damping for a short duration bump only ($t_p/t_n = 0.1$). The reason for this choice that short bumps give higher peak accelerations.

Piece-wise linear damper

The peak relative displacement and peak acceleration of the piece-wise linear damper are presented in Figure 5.5 corresponding to the rebound damping ratios $\zeta_r = 0.1, 0.3$ and 0.8 for a short duration bump ($t_p/t_n = 0.1$).

From Figure 5.5 (a), the previously held observation that the peak relative displacement is not affected much seems also to hold for low and high damping levels. Even though the amplitude of the peak relative displacement is similar to that of the linear damper, a benefit in reducing the peak acceleration can be obtained for $\alpha_p < 1$ as shown in Figure 5.5 (b). For example, the peak acceleration can be reduced as much as about 27% of that of linear damping at $\alpha_p = 0$ and $\zeta_r = 0.1$. From Figure 5.5 (b), it can be seen that the piece-wise damper has more benefit in reducing the peak acceleration as the overall level of damping is reduced.

Alternative bi-state damper

The peak responses of the alternative bi-state damper are presented in Figure 5.6. In the alternative bi-state damper, the overall level of damping in the system is quoted in terms of the damping ratio after the bump ζ_a. The peak relative displacement does not increase greatly as the damping level increases as shown in Figure 5.6 (a). This trend is very similar to that of the piece-wise linear damper as shown in Figure 5.5 (a). The peak acceleration can be also reduced for $\alpha_s < 1$ as shown in Figure 5.6 (b). However, it differs from the result for the piece-wise linear damper in that the peak acceleration can be reduced as the level of damping is increased.

The maximum benefit is achieved by setting the ratio of damping coefficients $\alpha_s = 0$. This is apparent from where the curves intersect the y axis in Figure 5.6 (b). Whilst this may be practically unacceptable, it is helpful to consider this case so as to give a bound on what is achievable from this damper model. An analytical approximation for this idealised case can be obtained as follows.

Since for a short duration bump the peak acceleration can be expected to occur during

the bump, it may be possible to approximate the system when $\alpha_s = 0$ as an undamped SDOF system for which the analytical solution has been found in Chapter 3. Therefore, an analytical expression for the peak acceleration of an undamped system is compared here with that of the linearly damped system in order to find the maximum benefit of the alternative bi-state damper.

Firstly, the peak acceleration for the undamped system can be found by setting $\zeta_d = 0$ in equation (3.3). For a short duration bump, the approximate equation (3.3) is given by

$$\frac{\ddot{x}(\tilde{t})}{\omega_n^2 h_b} = \zeta_d r \sin 2\pi\tilde{t} - \frac{1}{2}(1 - 4\zeta_d^2)\cos 2\pi\tilde{t} + \frac{1}{2}(1 - 4\zeta_d^2) + O(r^{-1}), \qquad 0 \leq \tilde{t} \leq 1 \tag{5.4}$$

Substituting for $\zeta_d = 0$, equation (5.4) reduces to

$$\frac{\ddot{x}(\tilde{t})}{\omega_n^2 h_b} \simeq -\frac{1}{2}\left(\cos 2\pi\tilde{t} - 1\right), \qquad 0 \leq \tilde{t} \leq 1 \tag{5.5}$$

Therefore, the peak normalised acceleration of the undamped system can be expressed as

$$\left(\frac{\ddot{x}(\tilde{t})}{\omega_n^2 h_b}\right)_{\text{max / min}} \simeq 1 \tag{5.6}$$

Finally, a simple relation between peak acceleration and system parameters can be found as

$$\ddot{x}_{\text{max / min}} \simeq \omega_n^2 h_b \tag{5.7}$$

From equation (5.7), it can be seen that the peak acceleration of the alternative bi-state damper is independent of the level of damping and duration of the bump for the ideal case when $\alpha_s = 0$.

Secondly, the approximate equation for the peak acceleration of a linearly damped sys-

tem has been found previously, and is expressed in equation (3.8). This can be rewritten as

$$\ddot{x}_{\max\,/\,\min} = \zeta r \omega_n^2 h_b \,, \qquad r \gg \left| \frac{1}{2\zeta} - 2\zeta \right| \tag{5.8}$$

Taking a ratio of the peak accelerations of the two systems gives

$$\frac{(\ddot{x}_a)_{\max\,/\,\min}}{(\ddot{x}_l)_{\max\,/\,\min}} = \frac{1}{\zeta r} \,, \qquad r \gg \left| \frac{1}{2\zeta} - 2\zeta \right| \tag{5.9}$$

where r is the frequency ratio and $(\ddot{x}_a)_{\max\,/\,\min}$ is the acceleration response of the alternative bi-state damper and $(\ddot{x}_l)_{\max\,/\,\min}$ is the acceleration response of the linear damper for a short duration bump. For a frequency ratio $r = 10$, these ratios of the peak accelerations of the two systems for the damping ratio $\zeta = 0.1$, 0.3 and 0.8 are also shown in Figure 5.6 (b). The numerical simulation for $\alpha_s = 0$ in Figure 5.6 (b) is in good agreement with the analytical result of this limiting case for $\zeta = 0.3$ and 0.8. For $\zeta = 0.1$, the analytical approximate value differs from the numerical result at $\alpha_s = 0$. The reason for this is that the frequency ratio r is not sufficiently large to satisfy the condition in equation (5.9).

The maximum achievable benefit of the alternative bi-state damper (i.e. when $\alpha_s = 0$) for reducing the peak acceleration is simply determined by the product of the damping ratio and the frequency ratio. Using this relationship, the performance of the alternative bi-state damper can be evaluated by defining the *improvement factor* as follows:

$$\textit{Improvement factor} = \frac{(\ddot{x}_l)_{\max\,/\,\min}}{(\ddot{x}_a)_{\max\,/\,\min}} \tag{5.10a}$$

$$\simeq \zeta r \tag{5.10b}$$

From equation (5.10b), the maximum achievable benefit from the alternative bi-state damping strategy can be estimated. For the $Improvement\ factor > 1$, the alternative bi-state damper has potentially better performance than the linear damper in reducing the peak acceleration. For the $Improvement\ factor = 1$, the performance of the alternative bi-state damper is the same as the linear damper. For the $Improvement\ factor < 1$, the alternative bi-state damper cannot out-perform the linear damper in reducing the peak acceleration.

5.4 PERFORMANCE OF BI-STATE DAMPERS FOR SHOCK ISOLATION

The previous section presented each of the bi-state dampers in turn and compared the performance of each with that of a linear damper. For short durations of bump, benefits in reducing the peak acceleration were observed with both types of bi-state damping when α_s and $\alpha_p < 1$.

In this section, the performances of the piece-wise linear and alternative bi-state dampers are compared directly in terms of the peak relative displacement and peak absolute acceleration. For short duration bumps, the responses of the piece-wise linear and alternative bi-state dampers are simulated numerically for the damping ratios $\zeta = 0.2$ and 0.5 which typify the bounds on the damping ratio in most passenger cars.

5.4.1 Peak relative displacement

In the automotive application of interest in this thesis, the relative displacement can be considered as a measure of the clearance between the vehicle body and the suspension. The

constraint on this clearance is often referred to as the rattle space.

The normalised relative peak displacements of the two types of bi-state damper for a short duration bump ($t_p/t_n = 0.1$) are shown in Figure 5.7. These curves are plotted as a function of ratio of damping coefficients, α_p and α_s. The damping levels (i.e. in jounce or after the bump) are taken as ζ_r, $\zeta_a = 0.2$ and 0.5.

For ζ_r and $\zeta_a = 0.2$ and 0.5, there is no difference of the peak relative displacement for both types of bi-state dampers as shown Figures 5.7 (a), (b). This means that neither type of bi-state damping has any benefit in reducing the peak relative displacement for α_p, $\alpha_s < 1$.

5.4.2 Peak acceleration

The peak acceleration can be used as a measurement of ride comfort for human occupants and a criterion for damage on a vehicle and its components.

The normalised peak acceleration of the two types of bi-state damper for a short duration bump, are plotted for different damping ratios, ζ_r and $\zeta_a = 0.2$ and 0.5 as shown in Figures 5.8 (a) and (b). For ζ_r and $\zeta_a = 0.2$, there is no difference in peak acceleration between the two bi-state dampers when α_p and α_s are greater than 0.6. However, when α_p and $\alpha_s < 0.6$, the alternative bi-state damping model has a marginally better performance in reducing the peak acceleration.

For ζ_r and $\zeta_a = 0.5$, the apparent difference in performance of shock isolation between the two types of bi-state damping models can be seen in Figure 5.8 (b). The alternative bi-state damping model is superior to the piece-wise linear as the damping ratio increases ($\alpha_p, \alpha_s < 1$). In particular, in the peak acceleration response, the alternative bi-state damper gives significant

reduction of the peak acceleration as much as 80% of a linear damping in a ideal case ($\alpha_s = 0$). For α_p, $\alpha_s = 0.5$, a practically applicable value for an automotive damper, the alternative bi-state damper can reduce the peak acceleration as much as 45% of the piece-wise linear damper.

5.4.3 Discussion

In Section 5.4, the peak relative displacement and acceleration responses of bi-state dampers in a SDOF system have been found. The performances between the piece-wise linear and the alternative bi-state damping models have been evaluated and compared. It has been found that the peak acceleration can be reduced by either of the bi-state dampers compared with that of a simple linear damper. In particular, the alternative bi-state damper which switches at the start and end of the bump has a significant advantage; the peak acceleration can be reduced with little requirement for an increased rattle space. For short durations of the bump, it can be established that:

(1) The two types of bi-state damping can reduce the peak acceleration compared to the system with linear damping for α_p, $\alpha_s < 1$;

(2) For the piece-wise linear damper, the peak acceleration increases as the level of system damping increases, however, for the alternative bi-state damper, it decreases for α_p, $\alpha_s < 1$;

(3) In the minimisation of the peak relative displacement, the alternative bi-state damper has the same performance as the piece-wise linear damper;

(4) In reducing the peak acceleration, the alternative bi-state damper is superior to the piece-wise linear damper for α_p, $\alpha_s < 1$ and higher level of overall damping.

5.5 CONCLUSION

In this chapter, two types of bi-state damping have been discussed for shock isolation in a SDOF system with base displacement motion. The effects of the ratio of damping values in each state, the duration of the bump and the level of system damping were investigated in terms of the peak relative displacement and peak acceleration. A comparison between two types of bi-state damper based on a linear damper was shown.

The piece-wise linear damper gives better isolation of peak acceleration than a linear damper for a short duration bump when the ratio of damping coefficients α_p is smaller than 1. For a long duration bump, the piece-wise linear damping does not have merit in reducing peak acceleration. The alternative bi-state damper which switches on during the bump and off after the bump, has good advantages in reducing the peak acceleration relative to the piece-wise linear damper without the penalty of increasing the peak relative displacement when the ratio of damping coefficient α_s is less than 1.

The theoretical maximum gain of the alternative bi-state damper is presented as an analytical expression. From this relation, the benefit in reducing the peak acceleration of the alternative bi-state damper increases as the damping ratio and the frequency ratio becomes higher.

The two types of bi-state dampers have some benefit for shock isolation compared to a linear damper. In particular, the alternative bi-state damper proposed has more potential to reduce the peak acceleration than the piece-wise linear damper. Considering the possibilities for further reducing the peak acceleration, the alternative bi-state damper is a potential semi-active damper.

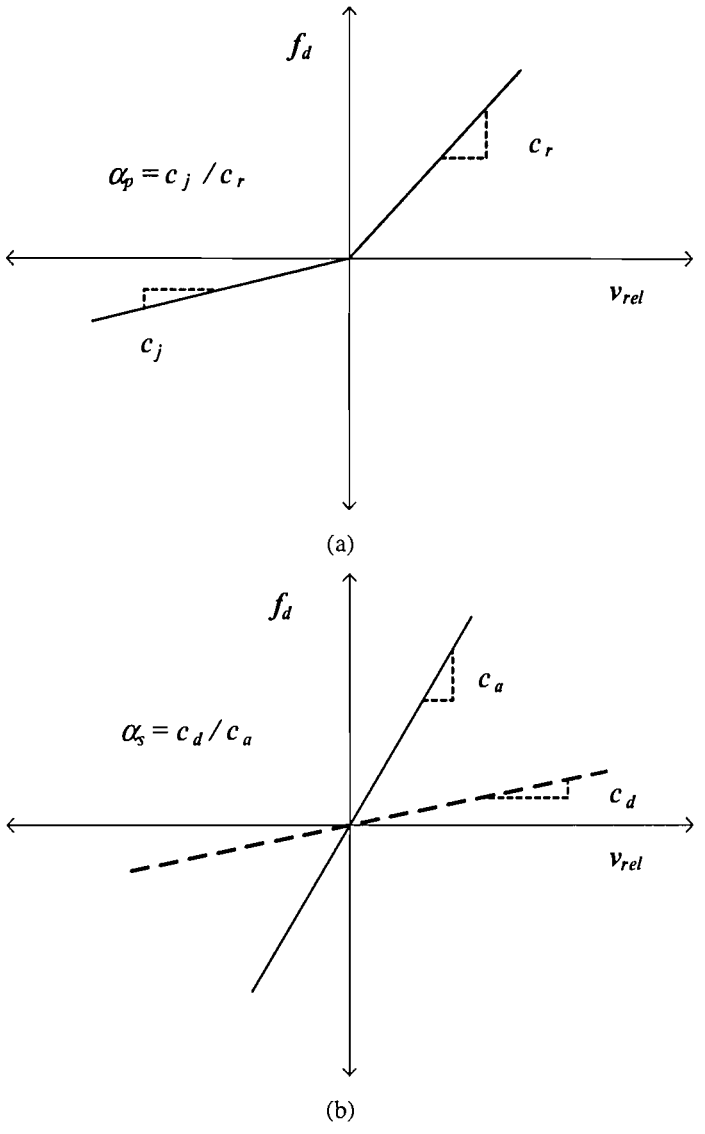

Figure 5.1: Characteristics of damping models. (a) a piece-wise linear damper, (b) an alternative bi-state damper switching at the start and end of a bump.

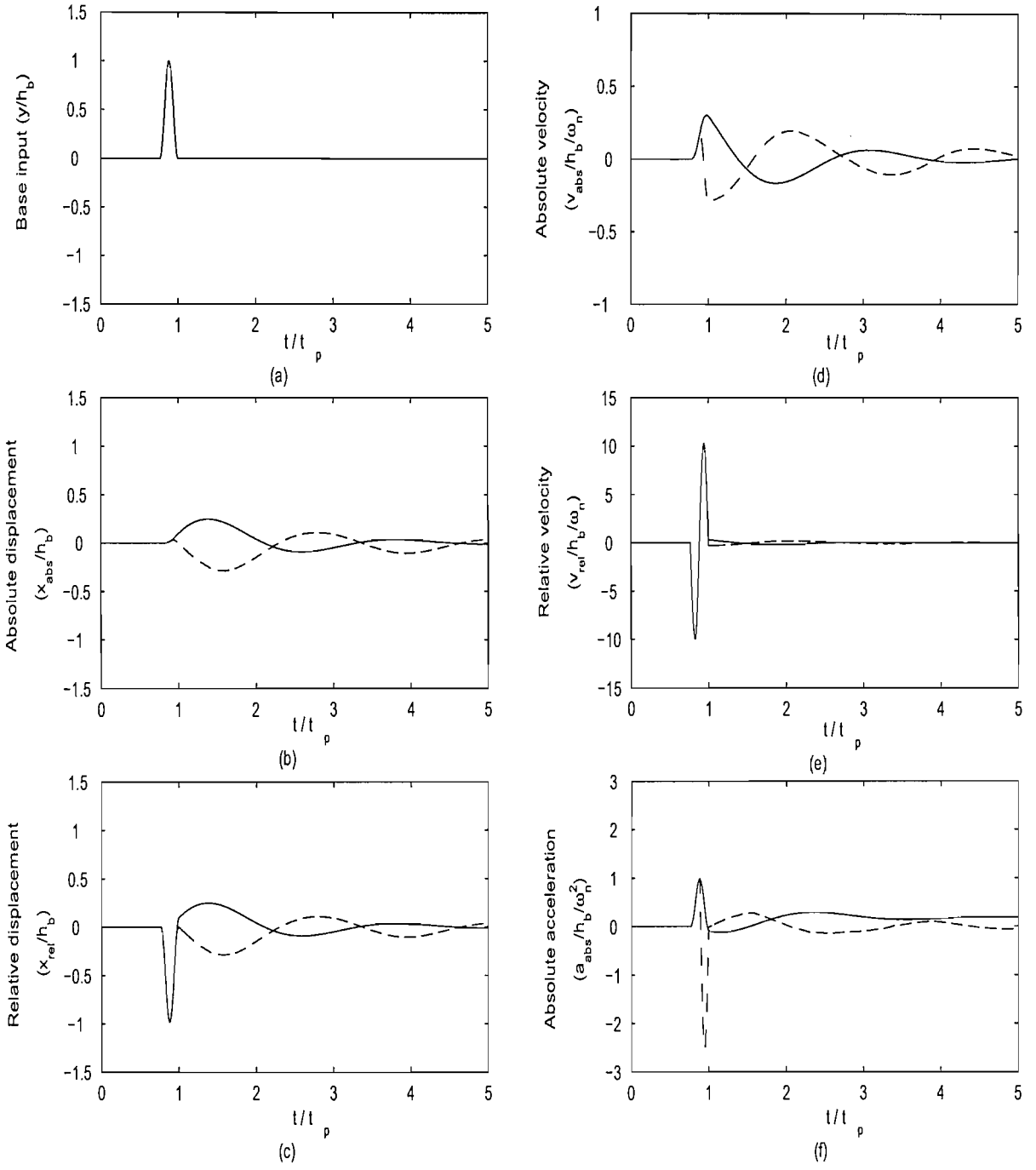

Figure 5.2: Comparison between time responses of the two types of bi-state damping. dashed line : piece-wise linear damping, solid line : alternative bi-state damping. (ζ_j and $\zeta_d = 0.0$, ζ_r and $\zeta_a = 0.3$, $t_n/t_p = 10$)

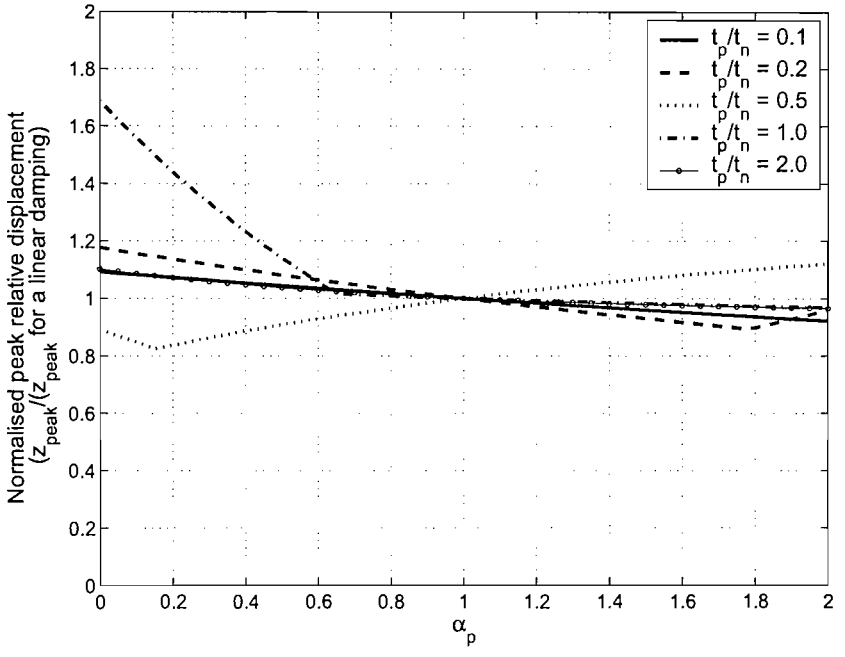

(a)

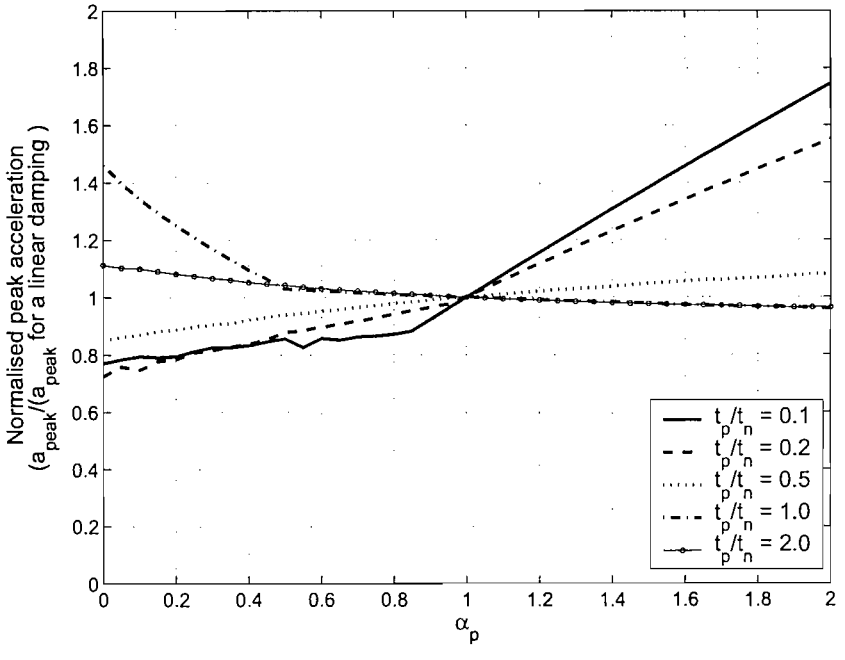

(b)

Figure 5.3: Normalised peak relative displacement (a) and normalised peak acceleration (b) as a function of the ratio of the damping coefficients α_p for the piece-wise linear damping corresponding to various durations of bump at a fixed rebound damping ratio, $\zeta_r = 0.3$.

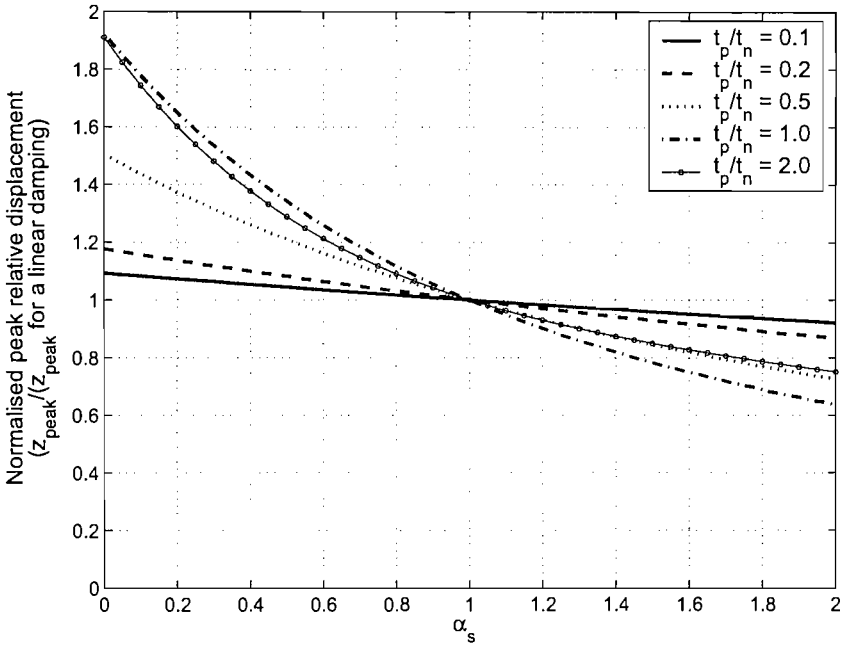

(a)

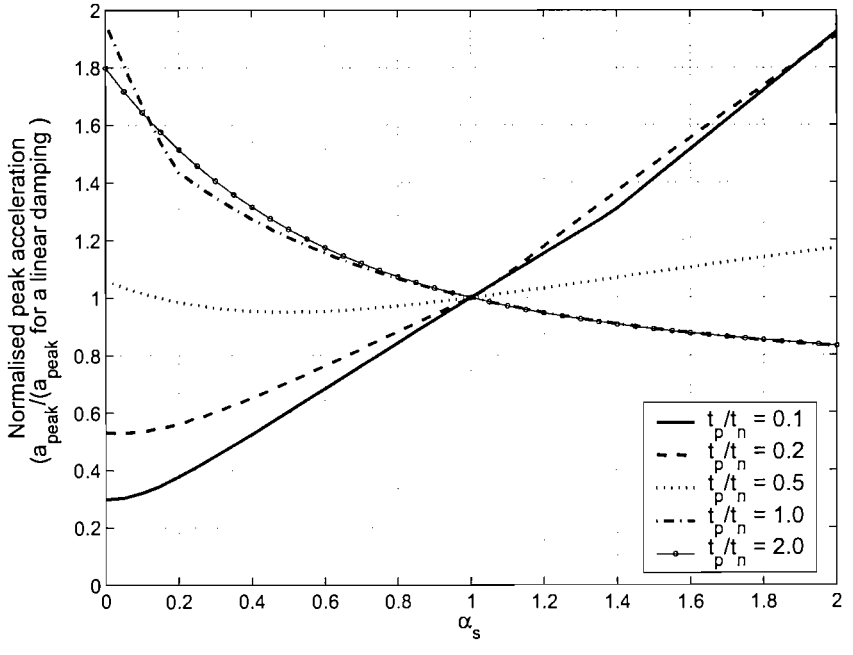

(b)

Figure 5.4: Normalised peak relative displacement (a) and normalised peak acceleration (b) as a function of the ratio of the damping coefficients α_s for the alternative bi-state damping, corresponding to various durations of bump at a fixed damping ratio $\zeta_a = 0.3$.

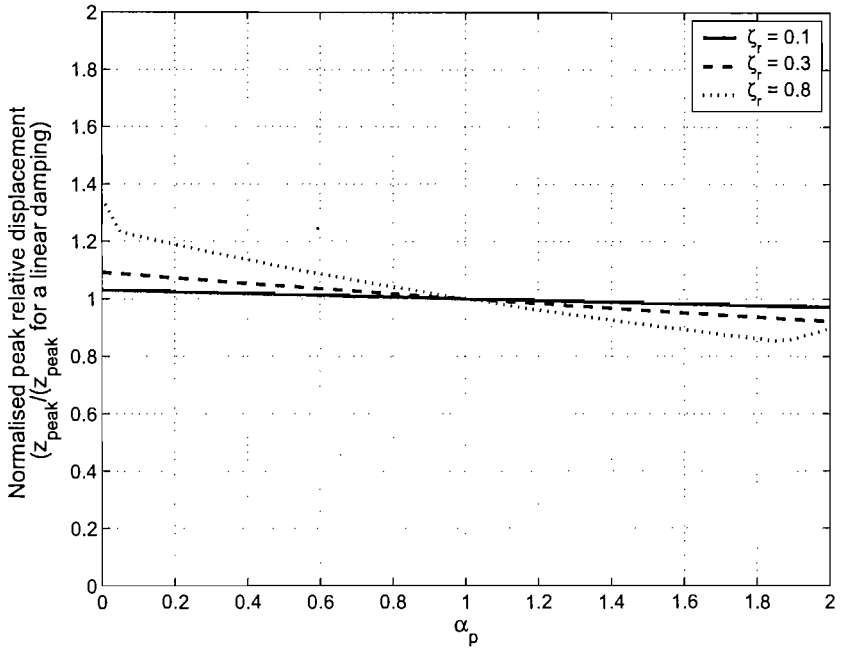

(a)

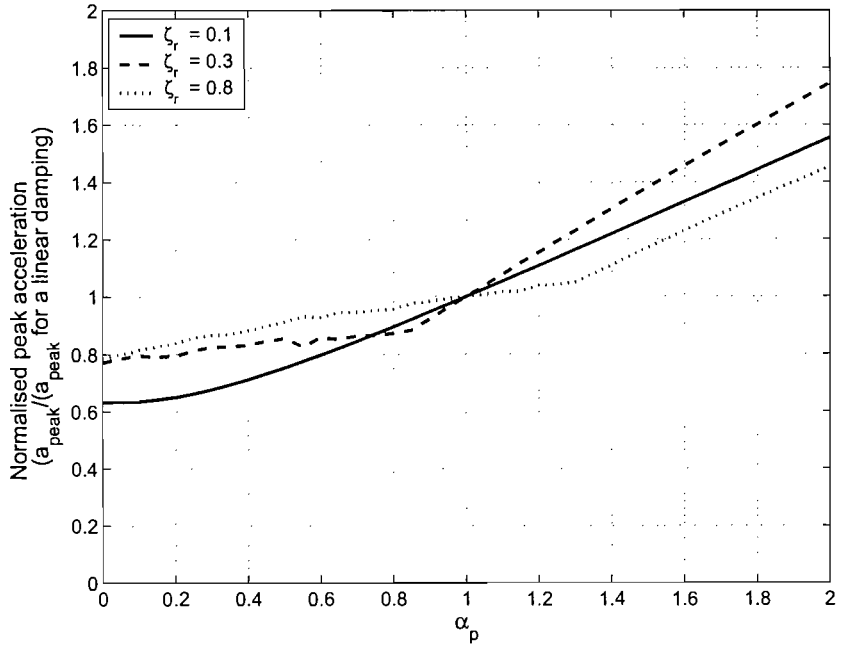

(b)

Figure 5.5: Normalised peak relative displacement (a) and normalised peak acceleration (b) as a function of the ratio of the damping coefficients α_p for the piece-wise linear damper corresponding to damping ratios $\zeta_r = 0.1, 0.3$ and 0.8 for a short duration bump ($t_p/t_n = 0.1$).

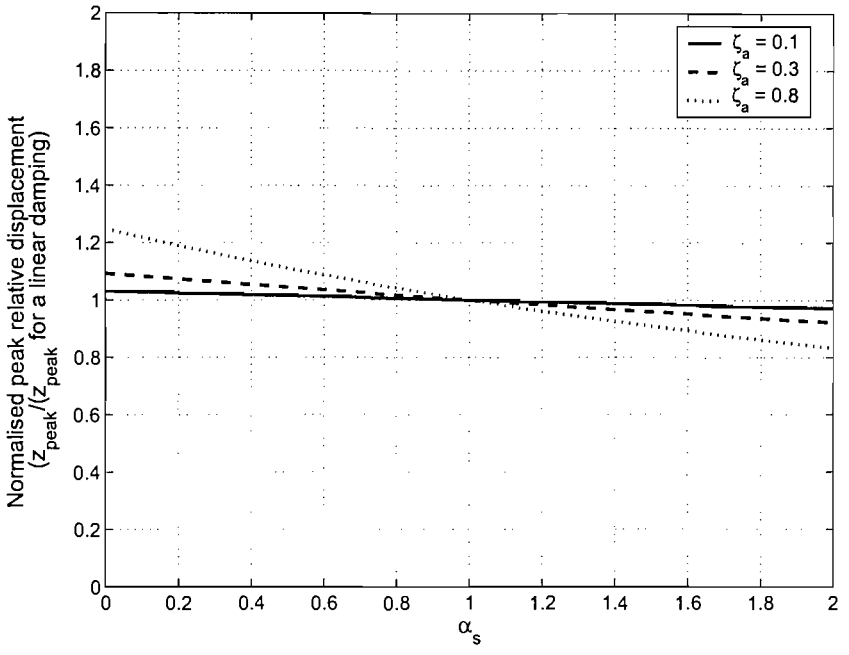

(a)

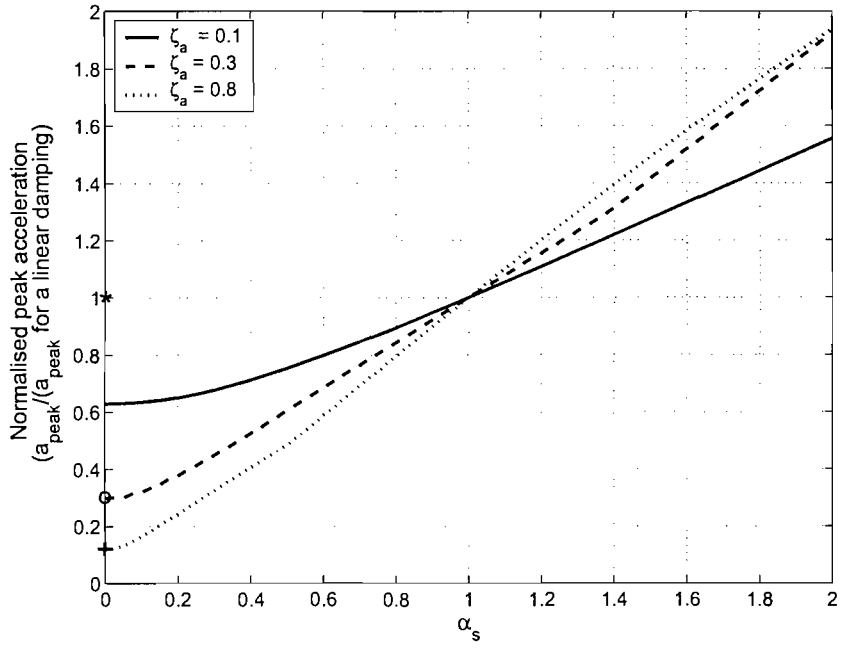

(b)

Figure 5.6: Normalised peak responses as a function of the ratio of the damping coefficients α_s in the alternative bi-state damper, corresponding to damping ratios after a bump $\zeta_a = 0.1, 0.3$ and 0.8 for a short duration bump ($t_p/t_n = 0.1$). Analytical approximations for $\alpha_s = 0$. (a) $*$: $\zeta = 0.1$, (b) o : $\zeta = 0.3$, (c) $+$: $\zeta = 0.8$.

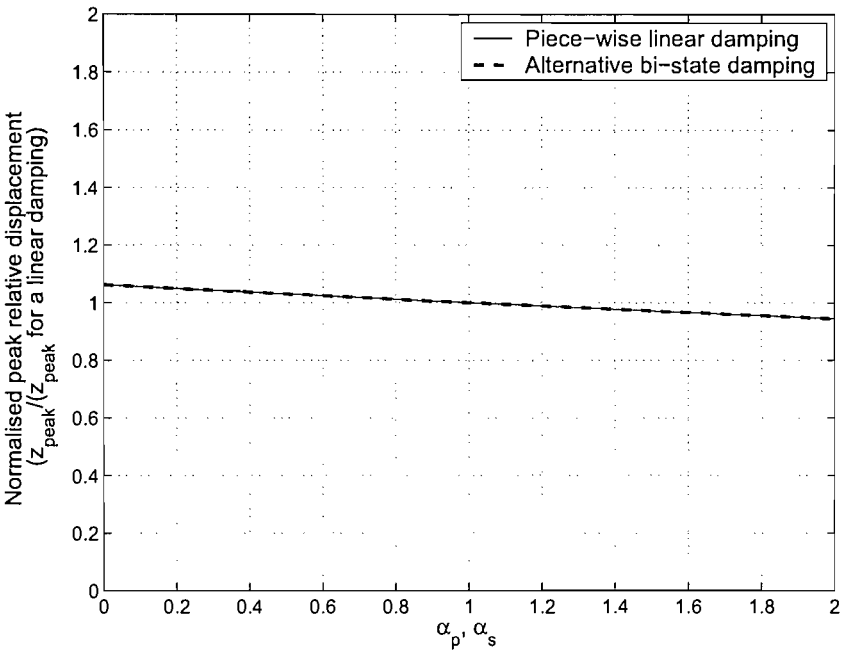

(a)

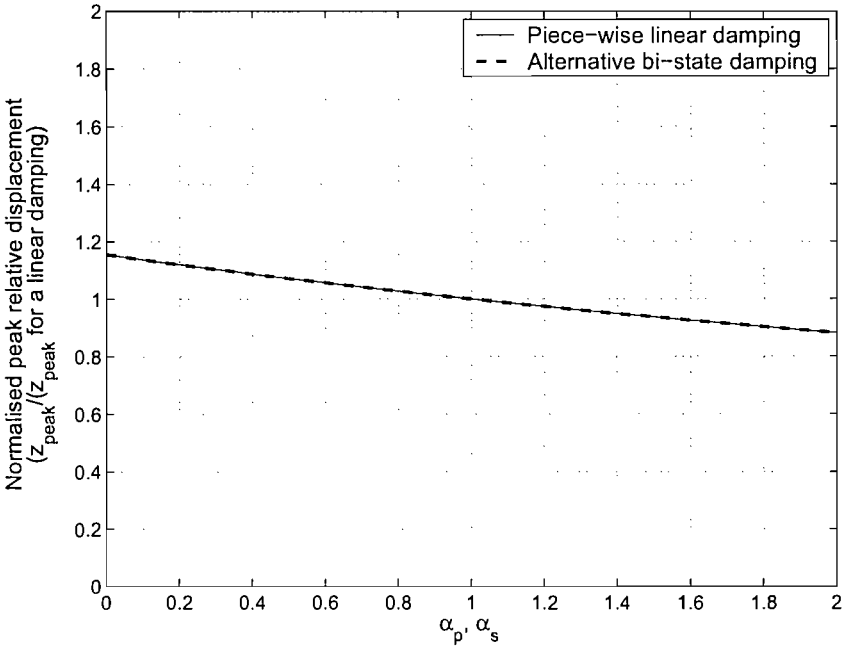

(b)

Figure 5.7: Comparison of normalised peak relative displacement between the piece-wise linear damping and the alternative bi-state damping in different damping ratios for a short duration bump ($t_p/t_n = 0.1$). (a) ζ_r and $\zeta_a = 0.2$, (b) ζ_r and $\zeta_a = 0.5$.

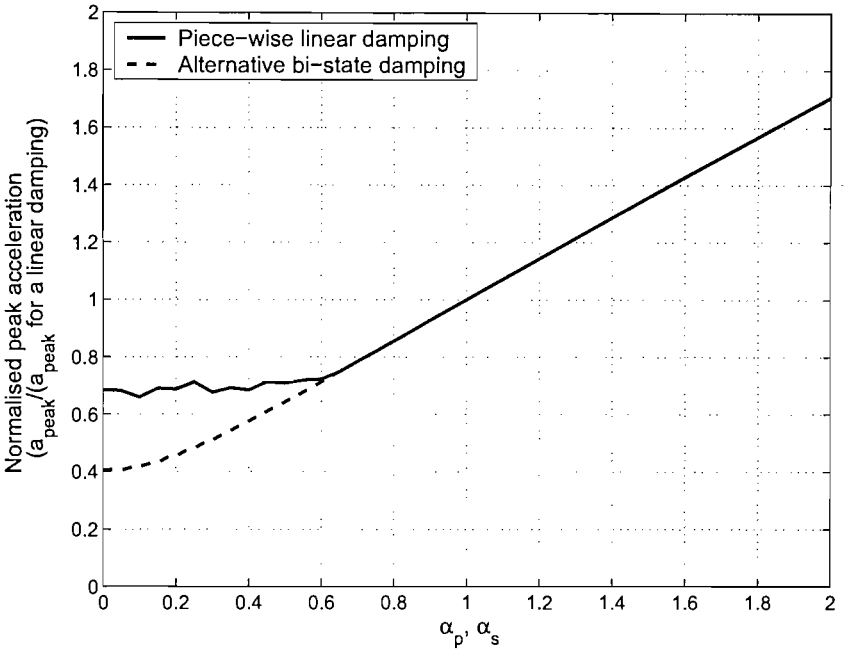

(a)

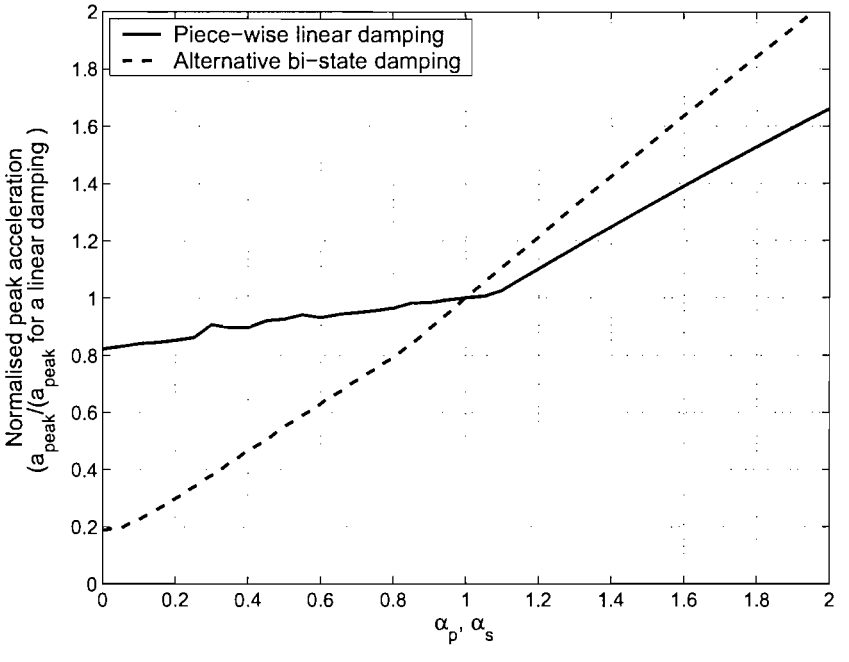

(b)

Figure 5.8: Comparison of normalised peak acceleration between the piece-wise damping and alternative bi-state damping in different damping ratios for a short duration bump ($t_p/t_n = 0.1$). (a) ζ_r and $\zeta_a = 0.2$, (b) ζ_r and $\zeta_a = 0.5$.

CHAPTER 6

GENERAL CONCLUSIONS

6.1 CONCLUSIONS

This chapter contains the general conclusions of this thesis. The details of the research in this thesis discussed in the previous chapters are summarised, and recommendations for future work are given. The aim has been to analyse suspension models of a vehicle with linear and bi-state damping excited by a single versed-sine displacement base motion using the numerical and analytical methods in order to investigate the relationship between peak responses and system parameters and present a switchable damper model in terms of shock isolation.

The introduction of this thesis and a literature review were presented in Chapter 1. In Chapter 2, the transient motion of a linear SDOF system with a versed sine base motion was reviewed using numerical and analytical methods. In the numerical method, the Runge-Kutta method, which is widely used to solve the differential equations, was adopted. In the analytical method, using Laplace transforms, the exact solution was presented using normalised parameters for the transient response. While the response of the system for the duration of the bump was mainly affected by the base excited motion, it was attenuated by damping during in free vibration after the bump.

In Chapter 3, the physical parameters which affect the response of a linear SDOF system were investigated in the time domain and the results presented using the shock response spectrum. The influence of physical parameters such as the damping ζ and the frequency ratio r of the system were analysed using the Taylor series approximation. The approximations allow the physical relationships between system parameters and responses to be expressed with sim-

ple equations. The role and effects of damping in transient vibration can then be investigated easily. It was found that for a short duration bump, the normalised peak acceleration is approximately proportional to the damping ratio and the frequency ratio, and for a long duration bump, the normalised peak acceleration is proportional to the square of the frequency ratio.

Using the two DOF quarter car model, the effect of base mass on the system responses and validity and limitation of the relationship between the peak acceleration and system parameters were investigated by numerical simulations. The peak acceleration response of the two DOF quarter car model was compared with that of the SDOF system. The approximate relationship between the peak acceleration and damping ratio ζ and the frequency ratio r in the SDOF system can be extended for the two DOF quarter car model for short duration bumps in a certain frequency range ($3 < r < 10$) and for long duration bumps. However, for a very short duration bump, this relationship may not be valid due to the effects of the unsprung mass. The relationship between the peak acceleration and system parameters measured experimentally in a passenger car was in good agreement with the simulation results of the two DOF system for limited frequency range.

In Chapter 4, a practical hydraulic automotive damper with a twin tube was discussed with reference to its non-linear characteristics. The fundamental principle for a viscous damping force can be expressed as the resistance to fluid flow, which is caused by the difference of pressure acting on both sides of the piston valve. The fluid flow is elaborately controlled by the bleed, blow-off valve and piston hole. From the experimental data of damping force and velocity in a practical damper, the non-linear relationship between the damping force and relative velocity was able to be modelled by a piece-wise linear system. This means that a simple mathematical relationship between the relative velocity and damping force could be expressed to give a convenient model for shock isolation problems.

In Chapter 5, A two state piece-wise linear damper and a new switchable damper were presented and compared for shock isolation in a SDOF system with a versed-sine displacement input of the base. The new strategy of a switchable damper, namely an alternative bi-state damper, is to switch it off while the bump is being traversed and to switch it on after the bump has been traversed. The ratios of the damping coefficients α_p of a piece-wise linear damper and α_s of an alternative bi-state damper were introduced to investigate the effect of duration of the bump and overall damping level. Generally, if the ratios of damping coefficients α_p, α_s is smaller than 1, the peak acceleration for the system with two bi-state dampers was smaller than when a linear damper is used. For a short duration, and the ratios of damping coefficients α_s, α_p smaller than 1, the alternative bi-state damper was able to further reduce the peak acceleration compared to the piece-wise linear damper as the level of damping was higher. The alternative bi-state damper was superior to the piece-wise linear damper in reducing the peak acceleration without the penalty of increasing the amplitude of the peak relative displacement for bumps of short duration. The alternative bi-state damping device has potential for a use in semi-active system.

In this work, the role and effect of damping in a vehicle traversing a bump was discussed using the approximate relationships between responses and parameters in a SDOF system. The validity and limitations of this relationship can be determined by comparing the results with a two DOF quarter car system and those from an experiment involving a passenger car. It was shown that the alternative bi-state damper which switches at the start and end of the bump has a better performance than the piece-wise linear damper in terms of shock isolation.

6.2 SUGGESTIONS FOR FUTURE WORK

The work in this dissertation has studied the peak response of suspension models subject to a shock input. Using bi-state dampers, the peak responses were investigated in terms of shock isolation. As far as future work is concerned, practical control strategies using the alternative bi-state damper can be investigated. This will require a suitable choice of the condition function to control when the alternative bi-state damper is switched on and off. It is important to observe which response quantity or combination of quantities are indicative of the start and end of the bump.

The effect of the alternative bi-state damper on the response to random excitation should be investigated to ensure that the improvement in shock isolation is not off-set by an increase in RMS response of a vehicle.

APPENDIX A. Runge-Kutta method

The Runge-Kutta computation procedure is popular because it gives an accurate solution. The 4^{th} order Runge-Kutta method is a single-step method with constant step size. With a constant step size, the total elapsed time taken can be estimated accuracy for each simulation, to ensure that the numeric integration routine is always stable, which is not always true for adaptive step size methods [29]. Care should be taken to ensure that the step size is much smaller than the duration of pulse input for a SDOF system.

The 4^{th} order Runge-Kutta method, which provides a numerical solution to $\dot{z} = f(x)$ with $z(0) = z_o$ and $\dot{z}(0) = \dot{z}_o$ and a constant step size (time step) h, can be stated as follows:

$$z(t+h) = z(t) + \frac{1}{6}(F_1 + 2F_2 + 2F_3 + F_4) \tag{A.1}$$

where,

$$F_1 = hf(t, x) \tag{A.2a}$$

$$F_2 = hf(t + \frac{1}{2}h, z + \frac{1}{2}F_1) \tag{A.2b}$$

$$F_3 = hf(t + \frac{1}{2}h, z + \frac{1}{2}F_2) \tag{A.2c}$$

$$F_4 = hf(t + h, z + F_3) \tag{A.2d}$$

Therefore, consider the differential equation for the SDOF system, which can be written as

$$\ddot{z} = f(t) - 2\zeta\omega_n\dot{z} - \omega_n^2 z = F(z, \dot{z}, t) \tag{A.3}$$

By letting $\dot{z} = w$, this equation is reduced to the following two first-order differential equations:

$$\dot{z} = w \tag{A.4a}$$

$$\dot{w} = F(z, w, t) \tag{A.4b}$$

Both z and w can be expressed using the Taylor series and ignoring the higher-order terms:

$$z_1 = z_o + \dot{z}h \tag{A.5a}$$

$$w_1 = w_o + \dot{w}h \tag{A.5b}$$

where, $z_o = z(0)$ and $w_o = \dot{z}(0)$ from initial conditions.

Therefore, the next step of z and w can be used in the following recurrence relations:

$$z_{i+1} = z_i + \frac{h}{6}(W_1 + 2W_2 + 2W_3 + W_4) \tag{A.6a}$$

$$W_{i+1} = W_i + \frac{h}{6}(F_1 + 2F_2 + 2F_3 + F_4) \tag{A.6b}$$

In MATLAB the Runge-Kutta method has been embedded in ODE45 solver which is widely used to solve second-order differential equations.

APPENDIX B. THE LAPLACE TRANSFORMS

B.1. Table of Laplace transforms

$f(t) = \mathcal{L}^{-1}[F(s)]$	$F(s) = \mathcal{L}[f(t)]$
$\int_{\sigma-j\infty}^{\sigma+j\infty} F(s)e^{st}ds$	$\int_0^\infty f(t)e^{-st}dt$
$af(t) = bg(t)$	$aF(s) + bG(s)$
$f'(t)$	$sF(s) - f(0)$
$f''(t)$	$s^2F(s) - sf(0) - f'(0)$
$\int_a^t f(t)dt$	$\frac{1}{s}F(s) - \frac{1}{s}\int_0^a f(t)dt$
$tf(t)$	$-f'(s)$
$\delta(t)$	1
$u(t)$	$\frac{1}{s}$
$u(t-a)$	$\frac{e^{-as}}{s}$
t	$\frac{1}{s^2}$
t^n	$\frac{\Gamma(n+1)}{S^{n+1}}, n > -1$
e^{-at}	$\frac{1}{s+a}$
te^{-at}	$\frac{1}{(s+a)^2}$
$\sin bt$	$\frac{b}{s^2+b^2}$
$\cos bt$	$\frac{s}{s^2+b^2}$
$e^{-at}\sin bt$	$\frac{b}{(s+a)^2+b^2}$
$e^{-at}\cos bt$	$\frac{s}{(s+a)^2+b^2}$
$e^{-at}(\cos bt + \frac{c-a}{b}\sin bt)$	$\frac{s+c}{(s+a)^2+b^2}$
$\frac{1}{b-a}(ae^{-at} - be^{-bt})$	$\frac{s}{(s+a)(s+b)}, a \neq b$

B.2. Partial Fraction

Generally, in order to break a complicated function $F(s)$ into a sum of simpler terms with known inverse Laplace transforms, partial fractions can be used. Any fraction with a polynomial denominator can be expressed as the sum of terms with first order denominators. The simpler terms are much easier to invert using tables of Laplace transforms. If a complicated function $F(s)$ can be expressed as,

$$F(s) = \frac{N(s)}{M(s)} = \frac{a_0 s^n + a_1 s^{n-1} + \cdots + a_n}{b_0 s^n + b_1 s^{n-1} + \cdots + b_n} \tag{B.1}$$

where, $N(s)$ and $M(s)$ are polynomials of degree n and m, respectively, with $m > n$, then $F(s)$ can be rewritten in the form

$$F(s) = \frac{A_1}{s - s_1} + \frac{A_2}{s - s_2} + \cdots + \frac{A_m}{s - s_m} \tag{B.2}$$

where, $s_1, s_2, \cdots, s_m$ are the roots of the algebraic equation

$$M(s) = 0 \tag{B.3}$$

Therefore, the inverse Laplace transform of $F(s)$ can be written as

$$\mathcal{L}^{-1}[F(s)] = A_1 e^{s_1 t} + A_2 e^{s_2 t} + \cdots + A_m e^{s_m t}$$

For example, in Section 2, equation (2.13) can be rewritten as

$$Z(s) = \left(\frac{\dot{z}(0) + (s + 2\zeta\omega_n)z(0)}{s^2 + 2\zeta\omega_n s + \omega_n^2}\right) + \left(\frac{-\frac{1}{2}\omega^2 s}{s^2 + \omega^2}\right)\left(\frac{1}{s^2 + 2\zeta\omega_n s + \omega_n^2}\right) \tag{B.4}$$

The term in the first set of brackets is determined by the initial condition of system, and the terms in the second and third set of brackets are determined by input acceleration of *cosine* function. Therefore, equation (2.13) can be rewritten as

$$Z(s) = Z_1(s) + Z_2(s) \tag{B.5}$$

where, $Z_1(s)$ is considered as free vibration from initial condition before or after bumping and $Z_2(s)$ is considered as forced vibration during bumping. The inverse Laplace transforms of $Z_1(s)$ and $Z_2(s)$ can be separately shown as below:

$$\begin{aligned} Z_1(s) &= \frac{\dot{z}(0) + (s + 2\zeta\omega_n)z(0)}{s^2 + 2\zeta\omega_n s + \omega_n^2} = \frac{(s + \zeta\omega_n)z(0)}{(s + \zeta\omega_n)^2 + \omega_d^2} + \frac{\dot{z}(0) + \zeta\omega_n z(0)}{(s + \zeta\omega_n)^2 + \omega_d^2} \\ &= \frac{(s + \zeta\omega_n)z(0)}{(s + \zeta\omega_n)^2 + \omega_d^2} + \frac{\omega_d}{(s + \zeta\omega_n)^2 + \omega_d^2}\frac{\dot{z}(0) + \zeta\omega_n z(0)}{\omega_d} \end{aligned}$$

Using the table of Laplace transforms, the inverse Laplace transform of $Z_1(s)$ is given by

$$\begin{aligned} z_1(t) &= z(0)e^{-\zeta\omega_n t}\cos\omega_d t + \frac{\dot{z}(0) + \zeta\omega_n z(0)}{\omega_d}e^{-\zeta\omega_n t}\sin\omega_d t \\ &= e^{-\zeta\omega_n t}\left(z(0)\cos\omega_d t + \frac{\dot{z}(0) + \zeta\omega_n z(0)}{\omega_d}\sin\omega_d t\right) \end{aligned} \tag{B.6}$$

The initial conditions at $t = 0$ are $z(0) = \dot{z}(0) = 0$, so $z_1(0) = 0$. At time $t = t_p$ when

the vehicle has traversed the bump, then $z_1(t)$ is given by,

$$z_1(t) = e^{-\zeta\omega_n(t-t_p)}\left(z(t_p)\cos\omega_d(t-t_p) + \frac{\dot{z}(t_p)+\zeta\omega_n z(t_p)}{\omega_d}\sin\omega_d(t-t_p)\right) \tag{B.7}$$

$Z_2(s)$ is given by

$$Z_2(s) = \left(\frac{-0.5\omega^2 s}{s^2+\omega^2}\right)\left(\frac{1}{s^2+2\zeta\omega_n s+\omega_n^2}\right) = -0.5\omega^2\left(\frac{s}{s^2+\omega^2}\right)\left(\frac{1}{s^2+2\zeta\omega_n s+\omega_n^2}\right) \tag{B.8}$$

Using the partial fraction, equation (B.8) can be decomposed as

$$Z_2(s) = -0.5\omega^2\left(\frac{A_1 s + A_2}{s^2+\omega^2} + \frac{A_3 s + A_4}{s^2+2\zeta\omega_n s+\omega_n^2}\right) \tag{B.9}$$

where the coefficients A_1, A_2, A_3, and A_4 are given by

$$\begin{aligned} A_1 &= \frac{\omega_n^2-\omega^2}{(2\zeta\omega\omega_n)^2+(\omega_n^2-\omega^2)^2}\,,\; A_2 = \frac{2\zeta\omega^2\omega_n}{(2\zeta\omega\omega_n)^2+(\omega_n^2-\omega^2)^2} \\ A_3 &= -\frac{\omega_n^2-\omega^2}{(2\zeta\omega\omega_n)^2+(\omega_n^2-\omega^2)^2}\,,\; A_4 = -\frac{2\zeta\omega_n^3}{(2\zeta\omega\omega_n)^2+(\omega_n^2-\omega^2)^2} \end{aligned}$$

Therefore, equation (B.9) can be written as

$$\begin{aligned} Z_2(s) &= \frac{-0.5\omega^2}{s^2+\omega^2}\frac{(\omega_n^2-\omega^2)s+2\zeta\omega^2\omega_n}{(2\zeta\omega\omega_n)^2+(\omega_n^2-\omega^2)^2} \\ &\quad -\left(\frac{-0.5\omega^2}{s^2+2\zeta\omega_n s+\omega_n^2}\right)\left(\frac{(\omega_n^2-\omega^2)s+2\zeta\omega_n^3}{(2\zeta\omega\omega_n)^2+(\omega_n^2-\omega^2)^2}\right) \\ &= \left(\frac{-0.5\omega^2(\omega_n^2-\omega^2)}{(2\zeta\omega\omega_n)^2+(\omega_n^2-\omega^2)^2}\right)\left(\frac{s+\frac{2\zeta\omega^2\omega_n}{\omega_n^2-\omega^2}}{s^2+\omega^2}\right) \\ &\quad -\left(\frac{-0.5\omega^2(\omega_n^2-\omega^2)}{(2\zeta\omega\omega_n)^2+(\omega_n^2-\omega^2)^2}\right)\left(\frac{s+\frac{2\zeta\omega_n^3}{\omega_n^2-\omega^2}}{s^2+2\zeta\omega_n s+\omega_n^2}\right) \end{aligned} \tag{B.10}$$

Using the table of Laplace transforms, the inverse Laplace transform of $Z_2(s)$ is given by

$$z_2(t) = \left(\frac{-0.5\omega^2(\omega_n^2-\omega^2)}{(2\zeta\omega\omega_n)^2+(\omega_n^2-\omega^2)^2}\right) \left((\cos\omega t + \frac{2\zeta\omega\omega_n}{\omega_n^2-\omega^2}\sin\omega t) - e^{-\zeta\omega_n t}(\cos\omega_d t + \frac{\zeta\omega_n(\omega_n^2+\omega^2)}{(\omega_n^2-\omega^2)\omega_d}\sin\omega_d t)\right) \quad \text{(B.11)}$$

APPENDIX C. Approximation for response spectrum

To simplify a long equation such as equation (2.24), a Taylor's expansion of the equation can be used. Generally, the Taylor series are most useful when it is possible to truncate the infinite sum and use only the first few terms of the series. Since x is usually small ($x < 1$), the higher order terms will all contain higher powers of x which should mean that they will be smaller than the first few terms. Truncating the series can lead to a reasonable approximation. A *sine*, *cosine* and *exponential* function can be simplified by taking the lower order terms of x as below,

$$\sin x = x - \frac{x^3}{3!} + \frac{x^5}{5!} - \cdots + O(x^n) \tag{C.1a}$$

$$\cos x = 1 - \frac{x^2}{2!} + \frac{x^4}{4!} - \cdots + O(x^n) \tag{C.1b}$$

$$e^x = 1 + \frac{x}{1!} + \frac{x^2}{2!} + \cdots + O(x^n) \tag{C.1c}$$

$$(1+x)^m = 1 + mx + \frac{m(m-1)}{2!}x^2 + \cdots + O(x^n) \tag{C.1d}$$

where, $O(x^n)$ is the higher order terms which can be neglected if x is smaller than 1.

For a short duration bump, the acceleration spectrum can be approximated using the Taylor series expansion and elimination of higher terms of the frequency ratio r. A frequency ratio r, much greater than 1, can be regarded as representing a bump of short duration. Therefore, for $1/r$, much smaller than 1, the exact solution of acceleration response can be simplified. To approximate equation (2.24), the normalised acceleration, $\ddot{x}(\tilde{t})/\omega_n^2 h_b$ can be expressed as shown in equation (2.25)

$$\frac{\ddot{x}(\tilde{t})}{\omega_n^2 h_b} = a(r)\left\{b(r) + c(r) + d(r)\right\} + e(r) \ , \quad 0 \leq \tilde{t} \leq 1 \tag{C.2}$$

where, r is ω/ω_n, h_b is height of a bump and

$$a(r) = \frac{1/2r^2(1-r^2)}{(2\zeta r)^2+(1-r^2)^2} \tag{C.3a}$$

$$b(r) = r^2\left(\cos 2\pi\tilde{t} + \frac{2\zeta r}{1-r^2}\sin 2\pi\tilde{t}\right) \tag{C.3b}$$

$$c(r) = \left(2\zeta^2 - \frac{2\zeta^2(1+r^2)}{(1-r^2)} - 1\right)e^{-2\pi\zeta\frac{1}{r}\tilde{t}}\cos 2\pi\sqrt{1-\zeta^2}\frac{1}{r}\tilde{t} \tag{C.3c}$$

$$d(r) = \left\{\frac{\zeta^3}{\sqrt{1-\zeta^2}}\frac{(1+r^2)}{(1-r^2)} + 2\zeta(1-\zeta^2)^2 - \zeta(\sqrt{1-\zeta^2})\frac{(1+r^2)}{(1-r^2)}\right\}$$
$$e^{-2\pi\zeta\frac{1}{r}\tilde{t}}\sin 2\pi\sqrt{1-\zeta^2}\frac{1}{r}\tilde{t} \tag{C.3d}$$

$$e(r) = \frac{1}{2}r^2\cos 2\pi\tilde{t} \tag{C.3e}$$

These equations can be simplified by using the condition that the frequency ratio r, is much greater than 1. First of all, the order of r in each term of equation (C.2) should be investigated in order to decide the order of r taken. $a(r)$, $c(r)$ and $e(r)$ are the zeroth order $O(r^0)$, $b(r)$ is the second order $O(r^2)$ and finally $d(r)$ is $O(\frac{1}{r})$ which do not need to be expanded. Therefore, $a(r)$ can be expanded as

$$\begin{aligned} a(r) &= \frac{1/2r^2(1-r^2)}{(2\zeta r)^2+(1-r^2)^2} = \frac{-1/2r^2(1-1/r^2)}{(2\zeta)^2/r^2+(1-1/r^2)^2} \\ &= \frac{-1/2r^2(1-1/r^2)}{(2\zeta)^2/r^2+(1-\frac{2}{r^2}+\frac{1}{r^4})^2} \\ &= -1/2(1-\frac{1}{r^2})(1+2(4\zeta^2-1)\frac{1}{r^2}+\frac{1}{r^4})^{-1} \\ &= -\frac{1}{2}-\frac{1}{2r^2}(1-4\zeta^2)+O(\frac{1}{r^4}) \end{aligned} \tag{C.4}$$

where, $O(\frac{1}{r^4})$ is the fourth or lower order of $1/r$. $a(r)$ should be expanded to keep $O(\frac{1}{r^2})$ since there are terms of $O(r^2)$ inside bracket in equation (C.2).

$b(r)$ can be expanded as

$$\begin{aligned} b(r) &= r^2(\cos 2\pi\tilde{t} + \frac{2\zeta r}{1-r^2}\sin 2\pi\tilde{t}) \\ &= r^2(\cos 2\pi\tilde{t} + \frac{2\zeta/r}{1-\frac{1}{r^2}}\sin 2\pi\tilde{t}) \\ &= r^2(\cos 2\pi\tilde{t} + 2\zeta/r(1-\frac{1}{r^2})^{-1}\sin 2\pi\tilde{t}) \\ &= r^2(\cos 2\pi\tilde{t} - 2\zeta/r\sin 2\pi\tilde{t}) + O(\frac{1}{r}) \end{aligned} \tag{C.5}$$

$O(\frac{1}{r})$ is the first or lower order of $1/r$.

$c(r)$ can be expanded as

$$\begin{aligned} c(r) &= (2\zeta^2 - \frac{2\zeta^2(1+r^2)}{1-r^2} - 1)e^{-2\pi\zeta\frac{1}{r}\tilde{t}}\cos(2\pi\sqrt{1-\zeta^2}\frac{1}{r}\tilde{t}) \\ &= (2\zeta^2 - \frac{2\zeta^2(\frac{1}{r^2}+1)}{\frac{1}{r^2}-1} - 1)e^{-2\pi\zeta\frac{1}{r}\tilde{t}}\cos(2\pi\sqrt{1-\zeta^2}\frac{1}{r}\tilde{t}) \\ &= (2\zeta^2 + 2\zeta^2(\frac{1}{r^2}+1)(1-\frac{1}{r^2})^{-1} - 1)e^{-2\pi\zeta\frac{1}{r}\tilde{t}}\cos(2\pi\sqrt{1-\zeta^2}\frac{1}{r}\tilde{t}) \\ &= (2\zeta^2 + 2\zeta^2(1+O(\frac{1}{r^2}) - 1)e^{-2\pi\zeta\frac{1}{r}\tilde{t}}\cos(2\pi\sqrt{1-\zeta^2}\frac{1}{r}\tilde{t}) \\ &= (4\zeta^2 - 14\zeta^2 - 1 + O(\frac{1}{r^2}))(1 - 2\pi\zeta\frac{1}{r}\tilde{t} + O(\frac{1}{r^2}))(1+O(\frac{1}{r^2})) \\ &= (4\zeta^2-1)(1+2\pi\zeta\frac{1}{r}\tilde{t}) + O(\frac{1}{r^2}) \end{aligned} \tag{C.6}$$

$O(\frac{1}{r^2})$ is the second or lower order of $1/r$.

Finally, when all terms are collated, the equation (C.2) can be expressed as

$$\begin{aligned} \frac{\ddot{x}(\tilde{t})}{\omega_n^2 h_b} &= -\left\{\frac{1}{2} + \frac{1}{2r}(1-4\zeta^2)\right\}\left\{(r^2\cos 2\pi\tilde{t} - 2\zeta r\sin 2\pi\tilde{t}) + (4\zeta^2-1)(1+2\pi\frac{\zeta}{r}\tilde{t}\right\} \\ &\quad + \frac{1}{2}r^2\cos 2\pi\tilde{t} + O(\frac{1}{r}),\ \ 0 \le \tilde{t} \le 1 \\ &= \zeta r\sin 2\pi\tilde{t} - \frac{1}{2}(1-4\zeta^2)\cos 2\pi\tilde{t} + \frac{1}{2}(1-4\zeta^2) + O(\frac{1}{r}),\ \ 0 \le \tilde{t} \le 1 \end{aligned} \tag{C.7}$$

where, $O(\frac{1}{r})$ is the low order term which can be ignored.

APPENDIX D. List of equipment used for experiments

Equipment	Serial number	Quantity
Passenger car (Chrysler Neon 2.0 auto)		1
Charge Amplifier with low frequency option	ADAUCA01	4
AD Converter (PMD 1608FS 16 bit USB interface)	ADAUCA01	1
Pulse type Speedometer (Peiseler MT100KFZ)	101.1177	1
B&K Accelerometer (4384 type)	1416873	1
	1417228	1
	1417231	1
	1417230	1
Data acquisition software (EngWaves ver.2.3)		
Commercial speed bump		2
12 Volt Battery box		1

REFERENCES

[1] C.M. Harris 2002 *Shock and Vibration Handbook(5^{th} edition)*, 31.6-31.39. New York: McGraw-Hill.

[2] S.S. Rao 1990 *Mechanical Vibration(2^{nd} edition)*. New York: Addison-Wesley Inc.

[3] T.D Gillespie 1992, *Fundamental of Vehicle Dynamics*. Warrendale, PA: Society of Automotive Engineers Inc.

[4] W.T. Thomson 1993 *Theory of Vibration with Applications*. London: Chapman & Hall.

[5] R.D Mindlin 1945 *Bell System Technical Journal,* **24:**353-467. Dynamics of Package Cushioning.

[6] J.C. Snowdon 1968, *Vibration and Shock in damped mechanical systems*. New York: John Wiley and Sons, Inc.

[7] M.S. Hundal 1980 *Journal of Sound and Vibration*, **76**(1):273-281. Response of shock isolators with linear and quadratic damping.

[8] D.C Karnopp, M.J. Crosby and R.A. Harwood 1974, *ASME Journal of Engineering for Industry* **96**: 619-626. Vibration control using semi-active force generators.

[9] S.J. Elliot, M. Serrand and P. Gardonio 2001, Transactions of the *ASME Journal of Vibration and Acoustics*, **123**: 250-261. Feedback stability limits for active isolation systems with reactive and inertial actuators.

[10] M. Ahmadian, B. Reichert and X. Song 1997, *ASME Design Engineering Technical Conferences*: 14-17. Sacramento, California. Harmonic Analysis of Semi-active Suspension.

[11] N. Jalili 2002, Transactions of the *ASME Journal of Vibration and Acoustics* **124**: 593-605. A Comparative Study and Analysis of Semi-Active Vibration-Control Systems.

[12] J. Alanoly and S. Sankar 1988 *Journal of Sound and Vibration* **126**: 145-156. Semi-active force generators for shock isolation.

[13] M. Ahmadian and N. Vahadati 2003, *International Mechanical Engineers Conference.* Washington, IMEC2003-43254. An analytical Evaluation of the Transient Dynamics of Semiactive Dampers.

[14] G. Yang, B. F. Spencer Jr, and F. Leban 2002 *Journal of structural control,* **9**: 135-152. Shock isolation using 'smart' damping.

[15] M.J Griffin 1996, *Handbook of Human Vibration*. London: Academic Press Limited.

[16] British Standard 1987, *British Standard 6841*. Guide to Measurement and evaluation of human exposure to whole-body mechanical vibration and repeated shock.

[17] F. Fahy and J. Walker 1998, Fundamentals of Noise and Vibration, London: Chapter 4. E&FN Spon.

[18] H.V.C. Howarth and M.J. Griffin 1991, *Journal of sound and vibration* **147**(3): 395-408. Subjective reaction to vertical mechanical shocks of various waveforms.

[19] Z. Zong and K.Y. Lam 2001, *Journal of Biomechanics* **35**: 45-43. Biodynamic response of shipboard sitting subject to ship shock motion.

[20] Y. Liu and J. Zhang 2001, *Mechanics Research Communications* **29**: 359-365. Nonlinear dynamic responses of twin-tube hydraulic shock absorber.

[21] Stefan W.R. Duym 2000, *Journal of vehicle system dynamics* **33**: 261-285. Simulation Tools, Modelling and Identification, for an Automotive Shock Absorber in the Context of Vehicle Dynamics.

[22] R. Mollica and K. Youcef-Toumi 1997, *Proceedings of the American Control Conference.* A Nonlinear Dynamic Model of a mono tube shock absorber

[23] M. Weigel, W. Mack and A. Riepl 2002, *Vehicle system dynamics* **38**(6): 415-432. Non parametric shock absorber modelling based on standard test data.

[24] S.O. Oyadiji and P. Sarafianos 2003, *International Journal of Vehicle Design* **33**(1-3): 251-278. Characterisation and comparison of the dynamic properties of conventional and electro-rheological fluid shock absorbers.

[25] L.F.P. Etman, and R.C.N. Vermeulen 2003 *Journal of vehicle system dynamics* **38**: 85-101. Design of a Stroke Dependent Damper for the Front Axle Suspension of a Truck Using Multibody System Dynamics and Numerical Optimization

[26] K. Cho and S. So 1999 *Transactions of the Korean Society of Automotive Engineers* **7**: 294-300. A Study of the New typed Stroke Dependent Damper.

[27] S. Dyne 2003 *Matlab Computation lecture notes*: ISVR, University of Southampton.

[28] T.P.Waters 2003 *Automobile Engineering Lecture notes:* ISVR, University of Southampton, 18, Vehicle Response to Road input.

[29] D. Kincaid and W. Cheney 1990 *Numerical Analysis,* 499-516. California: Brooks/Cole Publishing Company.

[30] K.S. Miller 1957 *Engineering Mathematics*, 196-217. New York: Rinehart & Company.

[31] L.A. Pipes 1958 *Applied Mathematics for Engineers and Physicists* 149-161. New York:McGraw-Hill Book Company.

[32] B.R. Mace 2003 *ISVR6031 Fundamental of Vibration Lecture notes:* Shock and Shock response.

[33] J.C. Dixon 1991 Tyres, Suspension and Handling 174-186 Cambridge: Cambridge University Press.

[34] J.C. Dixon 1999 *The shock Absorber Handbook*, 225-241. Warrandale: Society of Automotive engineers, Inc.

[35] Suspension and Damper Technology for Passenger Cars 2003, Technical brochure, ZF Sachs AG, http://www.sachs.de/owx_medien/media201/20126.pdf.

[36] Y. Hyun 2001 *Internal test report* R&D Technical Center in Hyundai Motor Co. Introduction of automotive shock absorber.

[37] R. Mollica and K. Youcef-Toumi 1997, *Proceedings of the American Control Conference* **6**: 704-708. Massachusetts Institute of Technology. A Nonlinear Dynamic Model of a Monotube Shock Absorber.

[38] J. Alanoly and S. Sankar 1988 *Journal of Sound and Vibration* **126**: 145-156. Semi-active force generators for shock isolation.

[39] D. Hrovat 1997, *Automatica* **33**(10): 1781-1817. Survey of Advanced Suspension Developments and Related Optimal Control Applications.

[40] S. Cafferty and G.R. Tomlinson 1997, *Journal of Automobile Engineering.* **211**(3): 181-203.Characterization of Automotive Dampers using Higher Order Frequency Response Functions.

[41] Test Report for shock absorber, 2004, Hyundai Motor Co.

[42] A. Best 1984, *Physics Technolgy of Modern Transportation.* **15**(8): 205-210. Vehicle ride - Stages in Comprehension.